MONTAN
UNIVERSITÄT
LEOBEN

Chair of Casting Research

Master's Thesis

Influence of alloying elements (Cu, Mg, Ag) and hot rolling on the solidification microstructure, precipitation microstructure and hardness of an Al-Cu-Mg-Ag alloy

Leon Heinl, BSc

November 2023

MONTANUNIVERSITÄT LEOBEN
www.unileoben.ac.at

EIDESSTATTLICHE ERKLÄRUNG

Ich erkläre an Eides statt, dass ich diese Arbeit selbständig verfasst, andere als die angegebenen Quellen und Hilfsmittel nicht benutzt, und mich auch sonst keiner unerlaubten Hilfsmittel bedient habe.

Ich erkläre, dass ich die Richtlinien des Senats der Montanuniversität Leoben zu "Gute wissenschaftliche Praxis" gelesen, verstanden und befolgt habe.

Weiters erkläre ich, dass die elektronische und gedruckte Version der eingereichten wissenschaftlichen Abschlussarbeit formal und inhaltlich identisch sind.

Datum 01.11.2023

Unterschrift Verfasser/in
Leon Heinl

Acknowledgement

I would like to express my special thanks to my supervisor Priv.-Doz. MSc PhD Jiehua Li for his time and efforts he provided throughout the last months. I would also like to thank my colleagues at the Chair of Casting Research for their support.

Besides them, I would also like to thank the Institute of Physics, in particular Mr. Mohammad Taha Honaramooz, MSc and Mag. et Dr.rer.nat. Rainer Lechner for their commitment. I would also like to thank the Institute of Forming Technology and the ÖGI Leoben, especially Mr. Albert Jahn, for their helpful cooperation.

Finally, I would like to thank my family, who made it possible for me to study at the Montanuniversität Leoben. Special thanks also go to my girlfriend for her patience and support during the last years.

Kurzfassung

Im Rahmen dieser Arbeit wurde zunächst untersucht welchen Einfluss der Cu-Gehalt auf das Erstarrungsgefüge, das Ausscheidungsgefüge und die Härte besitzt. Anschließend wurde der Einfluss der Zugabe von 0.7 wt.% Ag und 0.3 wt.% Mg bezüglich derselben Parameter betrachtet, dabei wurden die Elemente sowohl separat als auch gemeinsam zulegiert. Die Ziellegierung Al-4Cu-0.3Mg-0.7Ag wurde zuletzt auf sechs unterschiedliche Blechdicken bei 250 °C warm gewalzt und in drei verschiedenen Zuständen analysiert: (i) im verformten Zustand, (ii) nach einer T4 Lösungsglühung bei 540 °C für 6 Stunden und (iii) einer Alterung bei 170 °C für 12 Stunden. Die Betrachtung des Gefüges wurde für die Aufbaulegierungen nach einer Barker Ätzung unter dem Lichtmikroskop und für die Al-4Cu-0.3Mg-0.7Ag Legierung und die gerollten Proben unter dem REM durchgeführt. Die Ermittlung der Härte erfolgte nach Vickers, die T4 behandelten Proben wurden dabei für sieben Tage kalt ausgelagert. Das Verhalten der Ausscheidungen wurde mit Hilfe der Kleinwinkel-Röntgenstreuung (SAXS) bei 170 °C und DSC betrachtet.

Es konnte gezeigt werden, dass mit zunehmenden Cu Gehalt die Härte zunimmt, die Bildung einer signifikanten Menge von Ausscheidungen beginnt ab einem Gehalt von 4 wt.% Cu. Eine Zugabe von 0.3 wt.% Mg zu einer Al-4Cu Legierung führt zu einer Zunahme der Härte und verschiebt die Bildung der GP-Zonen bei 170 °C im SAXS zu einem späteren Zeitpunkt. Die Beimengung von 0.7 w.t% Ag zu einer Al-4Cu Legierung resultiert in einer gesteigerten Härte und Zunahme der Ausscheidungsdichte und Vergröberung. Die Härtemessung der Al-4Cu-0.3Mg-0.7Ag Legierung zeigt die höchsten Werten und die sich bildenden Ω-Phase vergröbert zunächst und zeigt anschließend eine exzellente thermische Stabilität im betrachteten Zeitraum von 40 Stunden. Die Härte der Proben nach dem Walzen liegen unabhängig von der nachfolgenden Behandlung unterhalb der ursprünglichen Legierung. Der Porod Radius der gerollten Proben ändert sich kaum, jedoch die Ausscheidungdichte zeigt leichte Unterschiede. Diese Masterarbeitet liefert ein grundlegendes Verständnis des Einflusses der Legierungselemente (Cu, Mg, Ag) und des Warmwalzens auf das Erstarrungsgefüge, Ausscheidungsgefüge und die Härte im Al-Cu-Mg-Ag Legierungssystem. Mit Hilfe dieser können weitere Legierungsentwicklungen durchgeführt werden.

Abstract

In this work, the influence of the Cu content on the solidification microstructure, precipitation microstructure and hardness was investigated firstly. Subsequently, the influence of the separate or combined addition of 0.7 wt.% Ag and 0.3 wt.% Mg on the same parameters was considered. Finally, the targeted alloy Al-4Cu-0.3Mg-0.7Ag was investigated under following conditions: (i) after hot rolling up to six different plate thicknesses at 250 °C and in the rolling state, (ii) after T4 solution treatment at 540 °C for 6 hours, and (iii) ageing at 170 °C for 12 hours. The observation of the microstructure was carried out with the use of the optical microscope for the build-up alloys after a Barker etching and under the SEM for the Al-4Cu-0.3Mg-0.7Ag alloy and the rolled respective samples. Hardness of the T4 treated samples after natural aged for seven days was determined according to Vickers. The the precipitation behaviour was investigated using small angle X-ray scattering (SAXS) at 170 °C and DSC, respectively.

It was found that with increasing Cu content the hardness increases, the formation of a significant amount of precipitates starts with a content of 4 wt.% Cu. The addition of 0.3 wt.% Mg into an Al-4Cu alloy leads to an increase in hardness and postpones the formation of GP zones at 170 °C in SAXS to a later stage. The addition of 0.7 wt.% Ag to an Al-4Cu alloy results in an increased hardness and an increase in the precipitation density and coarsening. The hardness measurement of Al-4Cu-0.3Mg-0.7Ag alloy shows the highest values and the Ω-phase formed coarsens firstly and then shows an excellent thermal stability in the considered period of 40 hours. The hardness of the samples after rolling are below the original alloy regardless of the subsequent treatment. The Porod radius of the rolled specimens hardly changes, but the precipitation density shows slight differences. This master thesis provides a fundamental understanding of the influence of alloying elements (Cu, Mg, Ag) and hot rolling on the solidification microstructure, precipitation microstructure and hardness in Al-Cu-Mg-Ag alloy system, which is of great help for the further alloy development.

Table of contents

1 Introduction

Al and its alloys play an important role in today's lightweight construction not only in the automotive industry, but also in the aerospace industry. There is a constant striving for ever lighter materials, which on the other hand should also have improved mechanical and thermal properties. Due to their relatively low density and high availability, and thus also their economic advantages, Al alloys are of great importance in these industries. Even the addition of low element contents can have a major influence on the formation of phases and precipitates. These in turn can have a big influence on material properties of the component. It is therefore particularly important to understand not only the mechanical properties but also the underlying mechanism that leads to the changes. With this understanding and the knowledge of the influence of certain alloying elements on the properties of the alloy, it is possible to produce requirement-specific materials. This is accompanied by an optimization of the process and increased efficiency in production. However, it is not always possible to know and understand the processes at the atomic level in a material to their full extent. Therefore, conclusions and assumptions are often made about the behaviour of the alloy during solidification and precipitation with the help of the already solidified material. Also, the technical progress over time brings new investigation methods to gain a deeper understanding.

The aim of this work is to consider the solidification, precipitation and hardness of Al-Cu-Mg-Ag based alloys. One special attention is paid to the influence of the additional elements (Mg and Ag), which lead to the formation of a thermodynamically more stable phase in the material. For this purpose, the alloy build-up was firstly carried out step by step, starting with high-purity Al and ending with the composition of the final targeted alloy. Diez samples of all materials were cast and then different heat treatments were applied to the samples. In addition, the targeted alloy was also hot rolled and considered both in the as-rolled condition and after an annealing treatment. Analysis of the phases and precipitates was then performed using a variety of methods. In addition to Barker etching and the optical microscope for determining the grain sizes in the non-grain refined materials, the Scanning Electron Microscope (SEM) was also used to perform more detailed microstructure characterisations. Different observations of the formed microstructure were carried out on this microscope. In addition, some samples in the T4 state (solution treatment) were subjected to in-situ small angle X-ray scattering.

The present work is divided into four main chapters. The chapter one starts with an overview of the theoretical principles of the alloy system, the possible solidification processes of an alloy, grain refinement and heat treatment. In addition, the age hardening mechanisms also play an important role in the properties of the material; precipitation hardening is of particular importance in this alloy. Subsequently, the chapter three (experimental methods) briefly describes the equipment used, the evaluation methods and casting of the various samples and their preparation. The next chapter four is the presentation of the results with a brief discussion, which is divided into the consideration of the influence of the alloying elements and the degree of deformation of the alloy, respectively. In the summary, the obtained results are summarized in a compact form and a brief outlook on possible further research activities is given.

2 Theoretical principles

2.1 Al-Cu alloys

The Cu content in an Al-Cu alloy has a great influence on the microstructure and the growth direction of the crystals. The microstructure of the α-Al also changes from columnar to columnar dendritic and, at high Cu contents, to equiaxed dendritic. Analogous to this change, the primary dendrite arm spacing also increases. All these microstructural changes can be attributed to the increase in constitutional supercooling. [1]

The binary phase diagram of Al and Cu is shown in **Figure 2-1 [2]**. These two elements form different compounds. But in the range of less than 10 % Cu, besides the α-Al, another phase is Al_2Cu (θ). This θ-phase is diamond-shaped in the microstructure when viewed under a microscope. The θ-phase is extremely brittle and therefore the technical Al-Cu alloys are almost entirely on the left side of the eutectic subsystem. They thus contain almost all primary α-phases and more or less eutectic. [3]

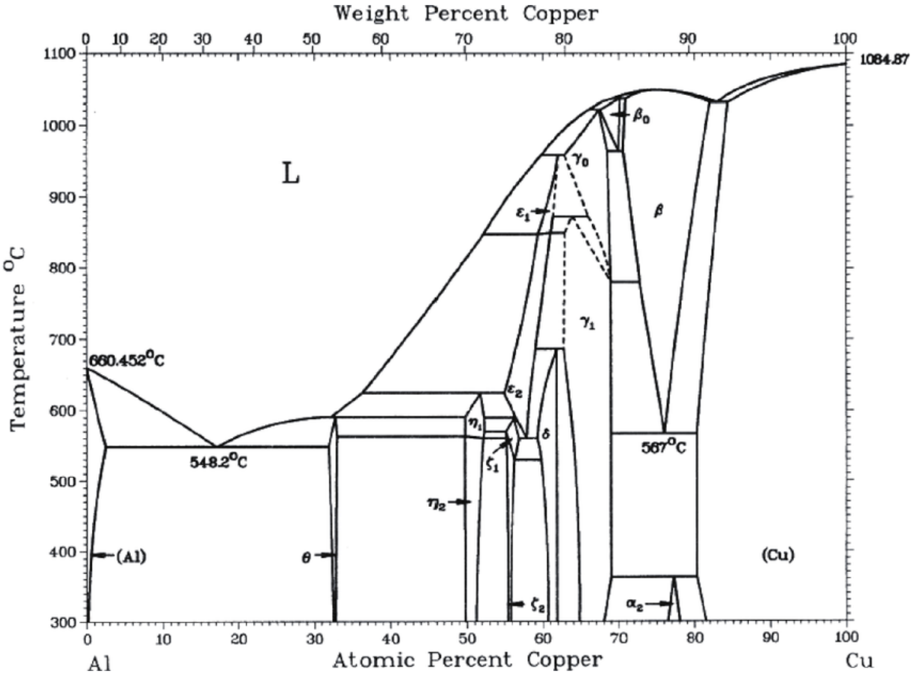

Figure 2-1: Al-Cu phase diagram. [2]

2.2 Al-Cu-Mg alloys

This type of alloy is characterized by the achievement of high values for tensile strength and yield strength with the help of age hardening. After its discovery in 1906 by A. Wilm, this alloy was used in the construction of zeppelin airships from 1914. However, its importance has declined due to its poorer corrosion properties compared with Al-Mg-Si. Al-Cu-Mg alloys are used purely as wrought alloys. A large number of further developments of this alloy have also been reported. In technical Al-Cu-Mg alloys, the θ-phase is predominantly formed as the equilibrium phase at low Mg concentrations, while the S-phase with a composition of Al_2CuMg precipitates at high Mg contents. Thereby, the hardenability of this alloy is based on the formed S-phase. During hardening, Guinier-Preston zones of Cu and Mg atoms appear on the (100) faces of the Al, on the one hand, and plate-like S precipitates, on the other hand. This can also be seen in **Figure 2-2 [4]**, the section of the ternary state diagram of Al-Cu-Mg for low contents of the alloying elements Cu and Mg. Cu plays a central role when the highest possible strength values are desired; the Cu content is usually between 4.0 and 4.8 %. The Mg is used for hardenability at room temperature and counteracts the influence of Fe, which is contained in pure Al in technical alloys. In addition, it also increases the speed of the hardening process in the alloy system. [4]

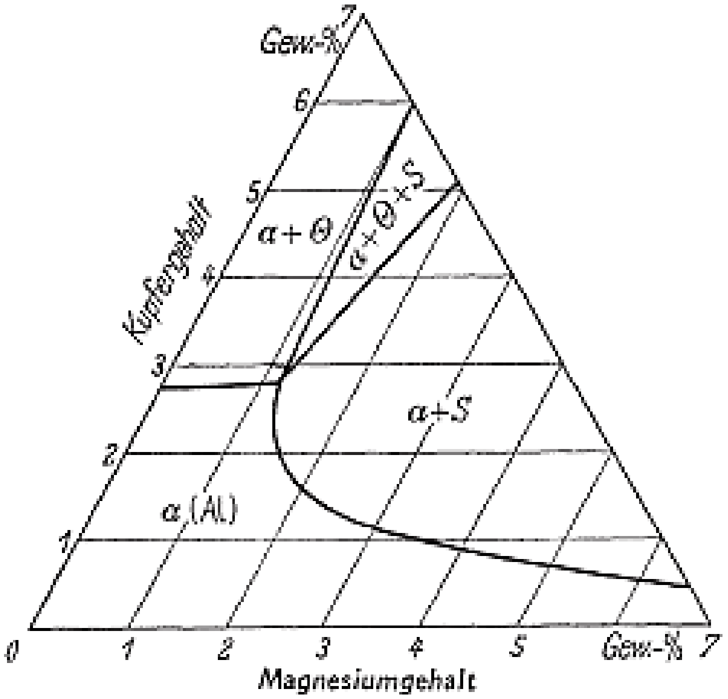

Figure 2-2: Part of the Al-Cu-Mg system at 460 °C. [4]

2.3 Al-Cu-Mg-Ag alloys

The Al-Cu-Mg-Ag alloy system is characterized by its high stability of mechanical properties at elevated temperatures. The system is characterized by high strength, low creep rates and high thermal stability, which makes it an interesting material for aerospace applications. The basis for these properties is the hardening of the alloy by the thermally relatively stable Ω-phase. Due to the high solubility of Mg and Ag in Al, these two elements do not tend to be precipitated by segregation, but form a stable state even in solid solution. However, Mg and Ag dissolved in the solid can affect the properties of the matrix and determine the hardening type. Small additions of Ag to an Al-Cu-Mg alloy with a high Cu/Mg ratio will cause the precipitation of the Ω-phase. This can be recognized in metallographic examination by its shape, which can be found as thin, hexagonal platelets in the {111} plane. The Ω-phase is not found in Al-Cu-Ag alloys, but it has already been detected in the absence of Ag in Al-Cu-Mg alloys. This suggests that Ag rather serves to kinetically enhance the precipitation of Ω-phase at the expense of θ'-phase. The most important age-hardening phases are listed in **Table 2-1 [5]**, where the type of phase depends mainly on the chemical composition. [5–7]

Table 2-1: Important hardening phases in Al-Cu-X alloys. [5]

Phase	Structure	Crystal habitus	Composition
Ω	orthorhombic	Thin plates on $\{111\}_{\alpha}$	~Al_2Cu
Θ‘	Tetragonal	Plates on $\{100\}_{\alpha}$	Al_2Cu
S‘	Orthorhombic	Slat on $\{210\}_{\alpha}$	Al_2CuMg
T	fcc	Rectangular plates on $\{100\}_{\alpha}$	Al_6CuMg_4

The composition of the Ω-phase corresponds chemically to the θ'-phase with the additional accumulation of Mg and Ag at the α/Ω-interface. The formation is preceded by the formation of Mg and Ag clusters after 15 s at 180 °C, which start to accumulate Cu atoms already after 30 s. The precipitation of the Ω-phase can be summarized as follow:

supersaturates solid solution (SSS) → Mg-Ag co-clusters → Ω-Phase [7]

2.4 Nucleation and crystal growth

In the production of cast materials, crystallization plays a central role in understanding material properties. For this reason, in the production of many metallic materials, attentions are paid to optimal smelting process control in order to achieve the targeted parameters. For the transition from liquid to solid a driving force is required, this is caused by the reduction of the temperature. The Gibbs free energy (G) is used to describe this model. It is defined with the use of the enthalpy (H), the temperature (T), and the entropy (S).

$$G = H - T * S \tag{1}$$

Figure 2-3 [8] shows the enthalpy curves of the melting phase and the crystal. At a certain temperature, the phase with the lower Gibbs free energy is thermodynamically stable. Thus, at the melting temperature T_E, both phases are in thermodynamic equilibrium and both have equal values for the free enthalpy.

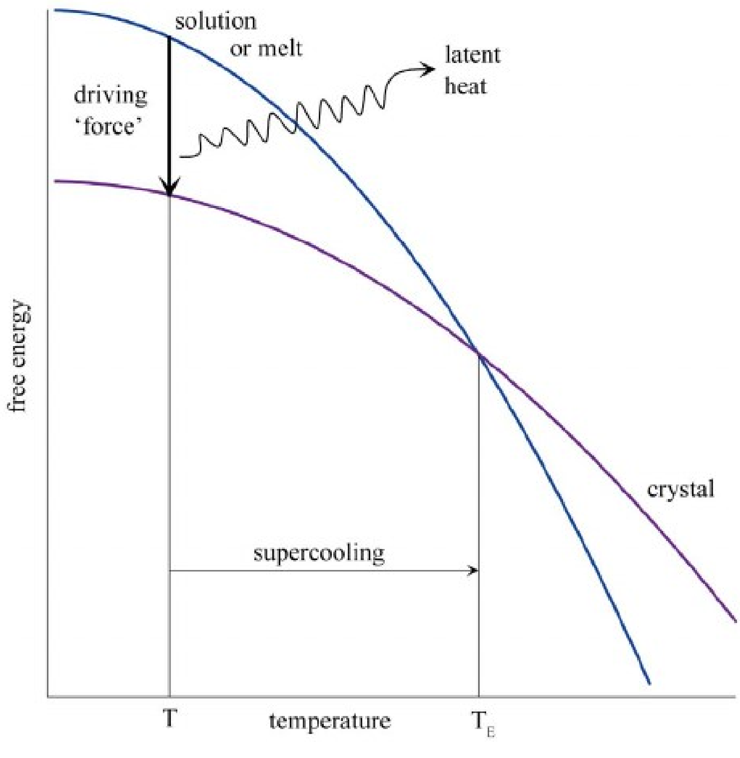

Figure 2-3: Dependency between free energy and temperature. [8]

A reduction in temperature leads to the liquid phase being metastable. If, on the other hand, the temperature is above the melting point, clusters are continuously formed, which, however, quickly disappear again. A supercooling (ΔT_c) causes the thermodynamic driving force as mentioned, this represents a change in Gibbs free energy (ΔG_c). The two equations for this are:

$$\Delta T_c = T_E - T \tag{2}$$

$$\Delta G_c = G_l - G_s \tag{3}$$

In these two equations, T corresponds to the current temperature, G_l and G_s represent the Gibbs free energy of the liquid and solid phases, respectively. If the temperature is below the melting temperature, clusters are formed which can form stable nuclei and grow as soon as they reach a critical radius (r*). However, this process is temperature-dependent and only takes place as soon as a certain temperature T below T_E has been reached. [9–11]

2.4.1 Homogeneous nucleation

An ideal homogeneous melt has no other solid compounds and nuclei formed, such as sulfides or oxides. This is the basic requirement for homogeneous nucleation from a melt. Assuming a spherical nucleus with radius (r), it is possible to calculate the critical nucleus size and nucleation enthalpy. The model for this is shown schematically in **Figure 2-4 [12]**.

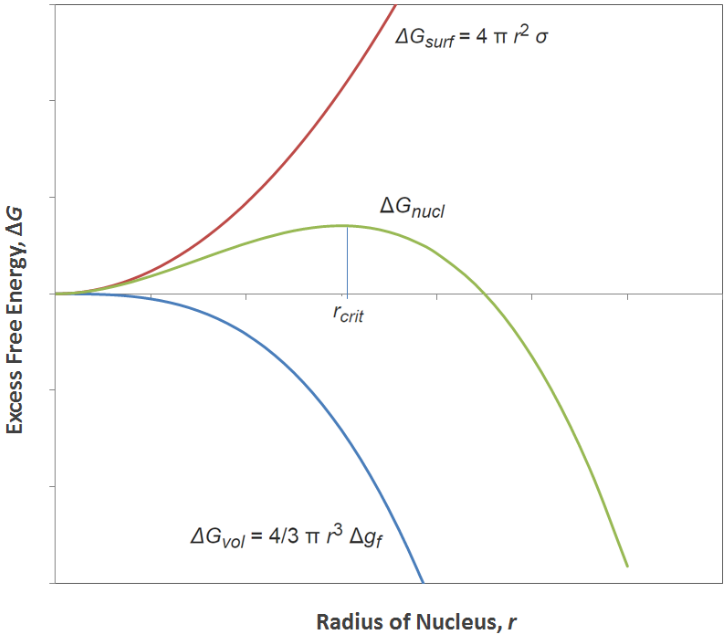

Figure 2-4: Gibbs free energy as a function of the radius. [12]

The total enthalpy (ΔG_{nucl}) consists of the volume fraction of the nucleus (ΔG_{vol}) and the surface fraction (ΔG_{surf}). Here σ describes the specific surface energy and Δg_f represents the driving force defined in the previous chapter. From these the equation for a spherical nucleus with radius r follows:

$$\Delta G(r) = 4\pi r^2\sigma - \frac{4}{3}\pi r^3\Delta g_f \tag{4}$$

However, homogeneous nucleation rarely takes place in technically applied melts, since particles and surfaces, which can serve as the nucleation sites for solidification, are usually present in the melt. In some cases, these are also systematically added in order to influence the morphology and properties of the material. [9; 13]

2.4.2 Heterogeneous nucleation

In practice, the occurrence of homogeneous nucleation is not very common, because heterogeneous solidification is preferred due to not only the large undercooling of the melt required for homogeneous nucleation but also the presence of particles in most alloys. In this case, the nuclei grow on the already existing surfaces such as the mold walls and the already mentioned particles within the liquid metal. This process is shown graphically in **Figure 2-5 [14]**, and the reduced Gibbs energy due to heterogeneous nucleation is also outlined. In the case of this mechanism, the critical nucleation radius for the formation of nuclei is reduced, since the necessary Gibbs (ΔG) energy is lowered.

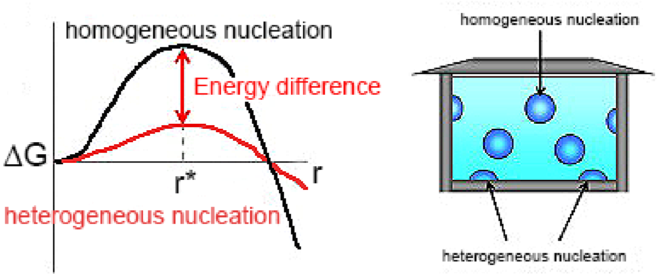

Figure 2-5: Homogeneous and heterogeneous nucleation. [14]

Due to the fact that, in contrast to homogeneous nucleation, the different interfacial energies between the nucleus, as shown in blue in **Figure 2-6 [14]**, and the melt γ_{CL}, between the nucleus and the mold wall γ_{CS}, and the melt and the mold wall γ_{SL} must also be taken into consideration, heterogeneous nucleation takes place before homogeneous nucleation. In summary, heterogeneous nucleation occurs relatively easier and earlier at a lower supersaturation of the melt, compared to homogeneous nucleation. [10; 14]

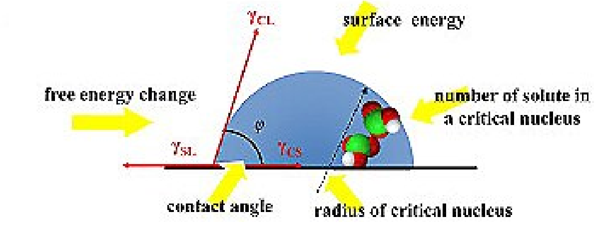

Figure 2-6: Equilibrium of a drop at a flat surface. [14]

2.5 Grain refining with TiB_2

An essential part of the manufacturing process of Al materials is grain refinement with the aim to reduce the size of the primarily Al grain by preventing the growth of long dendrites. This process offers many advantages for most alloys. In addition to casting parameters, mechanical properties are also positively affected. These include an improved feeding and thus a reduced tendency to shrinkage porosity, enhanced elongation properties, fatigue life and homogeneous distribution of the secondary intermetallic phase. To achieve this, small amounts of foreign elements are added to the melt before casting, which subsequently act as nucleating agents during crystallization. It should be observed that the added material has a higher melting point than the alloy to be cast. This is important to ensure that the added material is the first to solidify during cooling. An important parameter in the choice of grain refiner is the similarity of the crystallized phases, so that the crystals formed from the melt can attach well to the existing nuclei. The grain size of a material is inversely proportional to the degree of undercooling of the melt, this is due to the increased nucleation rate caused by this process. A fine and uniform microstructure is also ensured in this case. However, this is only theoretically possible and, depending on the component geometry, not always realizable in practice.

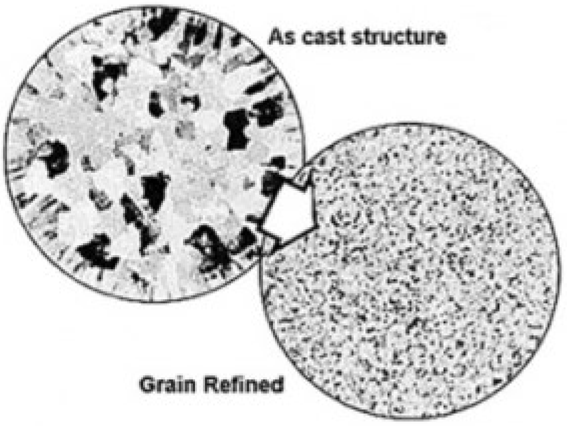

Figure 2-7: Influence of grain refining at the microstructure. [15]

For this reason, grain refiners are used in the solidification of many Al alloys. These ensure that growth is hindered when the eutectic temperature is reached, at which both α-phase and β-phase separate simultaneously. If there is a large amount of nuclei generated by a large undercooling or by the addition of nuclei, it happens that the melt solidifies evenly and finely distributed. The neighbouring nuclei hinder their mutual growth. The result of a grain refinement is shown exemplarily in **Figure 2-7 [15]**. [16–19]

For grain refinement with TiB_2, Al-Ti-B master alloys in the form of rods are usually used. In most cases, these are added a few minutes before casting to give the elements enough time to disperse in the melt. After the dissolution of the bar material, both TiB_2 and newly formed Al_3Ti particles are present in the melt. The latter is an extremely effective nucleating agent, but the Ti dissolves in the metal bath immediately after the addition, delivering free Ti to the melt. Solidification results in the deposition of α-Al on the Al_3Ti particles as shown in **Figure 2-8 [19]**.

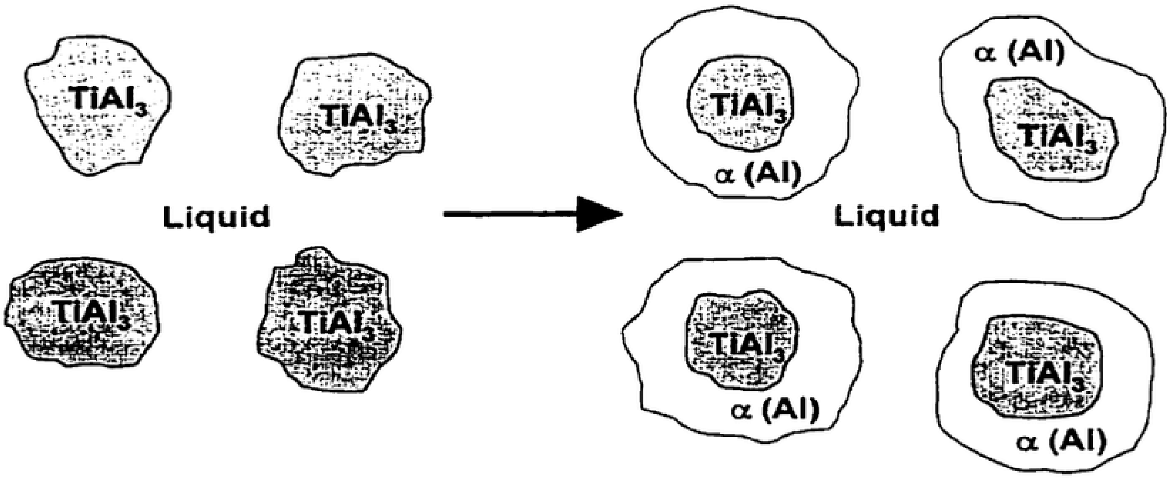

Figure 2-8: Grain refining mechanism of Al. [19]

However, this concept is highly simplified, since, as already mentioned, these particles dissolve in the melt. What remains are only TiB_2 particles on which monolayers of Al_3Ti form and on which the α-Al crystallizes. This layered structure is described in **Figure 2-9 [17]**. [17; 20]

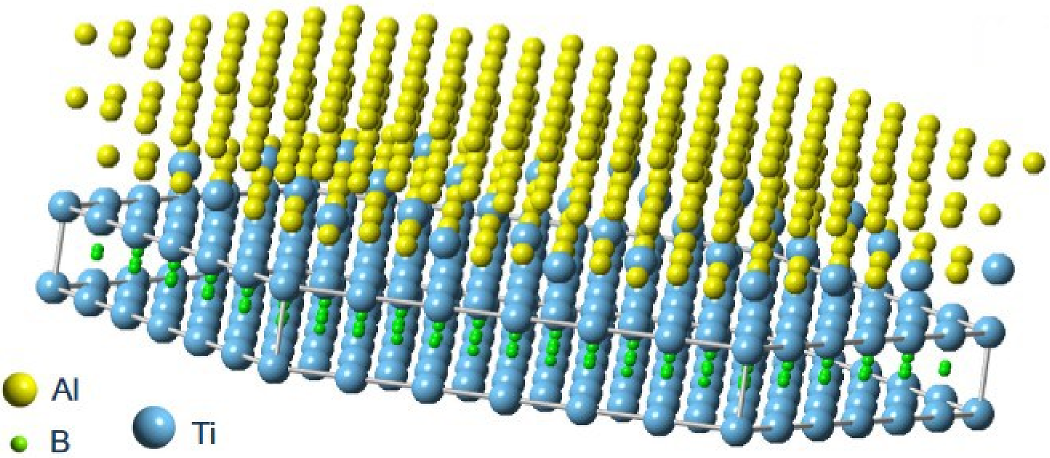

Figure 2-9: Different layers during grain refining with TiB. [17]

2.6 Strengthening mechanism

The most important strengthening mechanism in Al alloys is precipitation hardening. This central role of precipitation hardening is also reflected in the classification of alloys into hardenable and non-hardenable systems. The most important hardenable alloy systems including their IADS number class are Al-Cu and Al-Cu-Mg (2XXX), Al-Mg-Si (6XXX) and Al-Zn-Mg (7XXX). Using the binary Al-Cu alloy system as an example, the principle of precipitation hardening will be briefly illustrated with the aid of **Figure 2-10 [21]**.

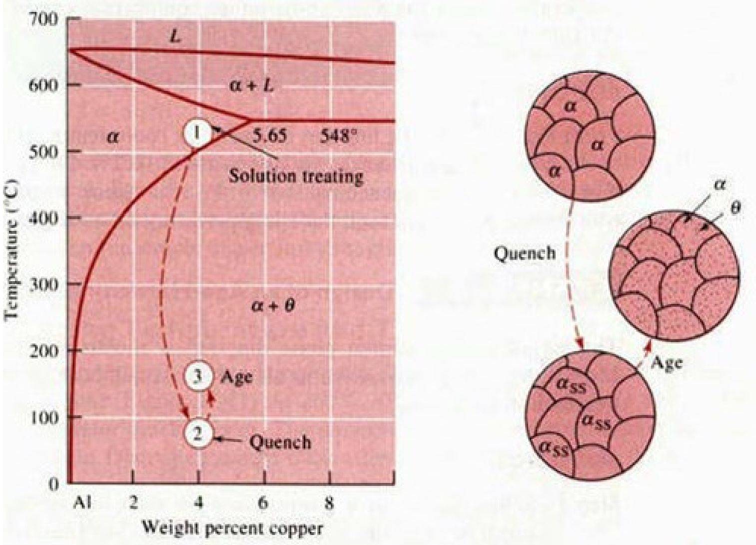

Figure 2-10: Three steps of age-hardening heat treatment and the microstructure of the Al-Cu phase diagram. [21]

The basic conditions for precipitation hardening are listed below:

1. The alloy exists wholly or partially as a solid solution at elevated temperatures.
2. The solubility of the second components in the crystal also decreases with decreasing temperature.

Both of these conditions are satisfied for an alloy containing less than 4 wt.% Cu, as in the systems considered for this work. The age hardening process itself consists of the three steps of solution treatment, quenching and ageing.

1. Solution treatment, this is the first step of the strengthening process. The alloy is heated above the solvus temperature and kept at this temperature until a homogeneous solid solution is formed. In the Al-Cu system, the θ-precipitates dissolve. Melting of individual phases must be prevented in this step in any case.

Temperatures that are too low to lead to a complete dissolution and homogenization must also be avoided. The optimum temperature range is often only 5 to 10 °C.

2. Quenching is the second step in which the workpiece is rapidly cooled, forming a supersaturated solution of α_{SS} and is not in equilibrium. In this process, the diffusion of Cu atoms in the solid solution is stopped, thus hindering the formation of coarse precipitates. In order to achieve the greatest possible supersaturation, it is necessary to cool the annealed material as quickly as possible; this is usually done with cold water.
3. Ageing is the last step, where the system is now heated below the solvus temperature. The goal here is the formation of finely dispersive precipitates. In this process, due to the low temperature, the atoms diffuse only over small distances, the excess Cu atoms diffuse to countless nucleation sites and the precipitates grow. A natural ageing describes the process at room temperature.

The transition of the supersaturated solid solution to the equilibrium state of the system usually occurs via a multistage process. In the Al-Cu system, the precipitation process takes place via several intermediate stages to the θ-phase according to:

$$\alpha_{SS} \rightarrow \text{GP-Zones} \rightarrow \theta' \rightarrow \theta$$

The resulting Guinier-Preston (GP) zones are Cu-rich, coherent, disk-shaped precipitates with a thickness of a few atomic layers. Due to the short diffusion paths, these precipitates are finely distributed and have a high density.

The strengthening mechanism is essentially based on the interaction between the dislocations and the precipitates. The greater the resistance to the dislocation movement, the greater the hardness and strength. [5; 21]

2.7 Heat treatment

The coarsening resistance and thermal stability of Al-Cu-Mg-Ag alloys through the Ω-phase is influenced by the chemical composition and thermomechanical processes. T4 heat treatment of a 2XXX alloy involves solution treatment followed by quenching in water and natural ageing. Whereas T6 heat treatment involves artificial ageing after quenching. The two possible treatments of the alloy are shown schematically in **Figure 2-11 [22]**.

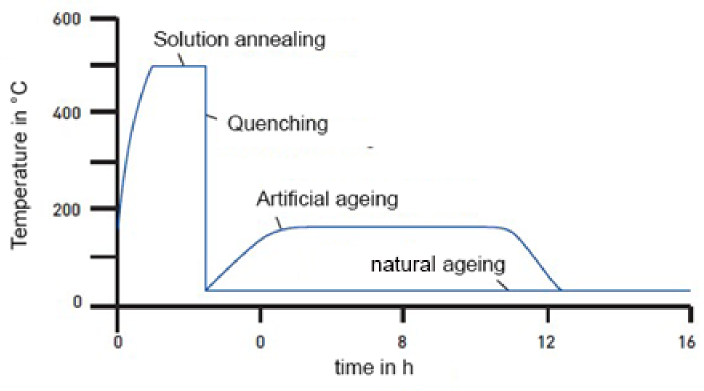

Figure 2-11: Schema of T4 and T6 of 2XXX-alloy. [22]

For this group of alloys, the temperature range at a Cu content of 4% plays a major role, since this already becomes very small in which a homogeneous microstructure is present. The relationship between the Cu content and the temperature is shown in **Figure 2-12 [22]**. Too high temperatures lead to a partially melting in the microstructure, and too low temperatures do not homogenize the microstructure. Artificial peak ageing of this type of alloy makes it possible to achieve higher strengths, but the corrosion resistance of the material decreases. [22]

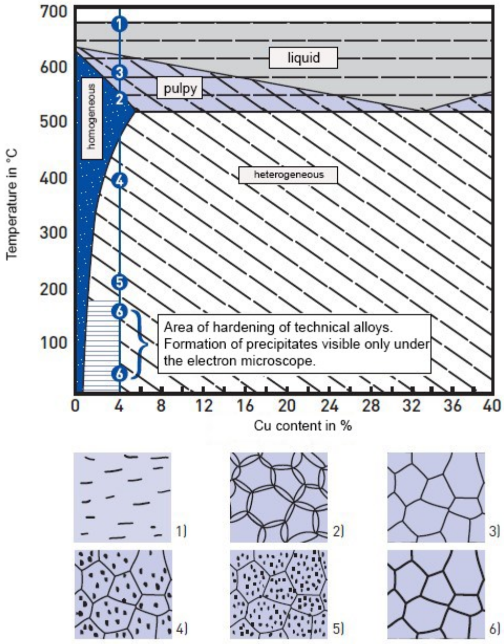

Figure 2-12: Relationship between temperature and microstructure in the Al-Cu-system. [22]

2.8 Precipitation behaviour of Al-Cu-Mg(-Ag) and the influence of hot rolling

De Geuser et al. use SAXS measurements to investigate a solution heat treated Al-4Cu-0.3Mg-0.4Ag alloy at 200 °C for up to 2 h in the as-received state and under the application of different loads. In all 3 samples, the clusters initially grow in the first hour until the Ω-precipitates form, which coarsen in the following hour. The precipitates have a size about 2 to 3 nm, with those of the sample without load being the highest. Whereas the applied stress shows no significant effect on the size of the clusters formed at the beginning. [23]

Chen et al. carried out investigations on an Al-5.11Cu-0.96Mg-0.58Mn-0.12Zr(-0.7Ag) alloy, on the one hand with the addition of 0.7 wt.% Ag and on the other hand without it. The examination of the two alloys by DSC in **Figure 2-13 [24]** shows a shift of the first peak, which corresponds to the cluster formation. The Ag-free alloy has a peak at a lower temperature because the Cu-Mg clusters have a lower binding energy than the Mg-Ag co-clusters. Their peak is at about 105 °C. The Al-Cu-Mg alloy shows a second clear peak at around 280 - 300°C, which can be assigned to be due to the formation of the S- and θ-phases. The peak of the Ω-phase of the Al-Cu-Mg-Ag alloy is at somewhat lower temperature of 260 °C. However, this peak is not exclusively based on this phase, but both the S-phase and the θ-phase form additionally.

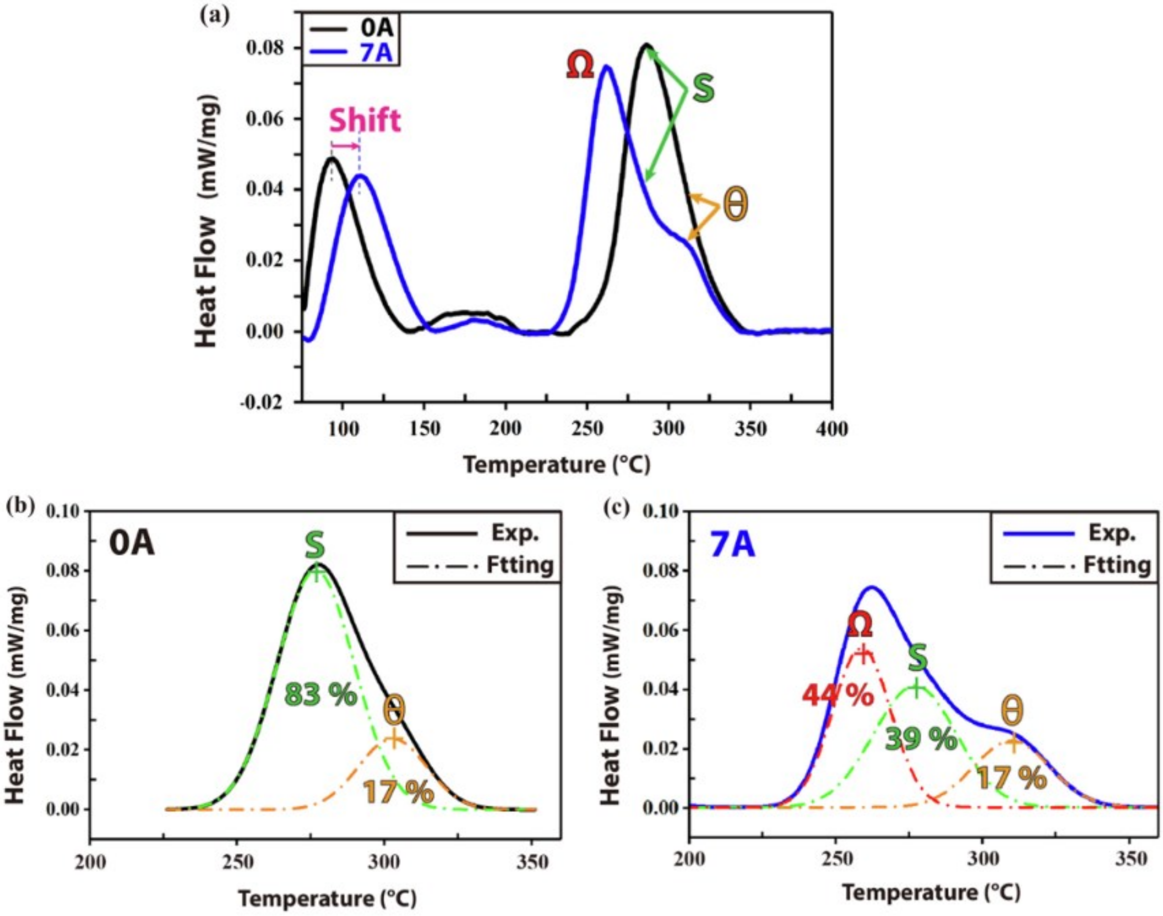

Figure 2-13: DSC curves of an Al-Cu-Mg alloy (0A) and an Al-Cu-Mg-Ag alloy (7A). [24]

The investigation of the alloy by means of in situ SAXS measurements at 185 °C shows that the size of the Mg-Ag co-clusters exceeds that of the Cu-Mg clusters. For the Ω-precipitates, the evaluation of the SAXS results shows that an almost constant thickness, but an increase in diameter with increasing annealing time can be observed. On the other hand the θ-phase dissolute during the ageing. This behaviour leads to the significantly higher values for hardness and thermal mechanical strength of the aged sample with Ag compared to the Al-Cu-Mg alloy. [24]

3 Experimental methods

3.1 Casting, heat treatment and rolling

Various Al alloys were prepared for a comparison with Al-4Cu-0.3Mg-0.7Ag alloy. These start with a cast of high-purity (HP) Al and build up to the targeted alloy. The chemical compositions of the various cast materials are listed in **Table 3-1**.

Table 3-1: Nominal composition of alloys in wt-%.

Alloy	Cu	Mg	Ag	Al
High-Purity Al				Bal.
Commercial-Purity Al				Bal.
Al-1Cu	1			Bal.
Al-2Cu	2			Bal.
Al-3Cu	3			Bal.
Al-4Cu	4			Bal.
Al-4Cu-0.3Mg	4	0.3		Bal.
Al-4Cu-0.7Ag	4		0.7	Bal.
Al-4Cu-0.3Mg-0.7Ag	4	0.3	0.7	Bal.

The material used for this was provided by the Chair of Casting Research. Commercial-purity (CP) Al was used for the production of all alloys, which means that traces of other elements may also be present. Casting is carried out in the institute's casting hall using the Nabertherm crucible furnace, which can be seen in **Figure 3-1**, into which the material is inserted after being cut and weighed. The melting temperature for all castings is 720 °C. The Al-4Cu-0.3Mg-0.7Ag sample is additionally grain-refined with Al-5Ti-1B. Diez specimens were cast in steel molds. The molds were previously coated with boron nitride and preheated in the Nabertherm convection oven at 150 °C for at least 30 minutes. This process serves to dry the coating and to reduce the temperature gradient between the melt and the mold.

Figure 3-1: Crucible furnace at the Chair of Casting Research.

In addition, a sample of the Al-4Cu-0.3Mg-0.7Ag alloy was cast with the same grain refiner using the melt spinning machine, as shown in **Figure 3-2**. Approximately 10 g of the material was melted in a vacuum chamber using induction heating. The molten metal was then ejected onto a rotating cooled Cu drum and solidified. The resulting ribbon of rapidly cooled material has a thickness of about 0.1 mm and a width of 7 mm.

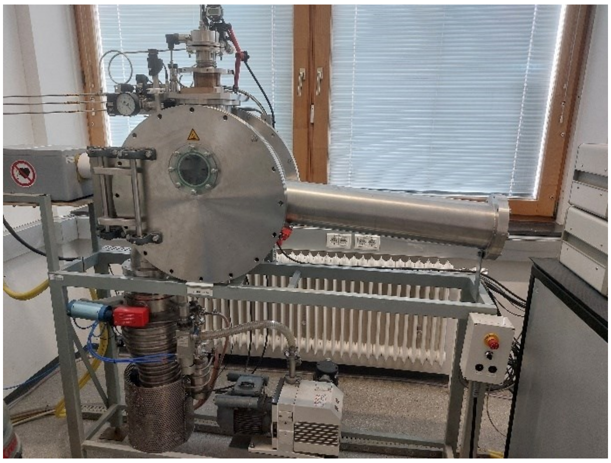

Figure 3-2: Melt spinning machine at the Chair of Casting Research.

Subsequently, T4 heat treatment at 540 °C for 6 hours and ageing of the specimens at 170 °C for 12 hours was performed in the Nabertherm NA120/85A convection oven, as shown in **Figure 3-3**.

Figure 3-3: Oven for heat treatment.

Subsequently, samples of the cast material were cut off for further investigations in the as-cast condition and, furthermore, larger pieces were cut off for T4 heat treatment with quenching in a water bath. The alloy Al-4Cu-0.3Mg-0.7Ag was also rolled into different thicknesses, as listed in **Table 3-2**.

Table 3-2: Dimension of rolled samples.

Designation	Thickness [mm]
A	0.3
B	1.2
C	2.05
D	3.14
E	4.25
F	6.74

The rolled materials were divided into three parts, one of which was considered in the as-rolled condition and the other two were subjected to two different heat treatments. One was a T4 solution heat treatment at 540 °C for 6 hours followed by quenching in a water bath and the other was an ageing at 170 °C for 12 hours. Finally, a sampling of all three conditions was made.

3.2 Hardness measurement

The hardness is measured at the Institute of Forming Technology in the Montanuniversität Leoben. The machine used for this is an EMCO Test M1C 010 as shown in **Figure 3-4**. The hardness test was carried out according to Vickers, whereby the impression created respectively the diagonals of the impression caused by the indenter are measured. The requirements are a flat ground surface, the thickness of the test material must be at a minimum of 10 times the indentation depth and the distance between the indentations must be at least 6 diagonal lengths. This serves to avoid an incorrect interpretation of the hardness due to a change in the properties of the surrounding material after deformation by the indentation.

Figure 3-4: EMCO Test at the Chair of Forming Technology.

3.3 Microstructure characterization methods

This chapter briefly explains the examination methods used in this thesis.

3.3.1 Optical microscope

For the analysis of the samples under the optical microscope, they were first ground with SiC abrasive paper with grades P80, P220, P600, P800 and P1200. The next step is polishing with diamond suspension (3 µm) and alkaline silica suspension (1 µm). These steps are performed manually at the Chair of Casting Research on an ATM Saphir 350 machine, as shown in **Figure 3-5**.

Figure 3-5: Grinding machine ATM Saphir 350.

In order to make the microstructure visible under the optical microscope, electrolytic etching according to Barker (35 ml HF, 13 g H_3BO_3, 800 ml H_2O) was also necessary. This takes place at the Österreichischen Gießereiinstitut (ÖGI). On the ATM Kristall 620 etcher used, as shown in **Figure 3-6**, the ground and polished specimen is placed with the side to be etched by immersing in the solution and connecting via a metallic connection as the anode. The etching time was two minutes for each sample. Subsequently, the microstructure could be distinguished with the polarized light mode in the optical microscope due to the contrast caused by the etching.

Figure 3-6: Barker etching with ATM Kristall 620.

In general, an optical microscope has only a shallow depth of field at a high magnification, which means that a good sample preparation is essential for optical observation of the microstructure. The resolution is limited to the wavelength range of visible light up to about 0.3 µm. However, this is sufficient for most investigations of a microstructure in the as-cast state or subsequent to heat treatment. The microstructural investigations were carried out at Chair of Casting Research by using a Carl Zeiss Axio Imager.A1m microscope. This has a maximum resolution of about 0.5 µm. In addition, a Nikon DS-Fi1 camera is integrated in this microscope, which enabled the observation and evaluation of the microstructure on the stationary computer with the aid of the NIS-Elements BR 3.0 software. For the evaluation of the etched microstructure and the determination of the grain size, the samples were viewed under a polarized light mode using the reflected light TC method. The setup of the microscope is shown in **Figure 3-7**.

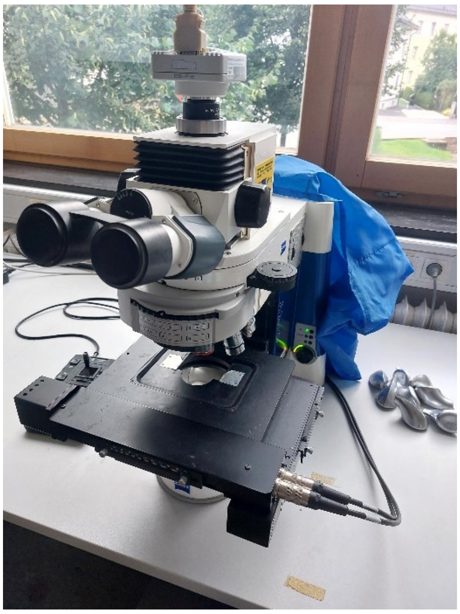

Figure 3-7: Light microscop Axio Imager A1m.

There are different analogous and also digital possibilities for determining the grain sizes of an Al alloy. Within the context of this work, the grain sizes are determined using the line intersection method. In addition to the NIS Elements BR 3.0 program, Origin is also used. In this method, measurement lines are placed in the sample, the length of which is known. The cutting points are then counted through the grain boundaries and the length divided by the number of grains is counted. The result of this step is an average grain boundary for this line intersection. To compensate for different grain orientations during solidification, a total of six grain size measurements are performed. Three lines are in horizontal and three in vertical direction. A common mean value and the standard deviation are then determined from these six grain size measurements.

3.3.2 SEM

Due to the fact that the resolution of the light microscope is limited, SEM is used for the observation and evaluation of grains in the submicrometric range. The requirements for these samples are much greater in terms of their surface area. The preparation of the samples includes the first step after mounting the same steps with grinding and polishing as in the light microscope. However, the materials to be examined were then subjected to a vibration polishing for at least 16 hours with the use of the ATM Saphir Vibro machine, as shown in **Figure 3-8**.

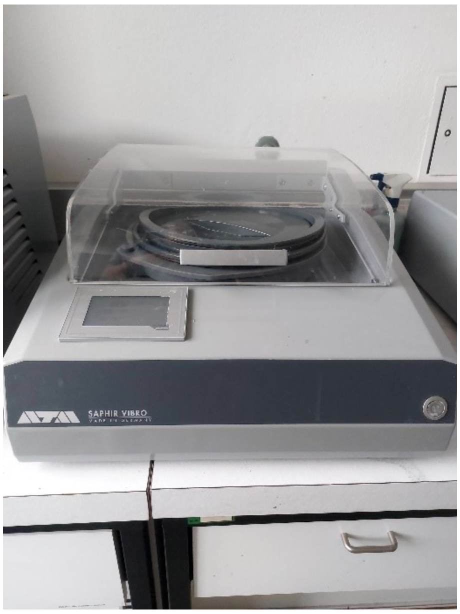

Figure 3-8: ATM Saphir Vibro for vibration polishing.

The samples were then broken out and ultrasonically cleaned in ethanol for about 20 minutes and finally attached to the sample holder using an Ag paste. The purpose of cleaning is to remove the specimen surface from any residues of polishing agent and mounting compound. The equipment used for this at the Chair of Casting Research is shown in **Figure 3-9**. This intermediate step is necessary because even small amounts of contamination can influence the analysis of the sample under SEM.

Figure 3-9: Ultrasonic cleaner.

SEM works on the basis of a focused, high-energy electron beam, which produces a multitude of signals at the sample surface. This beam has only a small size, which is why the area to be examined is scanned. The measurement duration and the size of the area to be examined correlate. The interactions between the beam and the sample contain a large amount of information about the examined part. This includes the morphology, the chemical composition, the crystal structure and the orientation of the grains. This data is usually output to a computer using a two-dimensional display. Resolutions up to 30,000 times can be reached and also point measurements of the chemical composition can be made. [25]

The chemical analysis of a sample with the use of a SEM is carried out by using energy dispersive X-ray spectroscopy (EDS). In addition to determining the chemical elements and their concentration, the distribution of the elements in the sample can also be detected. The basis for this method is X-ray microanalysis, which is based on the fact that each chemical element emits a characteristic X-ray radiation that is collected by the EDS detector. Using this technique it is possible to determine the composition of individual phases, small particles and impurities. The intensity of the peaks in an EDS spectrum is proportional to the concentration of the element in the sample. The position of the peaks depends on the electron energy used and thus the characteristic lines may differ depending on the investigation method.

Figure 3-10: Scanning electron microscope.

The SEM used in this work is a JOEL JSM-7200F located at the Department of Metallurgy, as shown in **Figure 3-10**. For taking the pictures this instrument is equipped with a backscatter electron detector and secondary electron detector. Next to this, an Oxford detector was used for the EBSD measurements. The data was then analysed with the help of the AZtec software package.

3.3.3 Small angle X-Ray scattering

The samples to be examined in SAXS have a greater requirement for their geometry. In return, the samples were not polished before the examination and only ground. The final machining step took place with a P2500 SiC abrasive paper. In order to keep the necessary thickness reduction as low as possible, the samples were cut at the ÖGI with the ATM Brillant 220 cutting machine as shown in **Figure 3-11** to a thickness of about 80 µm and a length between 17 - 18 mm and a width of 10 - 12 mm. Special attention had to be paid to the final thickness of the sample, since a sample that was too thick would have resulted in a low transmission of the X-rays in the test. On the other hand, it was also important that the thickness does not fall below 80 µm in order to obtain enough information from bulk samples.

Figure 3-11: Cutting machine ATM Brillant 220 at ÖGI.

SAXS is an analytical method used to determine the structure in terms of grain size and shape. X-rays are sent through the sample in a transmission mode and any particle in the beam will interact with it and emit a signal. The machine used at the Institute of Physics for the in-situ SAXS is shown in **Figure 3-12**. The method is extremely accurate, non-destructive and has low sample preparation requirements. The size of the particles that can be examined is in the range of 1 to 100 nm. The signal strength in SAXS is proportional to the squared volume of the particle. As a result, small objects are difficult to detect in the presence of larger ones. When a sample is irradiated with X-rays, the atoms within will reflect the incident radiation in all directions. This represents the background radiation of the material under investigation. In addition, particles such as precipitates inside the sample provide an additional scattering due to their different chemical compositions. Measuring this distribution of the radiation allows a detailed analysis about the structure of the particles. [26]

Figure 3-12: Machine used at the Institute of Physics for the SAXS.

3.3.4 Differential scanning calorimetry

Differential Scanning Calorimetry (DSC) is a thermal analysis method. It provides information about the amount of heat that is absorbed or released by a sample during heating, cooling or isothermal operation. Consequently, in addition to endothermic and exothermic processes, the transformation temperatures of a sample are also measured. It is therefore possible to detect and determine phase transitions within a sample using this method. The measuring device of Perkin Elmer, as shown in **Figure 3-13**, consists of two chambers, one containing an empty crucible as a reference and the other crucible with the sample. Both chambers are exposed to the same, user-definable measuring program. The endothermic and exothermic processes create a temperature difference between the reference and the sample. From this, the heat flow can be derived.

Figure 3-13: Machine of Perkin Elmer for the DSC measurements.

The samples for the DSC should be round, with a uniform thickness and should not exceed the crucible height. The preparation was done by hand with the help of SiC abrasive paper with a grade of P220. Before starting the measurement, all samples are weighed.

4 Results

The specimens described were subjected to different testing methods as outlined in the previous chapter. The aim is to identify the influences of the alloying elements, deformation and temperature on the properties. The first part starts with the consideration of the influences of the alloying elements on the grain size and the phases formed. In the second part, the effect of rolling on the microstructure is discussed. The morphology and chemical composition are first investigated using SEM, followed by SAXS studies on precipitation under a temperature exposure of 170 °C up to different ageing times.

4.1 Influence of Cu content

In the first part of this work, the influence of the alloying element Cu on the grain size and precipitates is examined. In addition to the optical microscope used for the determination of the grain size, the precipitation behaviour of the alloys is examined in the SAXS. **Figure 4-1** shows the acquired microstructures after casting and Barker etching. The microstructures of the pure Al samples (a and b) show elongated grains. The addition of more than 1 wt.% Cu leads to the formation of the equiaxed grains.

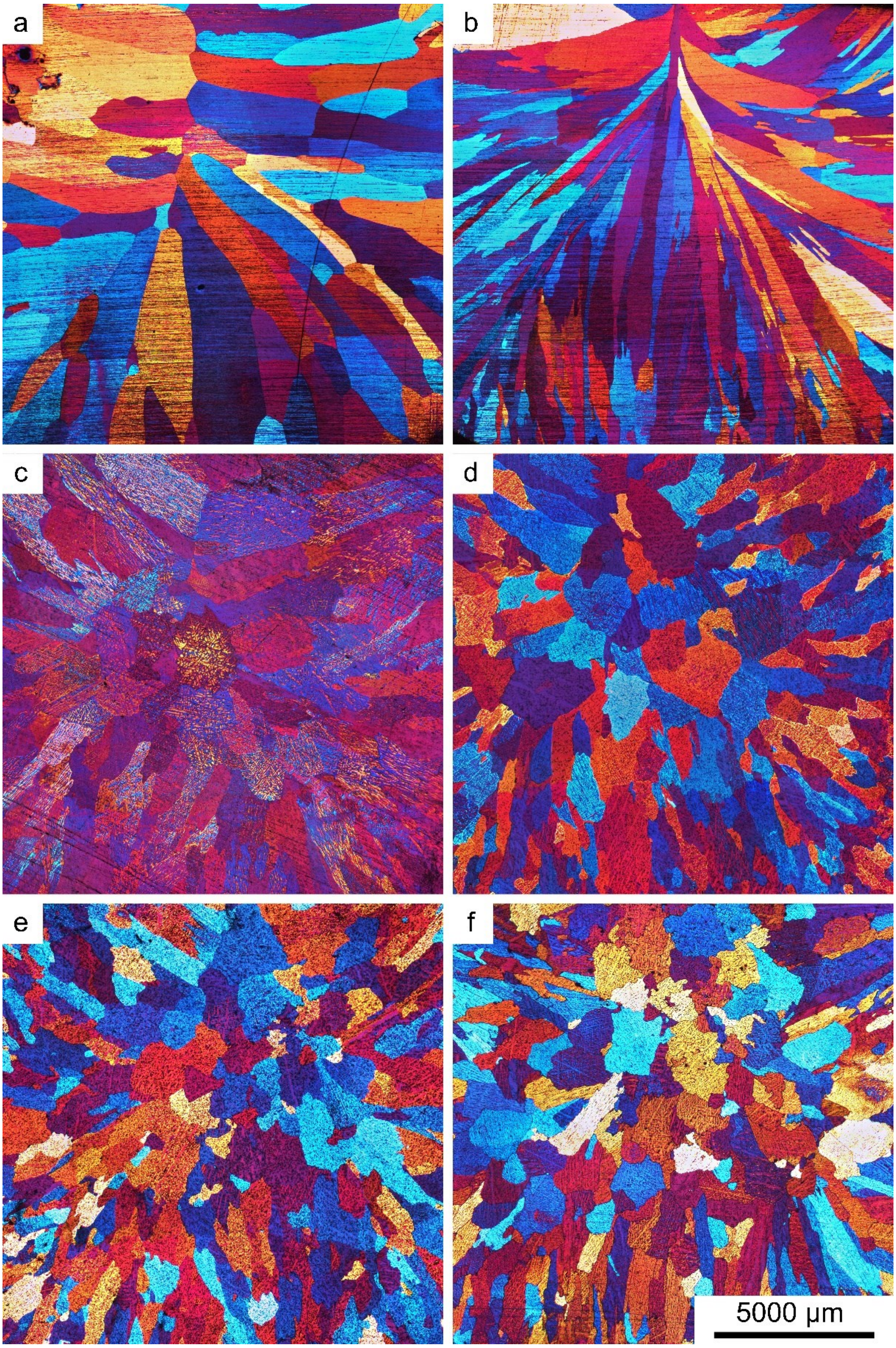

Figure 4-1: Microstructure of the samples after casting and Barker etching: a) HP-Al b) CP-Al c) Al-1Cu d) Al-2Cu e) Al-3Cu f) Al-4Cu.

After a solution treatment at 540 °C for 6 hours the microstructure is shown in **Figure 4-2**.

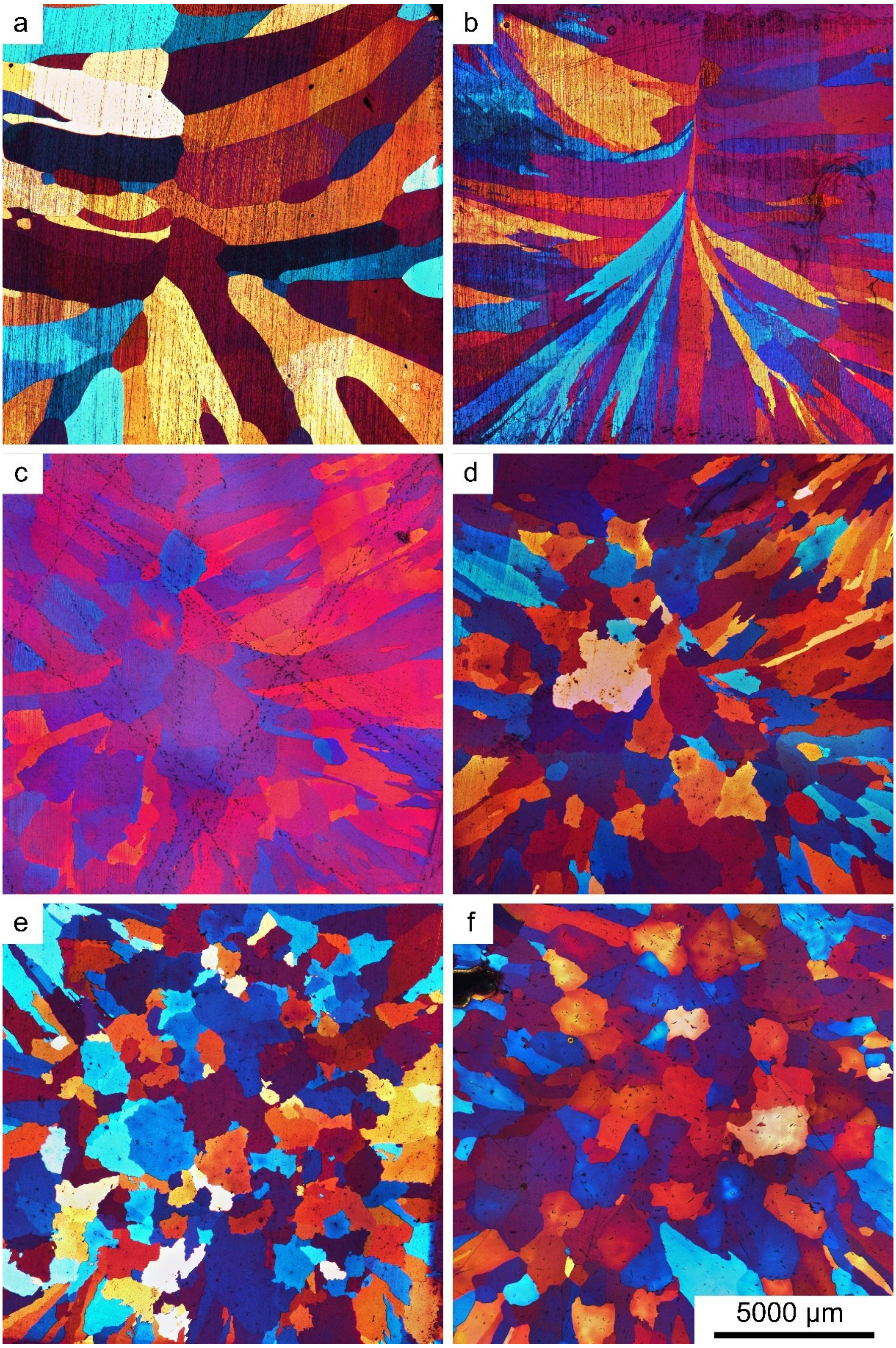

Figure 4-2: Microstructure of the samples after T4 solution treatment and Barker etching: a) HP-Al b) CP-Al c) Al-1Cu d) Al-2Cu e) Al-3Cu f) Al-4Cu.

4.1.1 Grain size

In the case of Barker etching, the grain size evaluation of 6 as-cast samples was performed. The results of the grain size determination are shown in **Figure 4-3**. This was necessary because no grain refining measures were set to be able to look at the direct influence of the elements and the purity of the Al. Due to the size of the grains, it was not possible to perform an automated determination of the grain size in the SEM as in the later investigations on rolled samples. It can be seen that the Al with a high purity has the largest mean grain size. The use of commercial purity Al leads to a decrease in grain size, while the addition of 1 wt% Cu to CP Al results in a slight coarsening. With the addition of 2 wt.% Cu the average grain size decreases and remains constant for higher amounts of Cu.

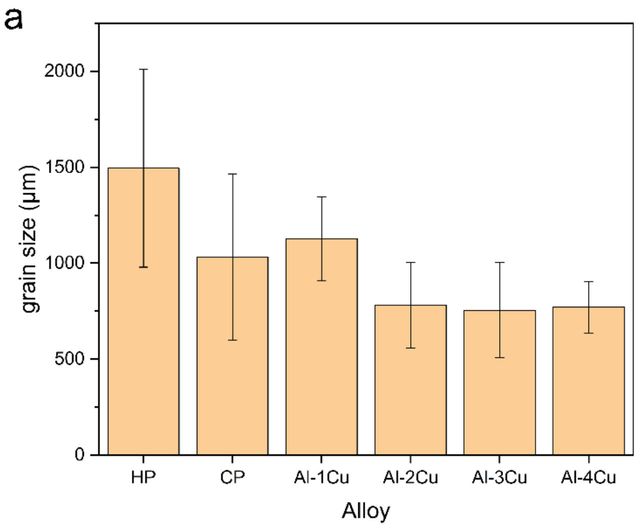

b

Alloy [-]	Grain size [µm]
HP	1494.7 ± 515.4
CP	1032.0 ± 433.4
Al-1Cu	1127.8 ± 217.9
Al-2Cu	780.9 ± 224.0
Al-3Cu	754.7 ± 247.9
Al-4Cu	769.7 ± 133.1

Figure 4-3: Grain size distribution after casting with different Cu contents: a) diagram b) table with mean and standard deviation.

A T4 solution heat treatment at 540 °C for 6 hours leads to coarsening. However, the coarsening of the Al-2Cu and Al-3Cu alloys is only slight compared to the other alloys.

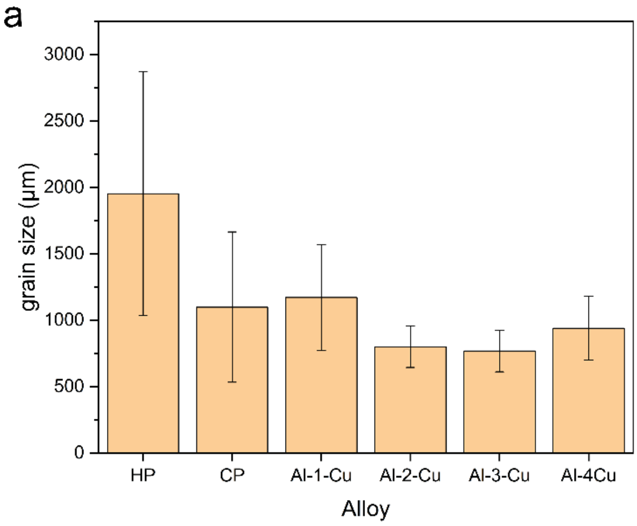

b

Alloy [-]	Grain size [µm]
HP	1953.2 ± 919.3
CP	1098.5 ± 565.0
Al-1Cu	1171.4 ± 397.2
Al-2Cu	799.4 ± 155.8
Al-3Cu	768.1 ± 156.7
Al-4Cu	939.3 ± 240.3

Figure 4-4: Grain size distribution after T4 with different Cu contents: a) diagram b) table with mean and standard deviation.

4.1.2 Hardness

The determination of the hardness was carried out according to Vickers. The samples were solution treated, quenched in water and natural aged for 7 days. The results of the measurements are shown in **Figure 4-5**. The hardness of the alloys increases with increasing Cu content. With the addition of 4 wt.% Cu more than quadrupled the hardness value compared to pure Al was observed.

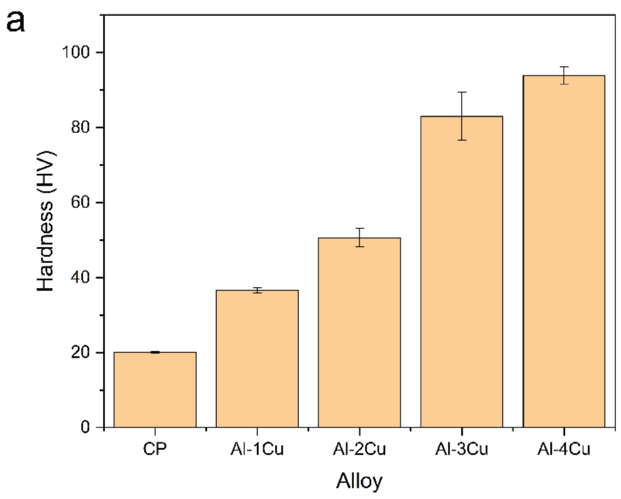

b

Alloy [-]	Hardness [HV]
CP	20.1 ± 0.2
Al-1Cu	36.6 ± 0.7
Al-2Cu	50.6 ± 2.4
Al-3Cu	83.9 ± 6.4
Al-4Cu	93.9 ± 2.3

Figure 4-5: Vickers hardness after T4 and natural ageing for 7 days with different Cu contents: a) diagram b) table with mean and standard deviation.

4.1.3 Precipitation behaviour

The observation of the intensity distribution in Figure 4-6 after 1.5 hours at 170 °C from the measurements carried out in the SAXS using the PeakFit2D software shows that an addition of 1 wt-% Cu does not lead to any precipitation. Above a content of 2 wt-%, first phases seem to form next to the α-Al. An Al-3Cu alloy already shows a 90° angle between the two peaks. These indicate a cubic precipitate phase in the material and corresponds to the θ-phase in the specific case. Similarly, the alloy with 4 wt.% Cu shows peaks with almost 90°, which supports the same conclusion. At this point, it should be noted that the exact location of the lines through the peaks are not always clear and there may be a slight deviation in the angles. It can also be seen that the intensity of all samples after 1 hour at 170 °C is lower than that after 20 hours.

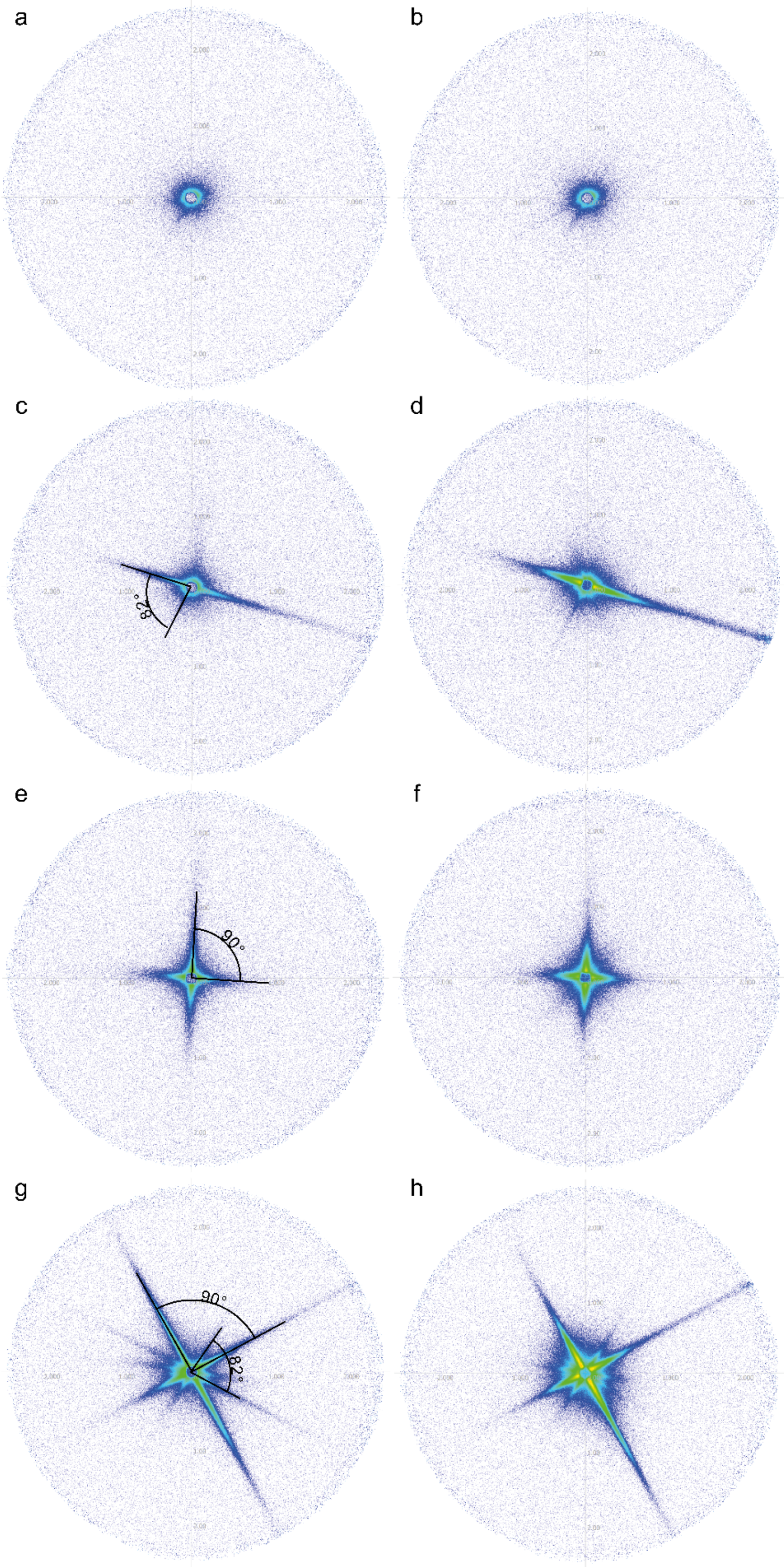

Figure 4-6: 2D scattering images obtained from the in-situ SAXS with different Cu contents and ageing time: a) Al-1Cu after 1 h. b) Al-1Cu after 20 h. c) Al-2Cu after 1 h. d) Al-2Cu after 20 h. e) Al-3Cu after 1 h. f) Al-3Cu after 20 h. g) Al-4Cu after 1 h. h) Al-4Cu after 20 h.

In the next step, the measured values were evaluated using the program MULIP SAXS-2D and the values for q and the corresponding intensity were inserted into Origin for a further detailed analysis. At first, only the influence of the Cu content on integrated intensity, number density and Porod radius is analysed. In **Figure 4-7**, the integrated intensity is plotted versus the duration of the in-situ observation. The Al-1Cu alloy, as also suggested by the previous figure (**Figure 4-6(a)**), shows no change over time. The alloys with 2 and 3 wt.% Cu show approximately the same trend. The Al-4Cu alloy, however, is clearly above the other three measurements. Al-4Cu is therefore chosen for further analysis with the addition of Mg and Ag respectively.

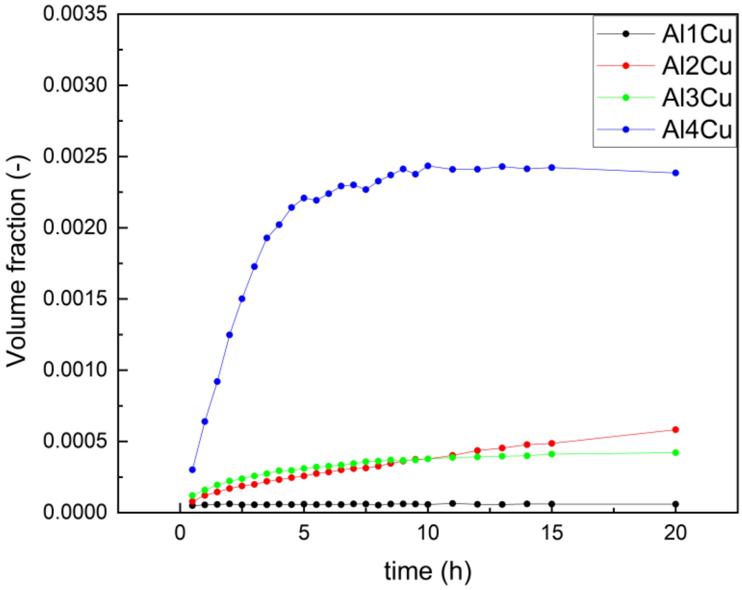

Figure 4-7: SAXS measurement, influence of Cu content on volume fraction.

When considering the number density N in **Figure 4-8**, those alloys with only 1 and 2 wt.% Cu show a small decrease in values over time. A somewhat larger amount of Cu, however, again leads to an increase in the number density. After an ageing for 5 hours, the values remain approximately constant for both alloys.

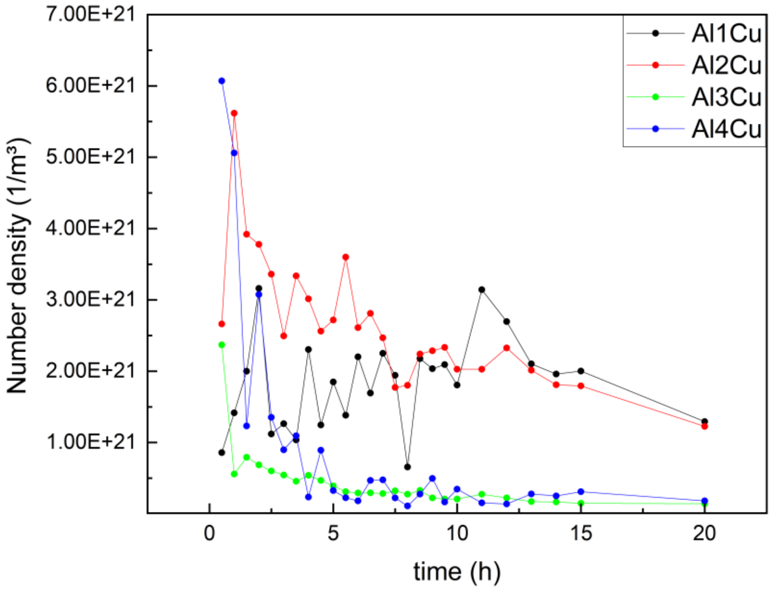

Figure 4-8: SAXS measurement, influence of Cu content on number density.

The Porod radius R_p represents the precipitates' radius calculated from the in-situ SAXS measurements. When considering the influence of the Cu content on the microstructure of the Al-Cu alloys, as shown in **Figure 4-9**, an increase in the Rp values with increasing Cu content can be seen. As outlined in **Figure 4-9**, adding 1 % Cu does not lead to the precipitation of any phases, and possibly the calculated value is related to the clusters. However, increasing the Cu content results in the growth and coarsening of the strengthening precipitates being clearly observed in the **Figure 4-9**. This is due to the fact that the higher Cu content leads to the higher diffusion rate and as a consequence, larger precipitates at the same time interval. The line begins to flatten out after about 5 hours. This is also the time in which the change of the volume fraction approaches zero.

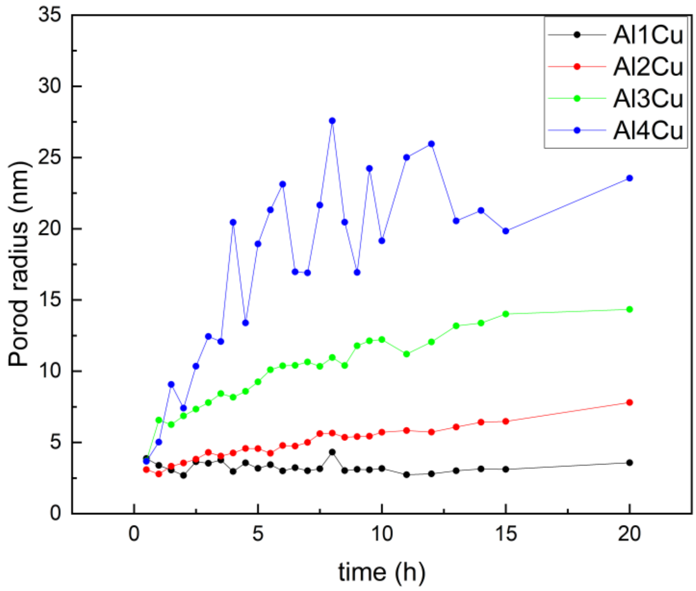

Figure 4-9: SAXS measurement, influence of Cu content on Porod radius.

In addition, the formation of the precipitates was observed by DSC. One sample of each alloy was analysed after solution treatment. The results are shown in **Figure 4-10**. The samples Al-1Cu and Al-2Cu show only minor peaks at 200 °C and 350 °C. The alloy with 3 wt.% Cu, on the other hand, shows a clear peak at 110 °C, which is due to the formation of clusters. With a content of 4 wt.% Cu, the peak of the clusters also appears at 100 °C and in addition a clear peak appears at 180 °C and 225 °C, whereby the former is due to the occurrence of the GP zones and the immediately following one is due to the formation of the θ-phase.

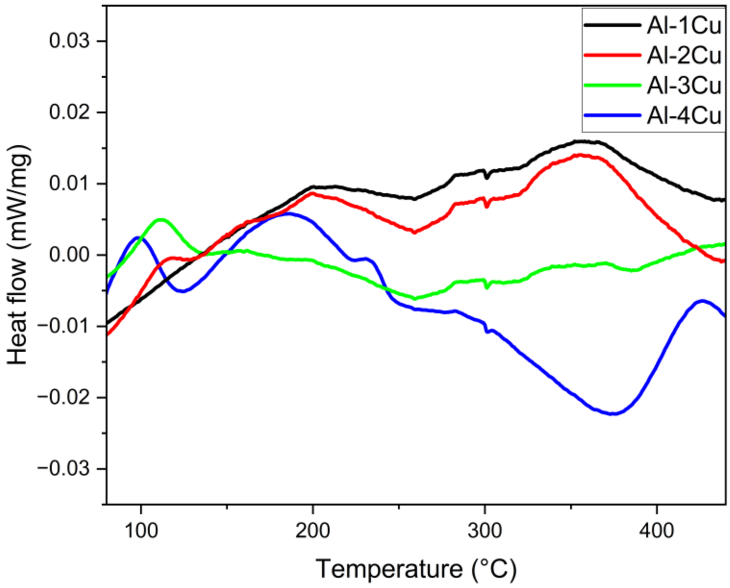

Figure 4-10: DSC curves after solution treatment with different Cu contents.

4.2 Influence of Mg addition

The addition of 0.3 wt.% Mg to an Al-4Cu alloy leads to the formation of a finer microstructure, as shown in **Figure 4-11** after Barker etching. Both larger grains comparable to the Al-4Cu sample (a) and significantly smaller grains can be found in the area under observation.

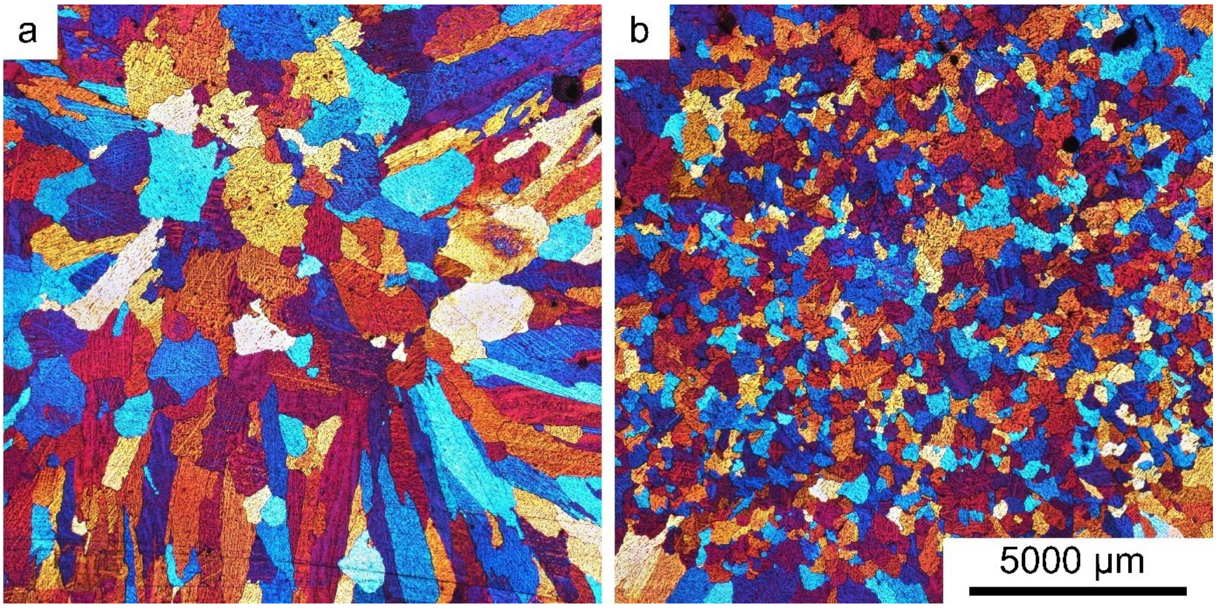

Figure 4-11: Comparison of the microstructure after casting: a) Al-4Cu b) Al-4Cu-0.3Mg.

4.2.1 Grain size

The evaluation of the mean grain sizes shows that an addition of 0.3 wt.% Mg leads to a significant decrease in the mean grain sizes according to **Figure 4-12**.

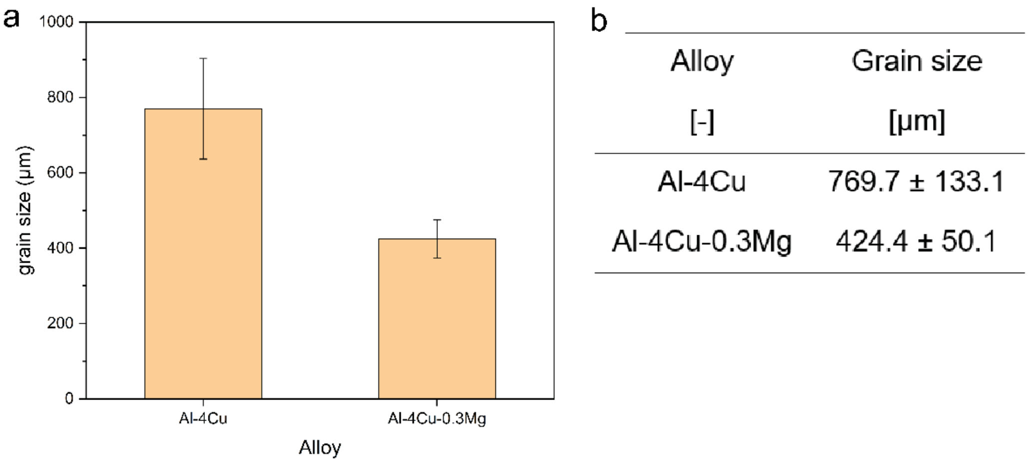

Alloy [-]	Grain size [µm]
Al-4Cu	769.7 ± 133.1
Al-4Cu-0.3Mg	424.4 ± 50.1

Figure 4-12: Grain size distribution after adding 0.3 wt.% Mg to Al-4Cu: a) diagram b) table with mean and standard deviation.

A subsequent solution heat treatment also leads to an increase in the grain size of the Al-4Cu-0.3Mg sample. However, the determined value is still significantly below that of the sample without Mg, as shown in **Figure 4-13**.

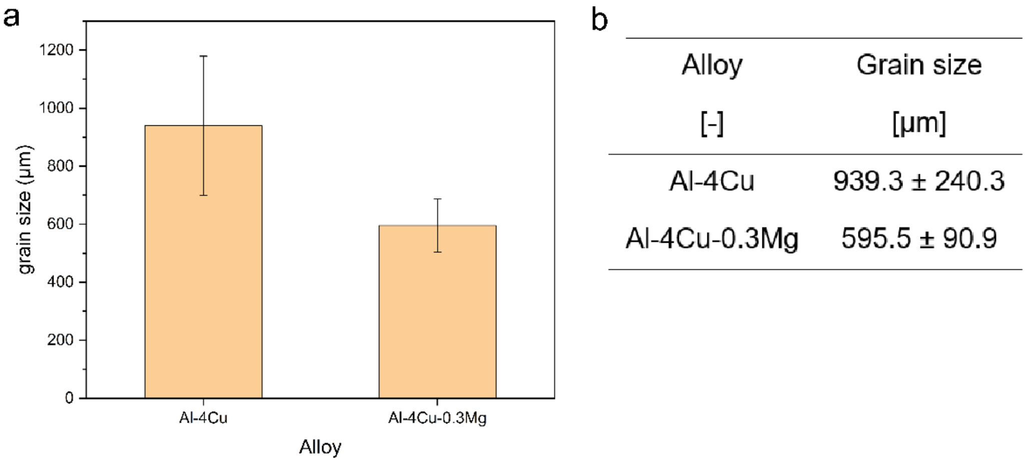

Alloy [-]	Grain size [µm]
Al-4Cu	939.3 ± 240.3
Al-4Cu-0.3Mg	595.5 ± 90.9

Figure 4-13: Grain size distribution of Al-4Cu and Al-4Cu-0.3 Mg after T4: a) diagram b) table with mean and standard deviation.

4.2.2 Hardness

The Al-4Cu-0.3Mg alloy was subjected to a hardness measurement after solution treatment, quenching in water and natural ageing for seven days. Subsequently, a comparison is made with the Al-4Cu alloy. The addition of 0.3 wt.% Mg leads to an increased hardness, as shown in **Figure 4-14**.

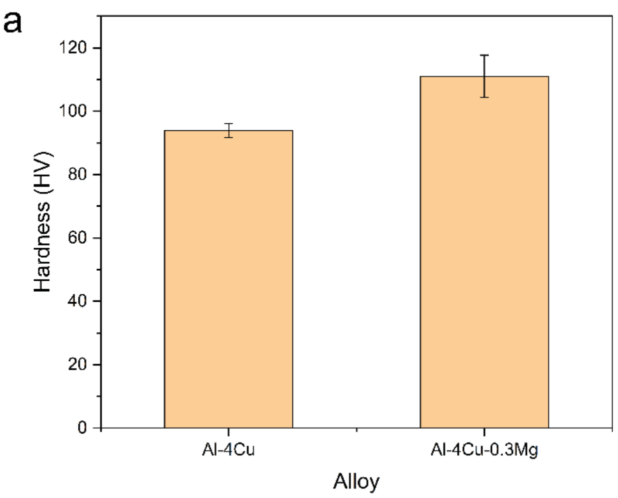

b

Alloy [-]	Hardness [HV]
Al-4Cu	93.9 ± 2.3
Al-4Cu-0.3Mg	111.0 ± 6.7

Figure 4-14: Vickers hardness after T4 (solution treatment) and natural ageing for 7 days of the Al-4Cu-0.3Mg alloy compared with the Al-4Cu alloy: a) diagram b) table with mean and standard deviation.

4.2.3 Precipitation behaviour

In **Figure 4-15** the 2D scattering images of the Al-4Cu-0.3Mg sample is shown. There is almost no difference between the scattering images recorded after 1 h and 20 h.

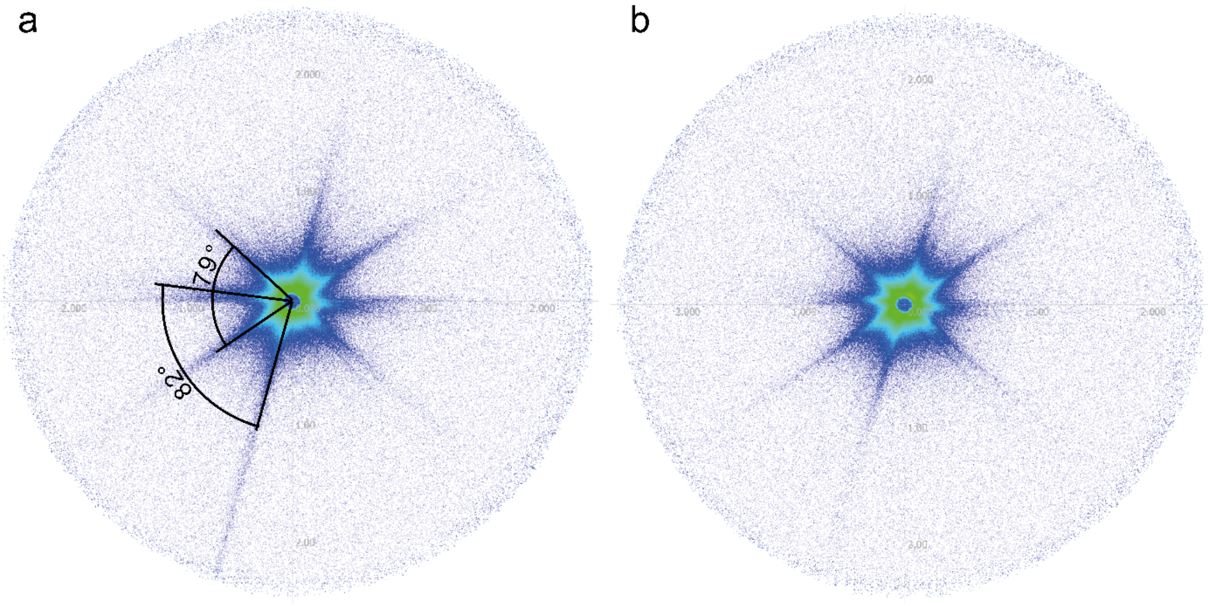

Figure 4-15: 2D scattering images obtained from the in-situ SAXS of Al-4Cu-0.3Mg: a) after 1 h. b) after 20 h.

First, **Figure 4-16** shows the integrated intensity of the alloys. Here, an addition of 0.3 wt.% Mg provides a rapid decrease in the determined volume fraction. There is only a slight increase at the beginning of the measurement, afterwards the determined values remain constant. The addition of Mg appears to inhibit the formation of precipitates in the material

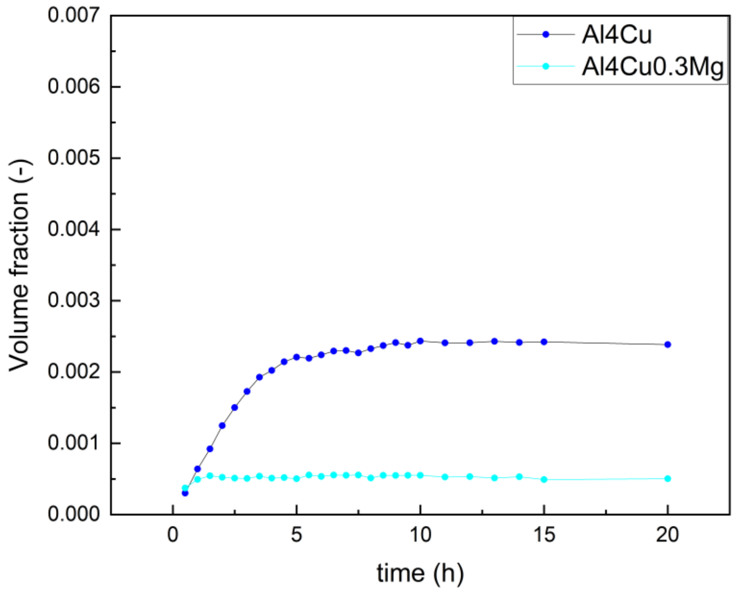

Figure 4-16: SAXS measurement, influence of Mg addition on volume fraction.

When looking at the number density of the alloys in **Figure 4-17** the alloy with 0.3 wt.% Mg also decreases over time, but a short increase in number density can be seen after 2 hours of ageing at 170 °C. Subsequently, the values of the Al-4Cu-0.3Mg sample are slightly above the Mg-free sample.

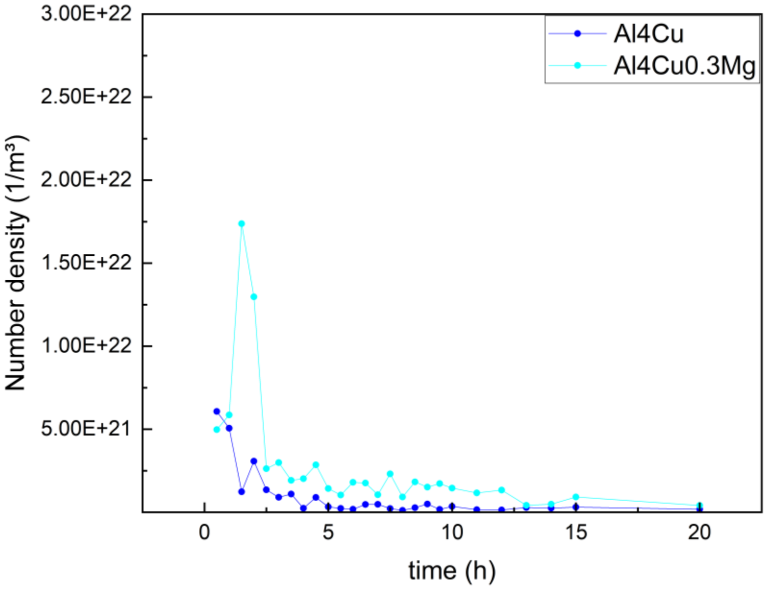

Figure 4-17: SAXS measurement, influence of Mg addition on number density.

The presence of Mg leads to a significant decrease in the size of the precipitates when looking at the Porod radius in **Figure 4-18**. The values for the size of the precipitates increases for both samples, but the Al-4Cu sample shows a significantly sharper curve in the first 5 hours.

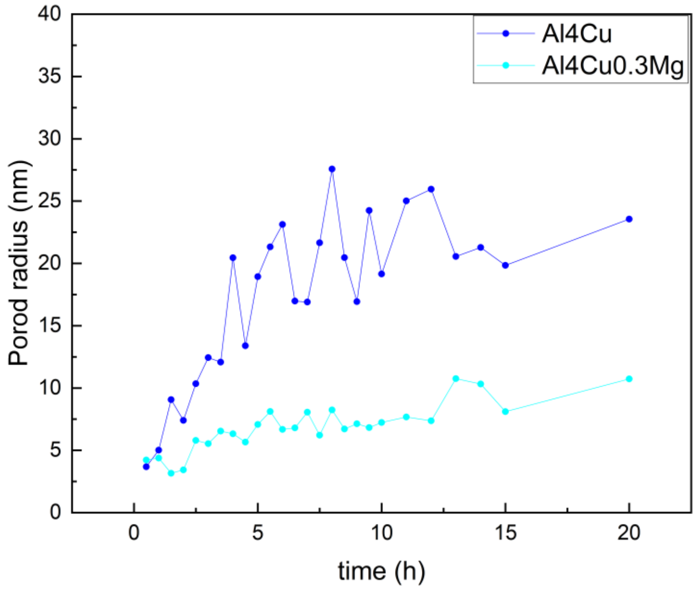

Figure 4-18: SAXS measurement, influence of Mg addition on Porod Radius.

A DSC curve was also recorded for the alloy Al-4Cu-0.3Mg after solution treatment at 540 °C for 6h and quenching. The results of the measurement at a heating rate of 10 °C / min are shown in **Figure 4-19**. The peak of the Cu-Mg cluster is found at 90 °C and at 220 °C the peak of the θ-phase is found. Both phenomena occur at lower temperatures compared to the Al-4Cu alloy.

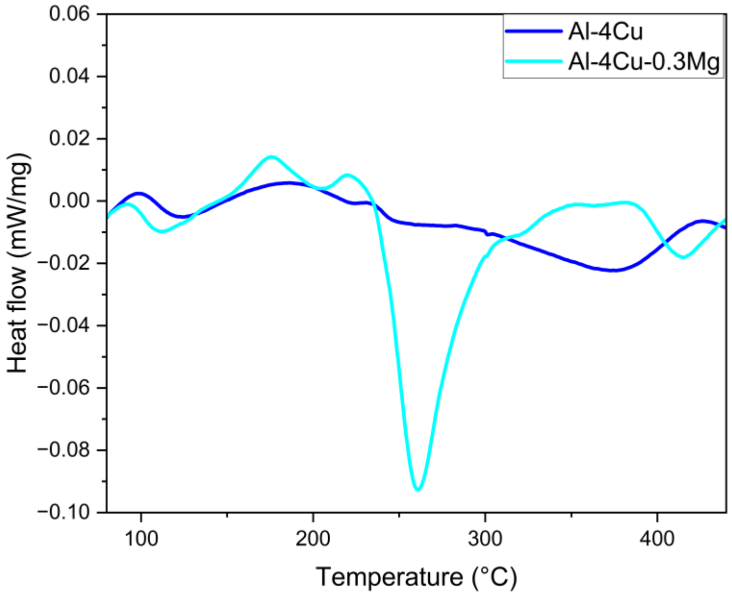

Figure 4-19: DSC curve of Al-4Cu-0.3 Mg compared with the curve of Al-4Cu after solution treatment.

4.3 Influence of Ag addition

As shown in **Figure 4-20**, the addition of 0.7 wt.% Ag to an Al-4Cu alloy does not lead to any significant change in the microstructure under the optical microscope.

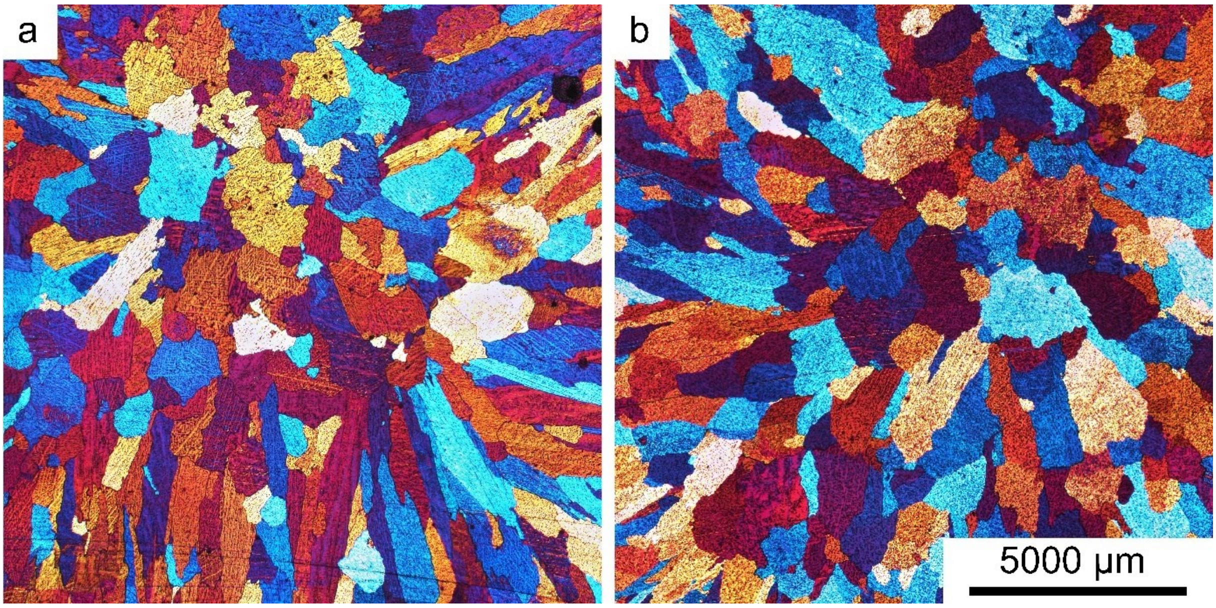

Figure 4-20: Comparison of the microstructure after casting: a) Al-4Cu b) Al-4Cu-0.7Ag.

4.3.1 Grain size

The observation of the determined grain sizes in **Figure 4-21** also shows that an addition of 0.7 wt.% Ag has no significant influence on the grain size after casting.

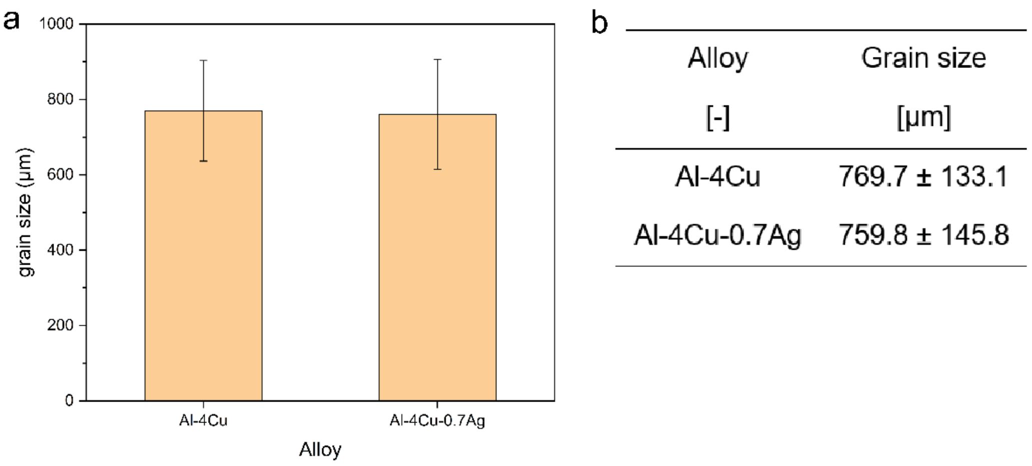

Alloy [-]	Grain size [µm]
Al-4Cu	769.7 ± 133.1
Al-4Cu-0.7Ag	759.8 ± 145.8

Figure 4-21: Grain size distribution after adding 0.7 wt.% Ag to Al-4Cu: a) diagram b) table with mean and standard deviation.

In contrast, the average grain size after T4 solution treatment is below the value of the Al-4Cu sample. There is a slight decrease in grain size for the Al-4Cu-0.7Ag sample, which can be attributed to the growth restriction caused by the addition of Ag.

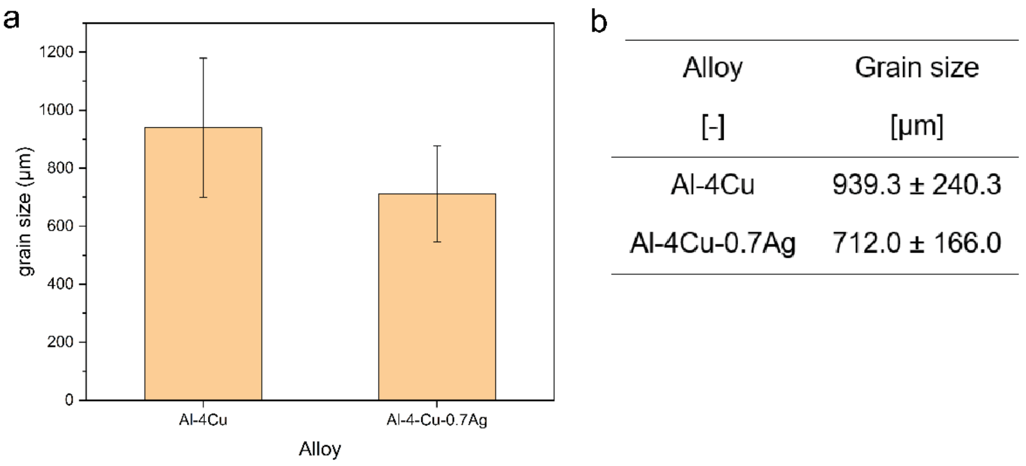

Alloy [-]	Grain size [µm]
Al-4Cu	939.3 ± 240.3
Al-4Cu-0.7Ag	712.0 ± 166.0

Figure 4-22: Grain size distribution of Al-4Cu and Al-4Cu-0.7 Ag after T4: a) diagram b) table with mean and standard deviation.

4.3.2 Hardness

The determined Vickers hardness of the Al-4Cu-0.7Ag alloy compared to the measured value of the Al-4Cu alloy is shown in **Figure 4-23**. The addition of 0.7 wt.% Ag increases the hardness. The value of this alloy is close to that of the Al-4Cu-0.3Mg alloy.

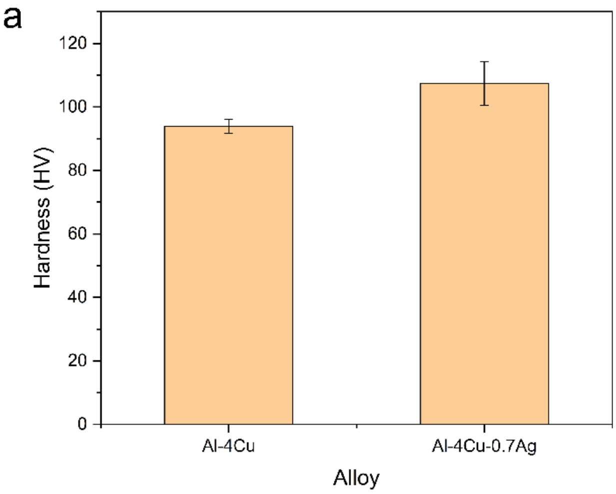

b

Alloy [-]	Hardness [HV]
Al-4Cu	93.9 ± 2.3
Al-4Cu-0.7Ag	107.4 ± 6.9

Figure 4-23: Vickers hardness after T4 and natural ageing for 7 days of the Al-4Cu-0.7Ag alloy compared with the Al-4Cu alloy: a) diagram b) table with mean and standard deviation.

4.3.3 Precipitation behaviour

When observing the precipitation behaviour with the aid of in-situ SAXS, **Figure 4-24** shows that there is an increase in intensity between 1h and 20 h at 170 °C. Furthermore, only one peak can be observed in both cases.

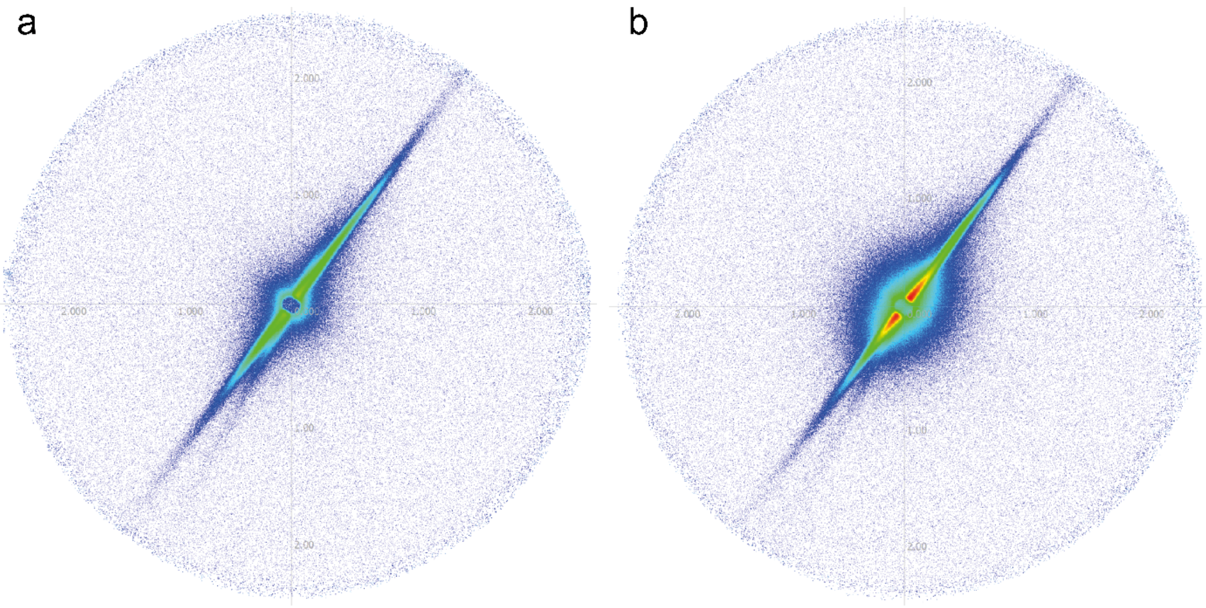

Figure 4-24: 2D scattering images obtained from the in-situ SAXS of Al-4Cu-0.7Ag: a) after 1 h. b) after 20 h.

Figure 4-25 shows the volume fraction of the Al-4Cu and Al-4Cu-0.7Ag samples. A clearly more significant increase of the curve of the Ag-containing alloy can be seen. In addition, the curve begins to flatten after 5 h at a value that is about twice as high as the curve of the Al-4Cu alloy.

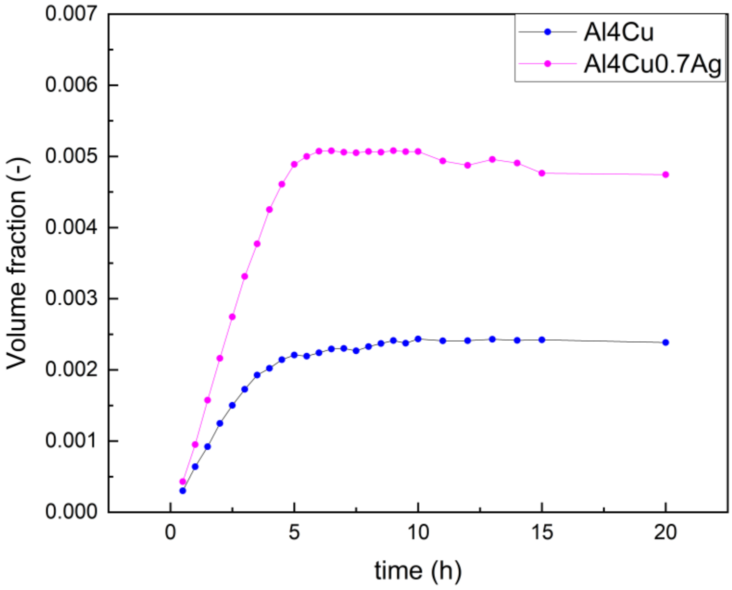

Figure 4-25: SAXS measurement, influence of Ag addition on volume fraction.

The number density curves in **Figure 4-26** show that the Al-4Cu-0.7Ag alloy has a higher value at the first time point of the measurement after 0.5 h and then drops rapidly. After 2.5 h, the curves of the two alloys are almost the same, whereby the Ag-containing alloy has slightly higher values.

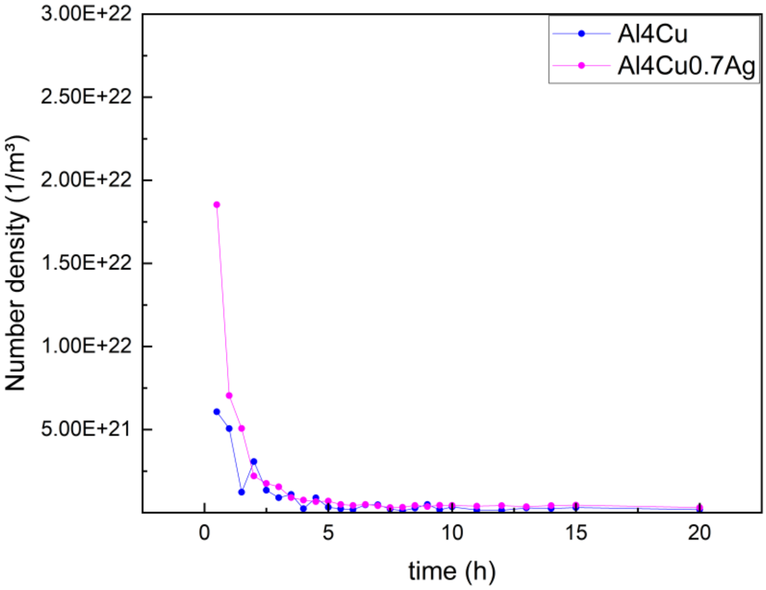

Figure 4-26: SAXS measurement, influence of Ag addition on number density.

Finally, the Porod radius is examined in **Figure 4-27**. The curves of the two samples are close to each other, but that of the Al-4Cu-0.7Ag sample is somewhat higher. The curve rises significantly up to a time of 7 h and then flattens out.

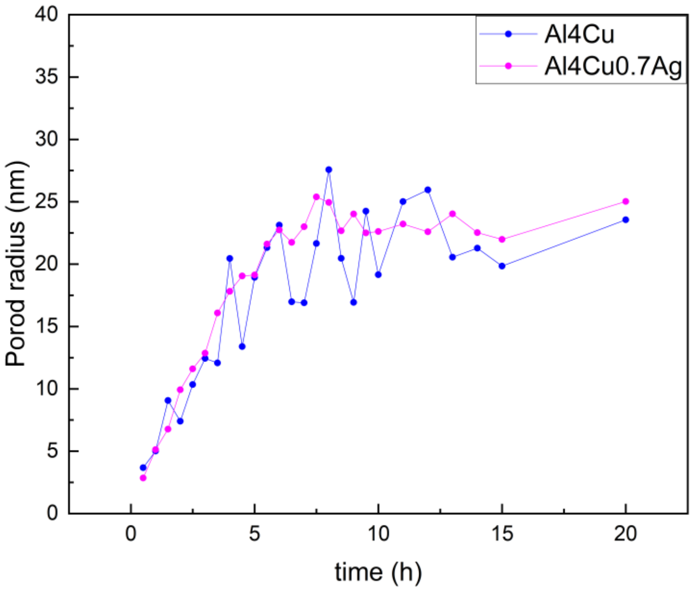

Figure 4-27: SAXS measurement, influence of Ag addition on Porod Radius.

The results of the DSC measurement of the Al-4Cu-0.7Ag sample are shown in **Figure 4-28**. The comparison with the Al-4Cu sample shows that the peaks of the two alloys hardly differ from each other. Only the first peak of the θ-phase at around 230 °C is not visible in the Ag-containing alloy.

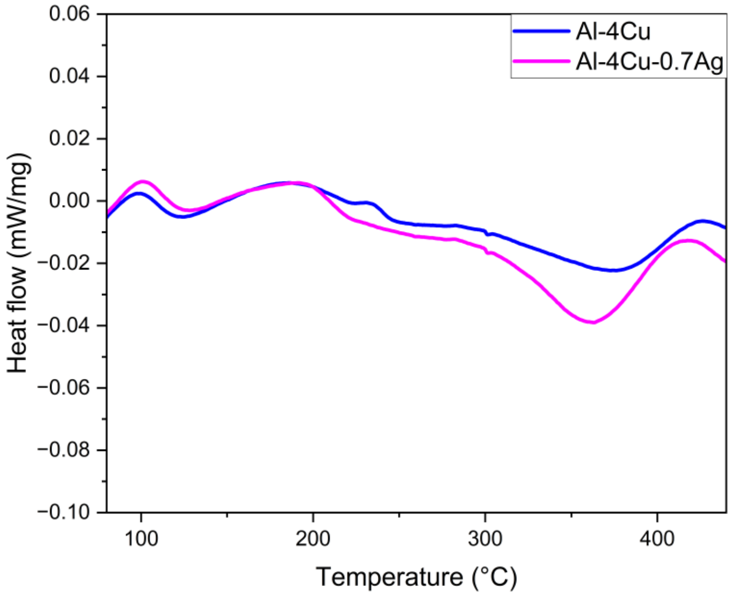

Figure 4-28: DSC curve of Al-4Cu-0.7Ag compared with the curve of Al-4Cu after solution treatment.

4.4 Influence of a combined addition of Mg and Ag

The Al-4Cu-0.3Mg-0.7Ag sample was additionally grain refined, which is the reason why a direct comparison with the previous alloys is not possible. In addition, the microstructure is analysed with the help of SEM after a T4 solution treatment.

4.4.1 EBSD analysis

Looking at the inverse pole figure (IPF) image in **Figure 4-29**, it can be seen that a uniform microstructure is obtained after the T4 heat treatment.

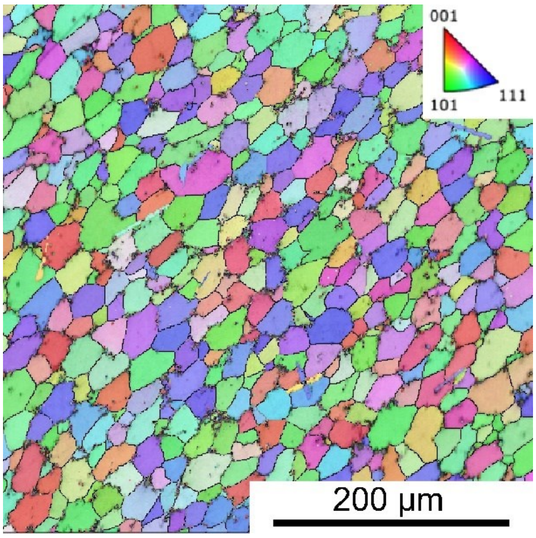

Figure 4-29: IPF image of the Al-4Cu-0.3Mg-0.7Ag alloy.

The texture analysis (pole figure) obtained from the sample is shown in **Figure 4-30**, where it can be seen that the grains are preferentially oriented in the <111> direction.

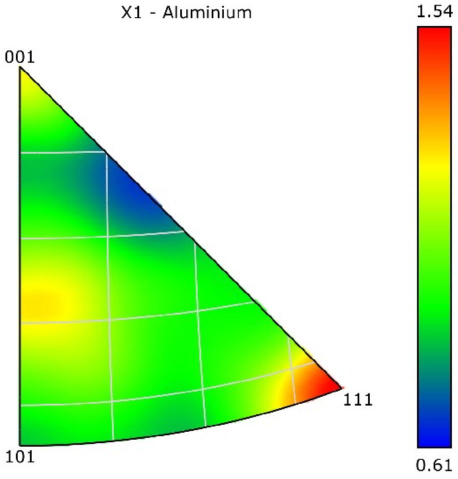

Figure 4-30: Texture analysis (PF) of the Al-4Cu-0.3Mg-0.7Ag alloy.

4.4.2 Grain size

The mean grain size of the Al-4Cu-0.3Mg-0.7Ag sample is 17.2 ± 8.1 µm. The distribution of the grain sizes is shown in Figure 4-31. It is noticeable that the grain size is uniformly distributed between 4 and 28 µm.

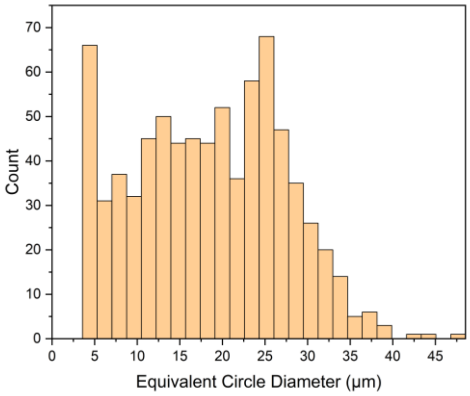

Figure 4-31: Grain size distribution of Al-4Cu-0.3Mg-0.7Ag.

4.4.3 Stress distribution

The kernel average misorientation (KAM) in **Figure 4-32** shows that there is hardly any internal stress in the microstructure after a T4 solution treatment. Slightly higher values are found at the grain boundaries of the sample.

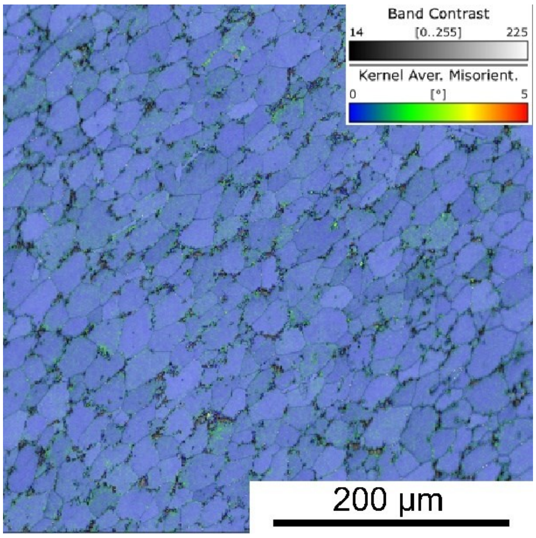

Figure 4-32: KAM of the Al-4Cu-0.3Mg-0.7Ag alloy.

4.4.4 Hardness

The resulting hardness from the combined addition of 0.3 wt.% Mg and 0.7 wt.% Ag to an Al-4Cu alloy is shown in **Figure 4-33**. The alloys were solution treated, quenched in cold water and natural aged for 7 days before the measurement. Compared to the Al-4Cu as well as to the alloys with the separate addition of Mg and Ag, a significant increased hardness can be observed.

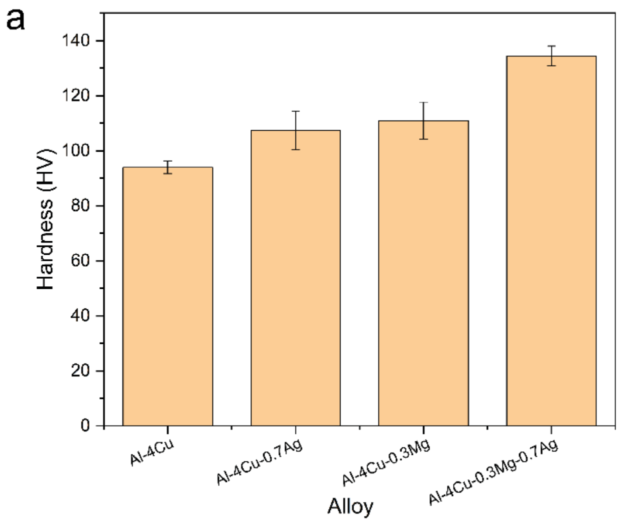

b

Alloy [-]	Hardness [HV]
Al-4Cu	93.9 ± 2.3
Al-4Cu-0.3Mg	111.0 ± 6.7
Al-4Cu-0.7Ag	107.4 ± 6.9
Al-4Cu-0.3Mg-0.7Ag	134.5 ± 3.6

Figure 4-33: Vickers hardness after T4 and natural ageing for 7 days of the Al-4Cu-0.3Mg-0.7Ag alloy compared with the Al-4Cu, Al-4Cu-0.3Mg and Al-4Cu-0.7Ag alloys: a) diagram b) table with mean and standard deviation.

4.4.5 Precipitation behaviour

The observation of the alloy using the in-situ SAXS leads to the 2D scattering images in **Figure 4-34**. Here, no clear peaks are recognisable any more. In addition, the intensity increases after 20 h in comparison to that after 1 h. The duration of the measurement was also therefore increased to 40 hours for this sample.

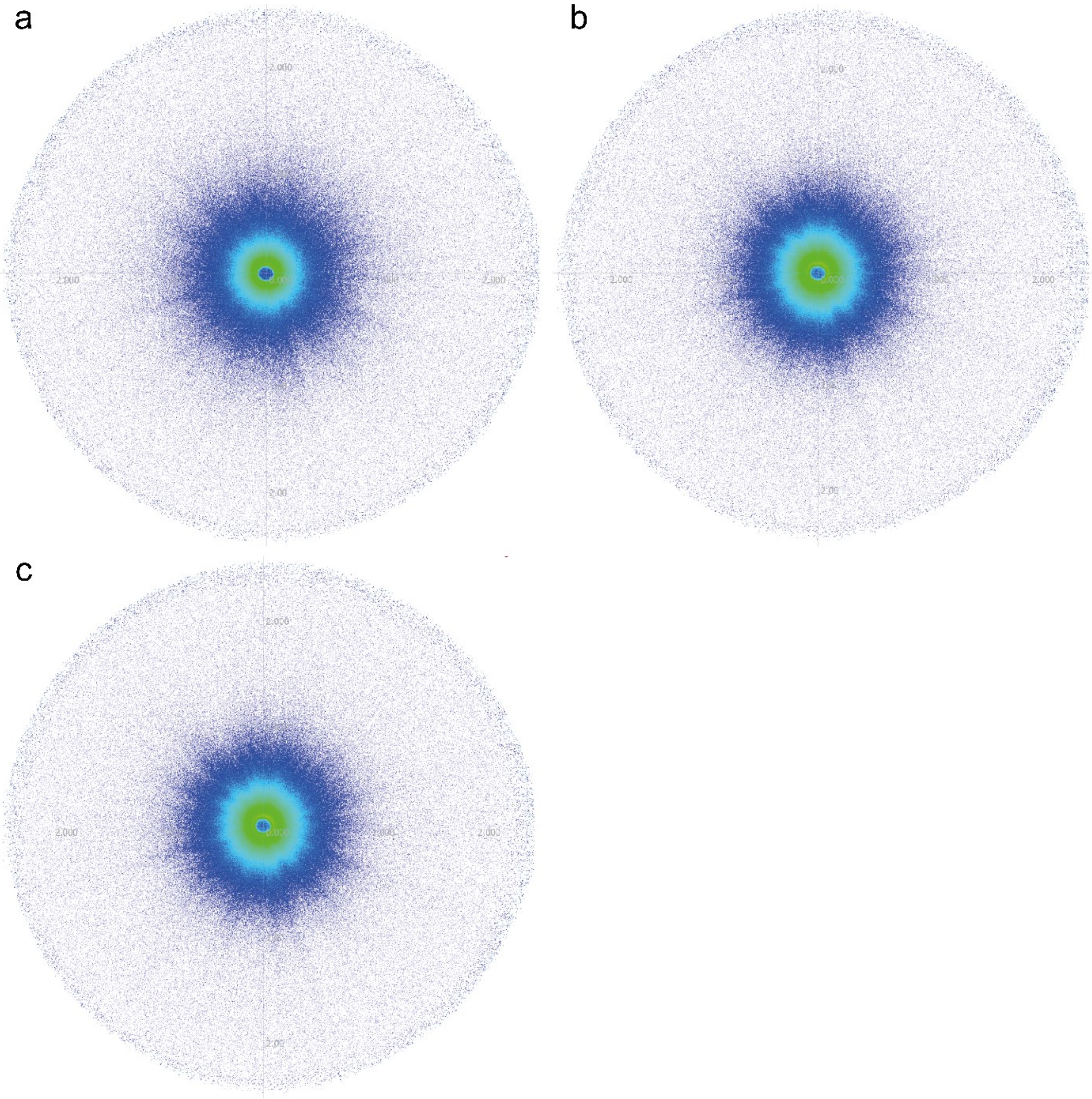

Figure 4-34: 2D scattering images obtained from the in-situ SAXS of the Al-4Cu-0.3Mg-0.7Ag: a) 1 h. b) 20 h. c) 40 h.

Figure 4-35 shows the volume fraction of the Al-4Cu-0.3Mg-0.7Ag alloy compared with the Al-4Cu, Al-4Cu-0.3Mg and Al-4Cu-0.7Ag alloys. A combined addition of both Mg and Ag elements causes a rapid increase in intensity at the beginning up to about 2.5 hours, after which the line runs below that of the base alloy. A possible interpretation is the formation of a thermodynamically more favourable phase at the beginning stage.

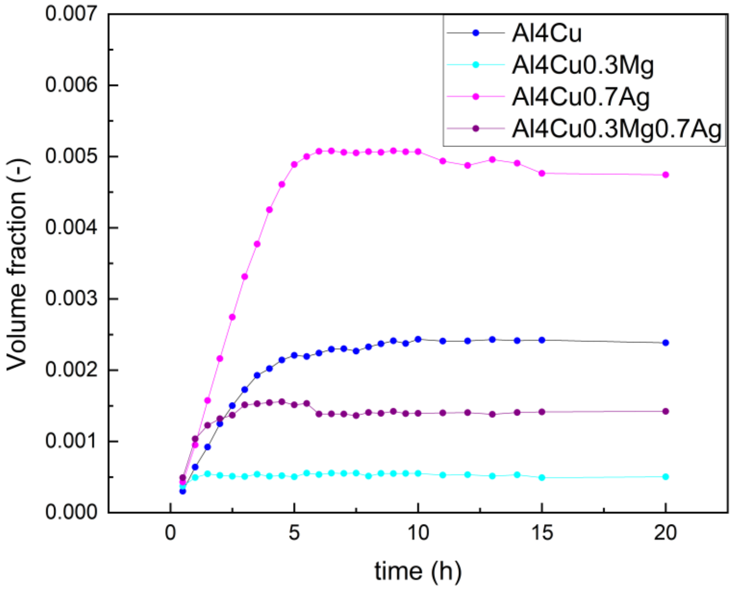

Figure 4-35: SAXS measurement, influence of a combined Mg and Ag addition on volume fraction.

When looking at the number density of the alloys in **Figure 4-36**, a small peak of the Al-4Cu-0.3Mg-0.7Ag alloy is visible at the beginning, which is roughly 0.5 h before the peak of the Al-4Cu-0.3Mg alloy. The graph of the alloy is above the other three alloys during the entire period under investigation and begins to flatten out after 3 hours.

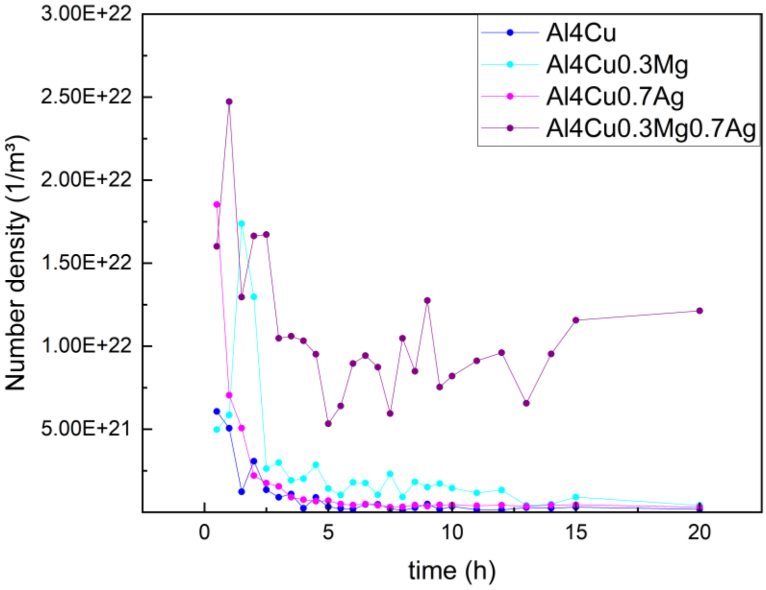

Figure 4-36: SAXS measurement, influence of a combined Mg and Ag addition on number density.

Finally, the Porod radius of the Al-4Cu-0.3Mg-0.7Ag alloy is compared with the previous alloys. The paths of the Al-4Cu-0.3Mg and Al-4Cu-0.3Mg-0.7Ag are similar in the first 5 hours of ageing. Subsequently, the values of the latter are less than those of the Ag-free alloy, indicating a very beneficial effect of Mg and Ag on the size of precipitates. The maximum size of the particles was reached after 15 h, whereas the precipitates of the Al-4Cu-0.3Mg alloy continue to coarsening, indicating a very beneficial effect of Ag on the thermal stability of precipitates.

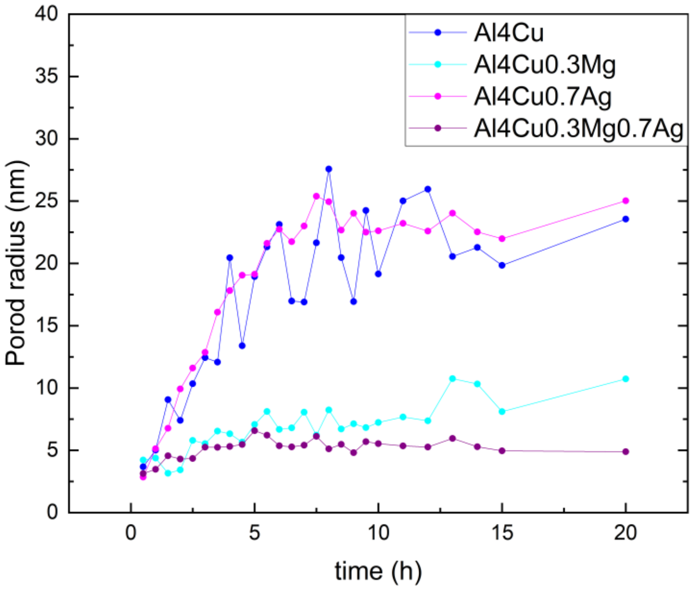

Figure 4-37: SAXS measurement, influence of a combined Mg and Ag addition on Porod radius.

In addition, the measurement was extended to 40 h as mentioned at the beginning. As shown in **Figure 4-38**, the volume fraction, number density and Porod radius still have the same values as that after 20 h, even after a longer ageing time at 170 °C. This means that the precipitates that form do not show any significant coarsening even after 40 hours and are thermally stable.

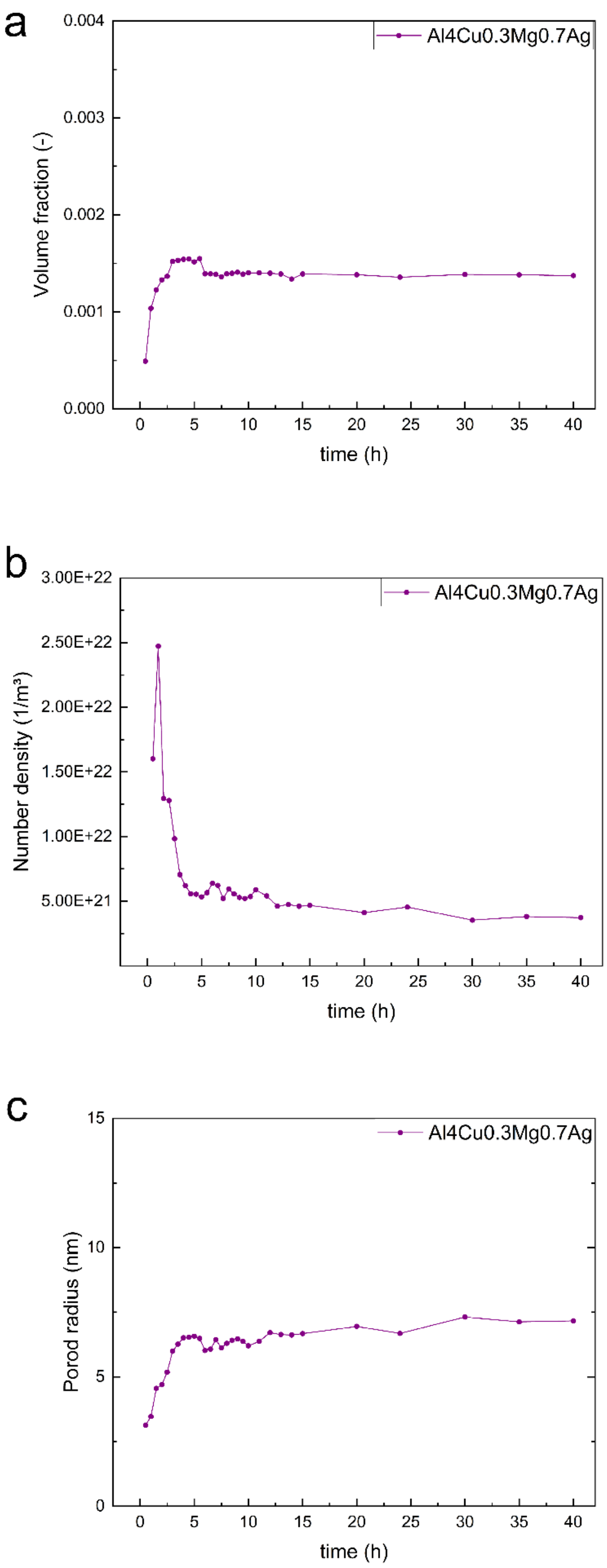

Figure 4-38: SAXS measurement of the Al-4Cu-0.3Mg-0.7Ag: a) Volume fraction b) Number density c) Porod radius.

The DSC measurement of the alloy yields the curve shown in **Figure 4-39**, with the peak at about 300 °C belonging to the θ-phase and at about 270 °C to the Ω-phase. An exothermic peak is found at about 200 °C, which is the same as the previous investigations.

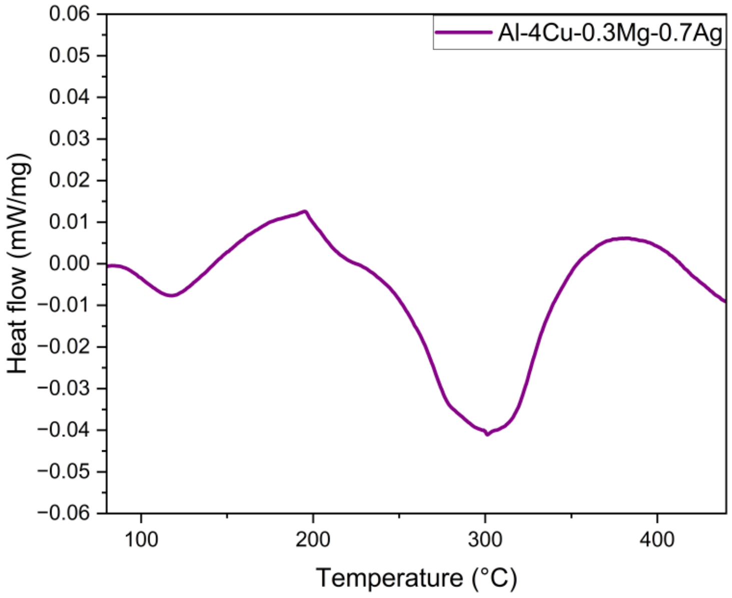

Figure 4-39: DSC curve of Al-4Cu-0.3Mg-0.7Ag after solution treatment.

4.5 Influence of rapid solidification on Al-4Cu-0.3Mg-0.7Ag

In addition, ribbons of the material are prepared in the melt spinning machine at the Chair of Casting Research. This makes it possible to compare the microstructure with different solidification rates. The casting in the melt spinning machine results in a good strip, which could also be prepared appropriately.

4.5.1 EBSD analysis

The next step is the observation of the IPF using SEM. This is shown in **Figure 4-40**. A significant grain refinement and orientation of the grains is visible.

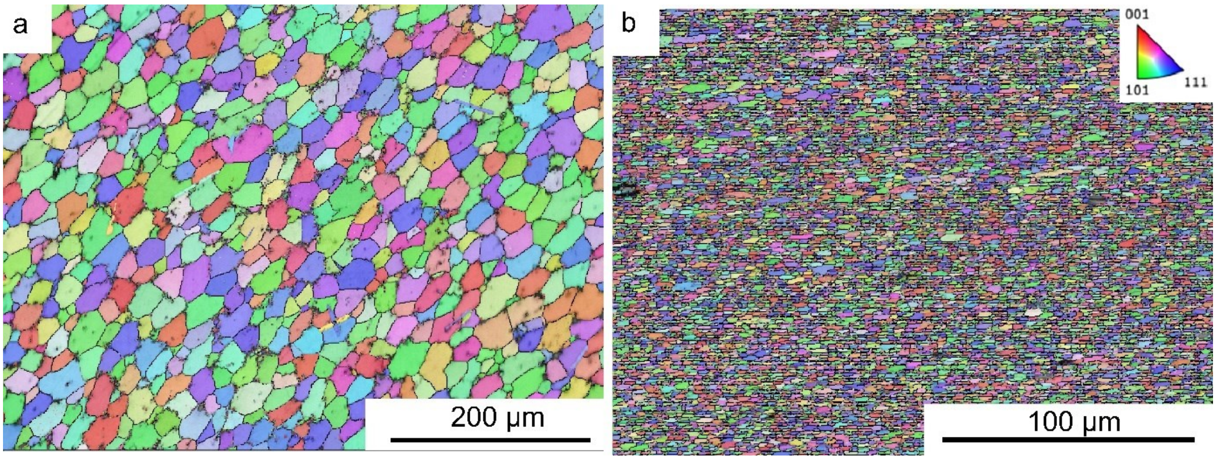

Figure 4-40: IPF images of as cast and melt spun samples; a) Al-4Cu-0.3Mg-0.7Ag with TiB2 casted b) Al-4Cu-0.3Mg-0.7 Ag with TiB2 melt spun.

Examination of the corresponding texture in **Figure 4-41** shows that the orientation of the grains in the alloy after casting is in the <111> direction. In contrast, the orientation of the grains in the Al-4Cu-0.3Mg-0.7Ag alloy after melt spinning shifts almost entirely in the <001> direction, which corresponds to the different solidification conditions produced by the rotating wheel.

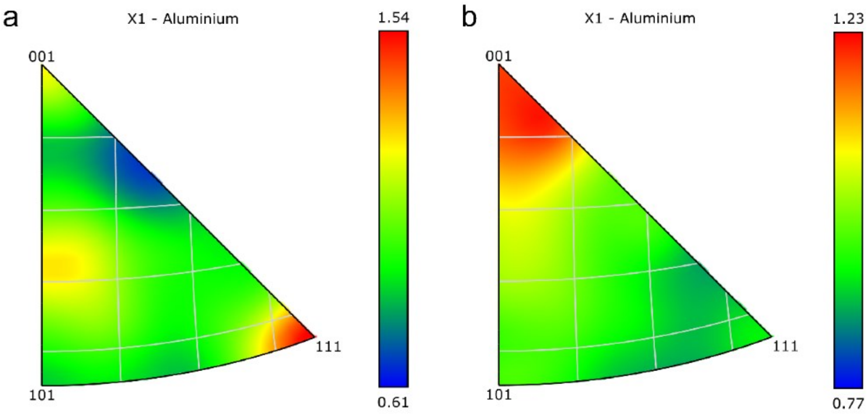

Figure 4-41: : Texture analysis (PF) of as cast and melt spun samples; a) Al-4Cu-0.3Mg-0.7Ag with TiB2 casted b) Al-4Cu-0.3Mg-0.7 Ag with TiB2 melt spun.

4.5.2 Grain size distribution

The evaluation of the grain size with the help of the SEM leads to an average size of 2.4 ± 0.6 µm. The distribution of the grain size is shown in **Figure 4-42**.

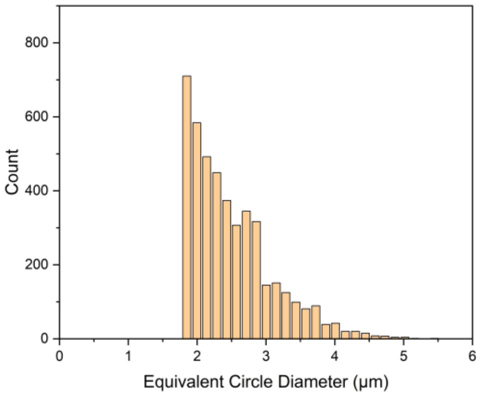

Figure 4-42: Grain size distribution of the Al-4Cu-0.3Mg-0.7Ag after melt spinning.

4.5.3 Stress distribution

Figure 4-43 show the KAM maps. The largest stresses are located at the grain boundaries. The reason for this can be seen in the uniform orientation of the grains in the Al-4Cu-0.3Mg-0.7Ag alloy. A reduced deviation of orientation reduces the stress differences between grains and leads to lower intergranular stresses. This property is favourable for the deformation of the material and provides continuous and uniform deformation when force is applied, which can lead to a reduction in the stresses generated.

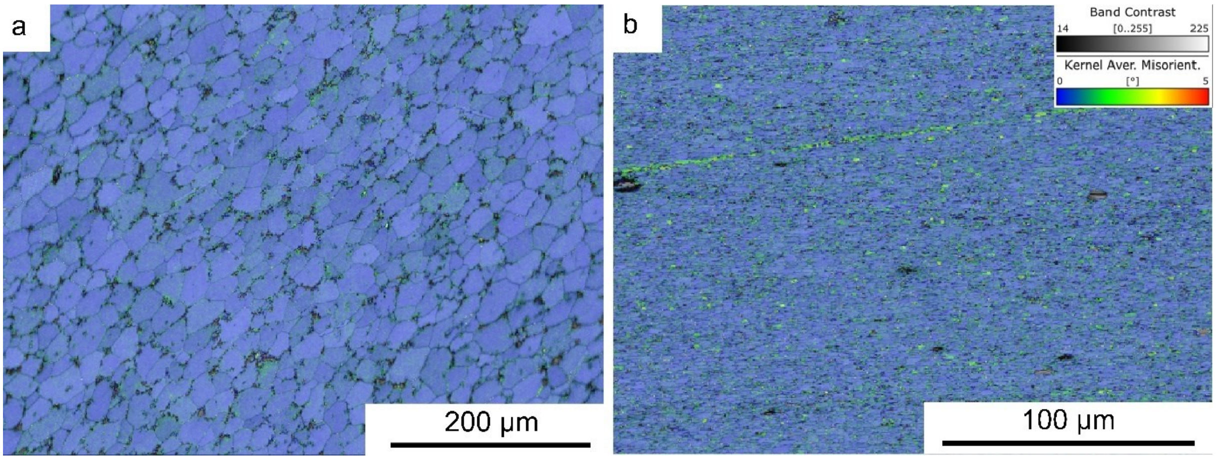

Figure 4-43: KAM of as cast and melt spun samples; a) Al-4Cu-0.3Mg-0.7Ag with TiB2 casted b) Al-4Cu-0.3Mg-0.7 Ag with TiB2 melt spun.

4.6 Influence of hot rolling

In the second part of this work, the influence of hot rolling on the microstructure and the precipitates formed after a temperature application of 170 °C and a T4 heat treatment is considered. The investigation methods are analogous to those in the previous chapter.

In the first step, the rolled samples are observed SEM. At this point, no further heat treatment has taken place. **Figure 4-44** shows the microstructure obtained after hot rolling at 250 °C of an Al-4Cu-0.3Mg-0.7Ag sheet. The visible precipitates are all in the same size range, with the shape changing from largely elongated phases to uniformly shaped particles with decreasing thickness. There is also a slight tendency towards finer precipitates with increasing deformation.

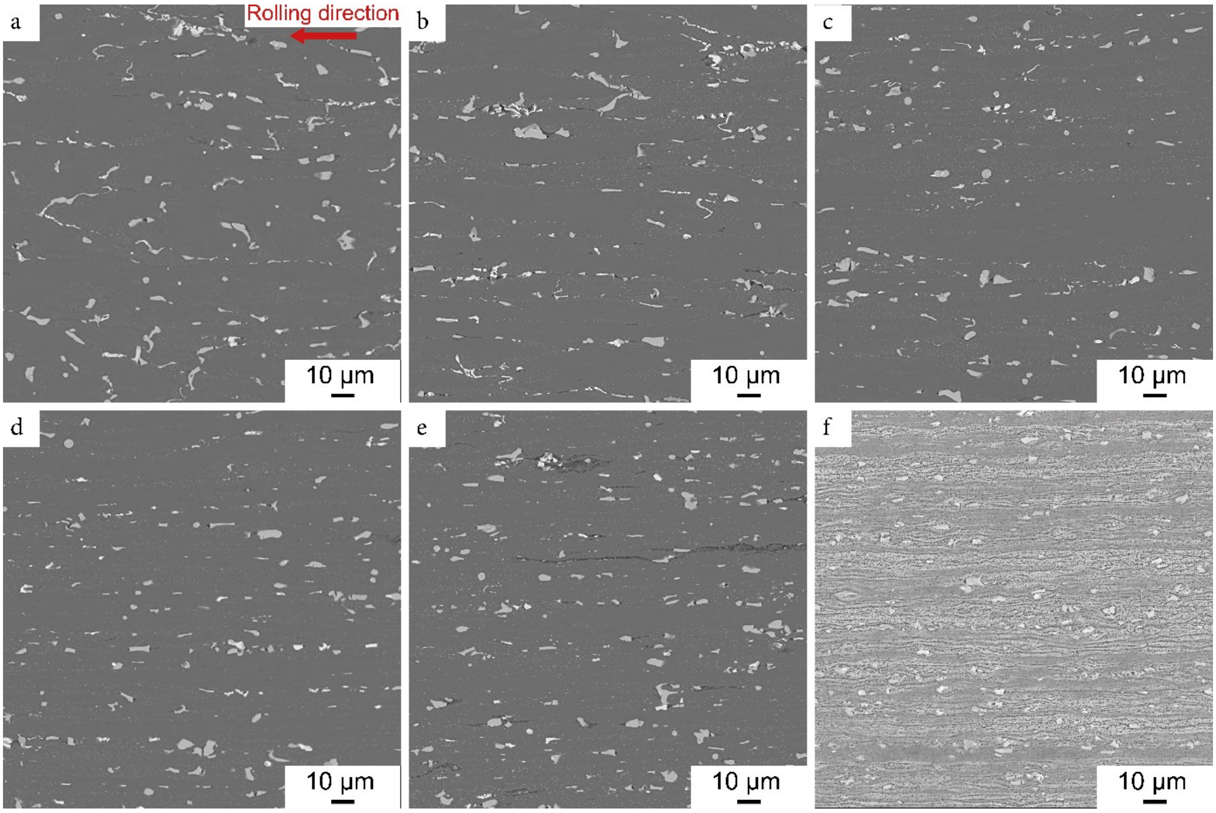

Figure 4-44: SEM image of rolled samples: a) 6.74 mm b) 4.25 mm c) 3.14 mm d) 2.05 mm e) 1.2 mm f) 0.3 mm.

4.6.1 EBSD analysis

The observation of the rolled samples with the help of IPF makes it possible to gain information about the crystal orientation and the texture. Here, individual crystals have the same colour. The crystals already show a slight directional orientation after the first rolling pass, but still have comparatively coarse and uniform grain sizes. Local large elongated grains and also very fine microstructures can be found next to each other. Up to a thickness of 3.14 mm many different orientations are found, after the last thickness reduction to 0.3 mm a fine structure with a relatively uniform orientation is present.

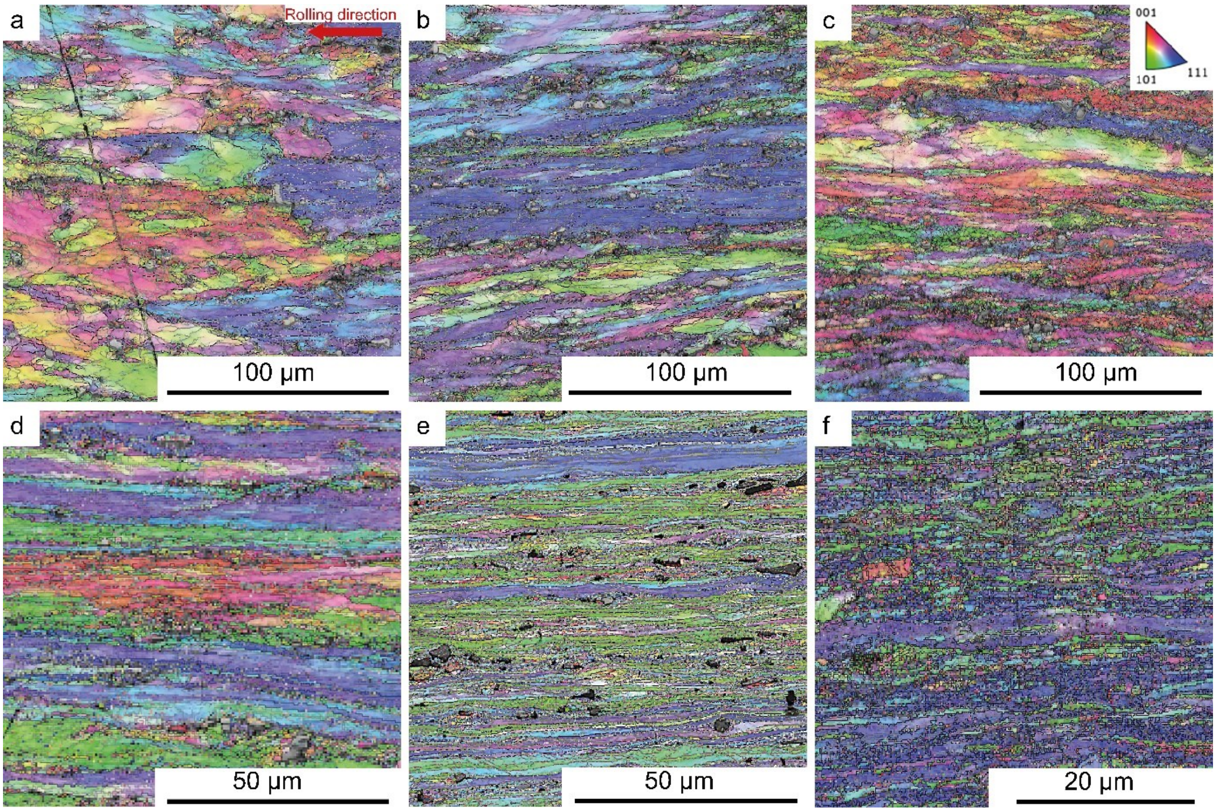

Figure 4-45: IPF image of rolled samples: a) 6.74 mm b) 4.25 mm c) 3.14 mm d) 2.05 mm e) 1.2 mm f) 0.3 mm.

The precise analysis of the texture of the samples, as shown in **Figure 4-46**, also supports the assumptions that were already visually apparent. The orientation of the grains of the samples with a thickness of 0.3 mm, 1.2 mm, and 2.05 mm is mainly in the <111> direction. The 3.14 mm and 4.25 mm specimens also prefer this direction, which also represent the orientation of the grains in the as-cast state. Only the specimen after the first rolling pass has a deviating orientation of the grains in <101> direction, which represents the rolling direction. It is possible that recrystallization due to a high rolling temperature (250 °C) has occurred as a result of the increasing rolling pass. Only in the first reduction step was this energy input too low and the microstructure still clearly showed a rolling structure.

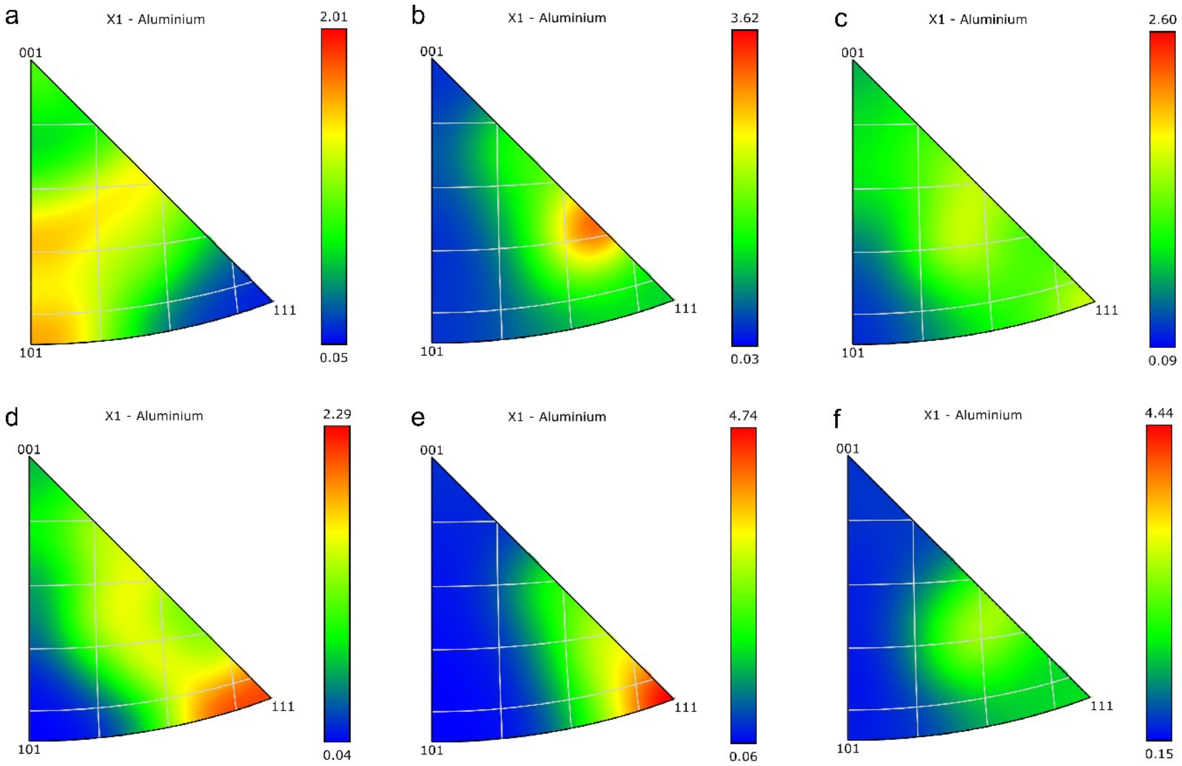

Figure 4-46: Texture analysis (PF) of hot rolled samples: a) 6.74 mm b) 4.25 mm c) 3.14 mm d) 2.05 mm e) 1.2 mm f) 0.3 mm.

4.6.2 Grain size distribution

The graphical evaluation of the determined grain sizes of the Al phases with the aid of the EBSD in SEM is shown in **Figure 4-47**. Several ranges were considered for each of the samples. It can be seen that the samples with a thickness of 6.74 mm, 4.25 mm and 2.05 mm show a greater variation in the determined grain sizes.

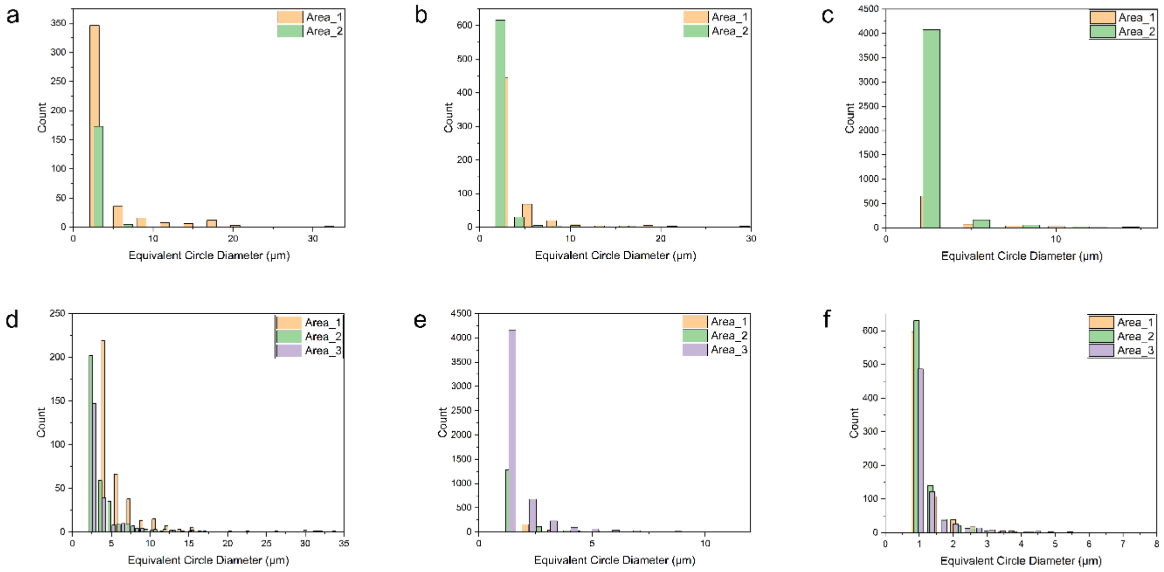

Figure 4-47: Grain size distribution of the samples after rolling: a) 6.74 mm b) 4.25 mm c) 3.14 mm d) 2.05 mm e) 1.2 mm f) 0.3 mm.

The results of the measurement are also clearly displayed in **Table 4-1**. It is noticeable that the sample with a thickness of 2.05 mm deviates strongly from the others, which still needs to be double checked.

Table 4-1: Average grain size of the Al phase after rolling.

Sample thickness [mm]	Grain size [µm]
6.74	4.22 ± 8.04
4.25	2.99 ± 4.93
3.14	1.86 ± 2.54
2.05	4.59 ± 3.56
1.2	1.50 ± 1.52
0.3	1.13 ± 0.73

In addition, the size of the Al_2Cu phases was determined with the help of the SEM. The results are listed in **Table 4-2**. This phase was not found in the sample with a thickness of 0.3 mm in the areas considered. A correlation between the sizes of the Al phases and the Al_2Cu phases can be seen.

Table 4-2: Average grain size of the Al_2Cu phase after rolling.

Sample thickness [mm]	Grain size [µm]
6.74	2.20 ± 0.6
4.25	2.20 ± 0.8
3.14	1.30 ± 0.9
2.05	2.03 ± 0.9
1.2	1.10 ± 0.4

4.6.3 Stress distribution

By observing the KAM maps, it is possible to visualize internal stresses in the microstructure. The areas with higher stresses are the places where new phases are preferentially formed during solution treatment (540 °C for 6 hours) or ageing (170 °C for 12 hours) in order to relieve the stresses in the microstructure. **Figure 4-48** shows the KAM of the rolled samples. It can be seen that there are stresses almost throughout the microstructure of the samples. Only in the specimen with a thickness of 4.25 mm are there large areas where any stresses are hardly found.

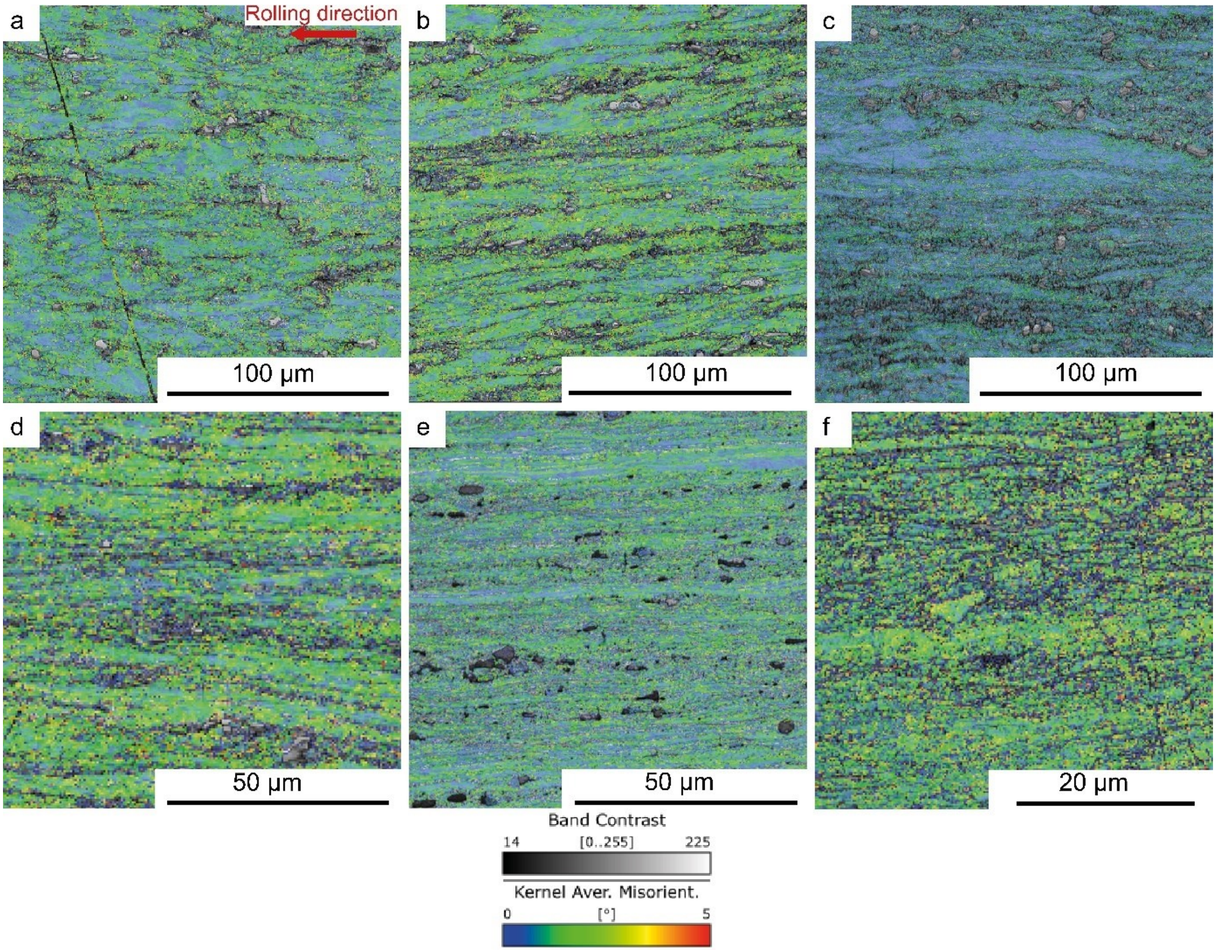

Figure 4-48: KAM of rolled samples: a) 6.74 mm b) 4.25 mm c) 3.14 mm d) 2.05 mm e) 1.2 mm f) 0.3 mm.

4.6.4 SEM EDS analysis

For the observation of the elements the EDS analysis is used in this work. This provides a quantitative analysis of the elements and their distribution in the considered area. However, this method does not yield quantitative values for the composition. **Figure 4-49** shows the EDS maps of the sample with a thickness of 6.74 mm, clearly indicating that the microstructure consists mainly of Al. However, the added elements (Ag and Mg) are also present in the matrix along with Mn, which is present in the alloy due to impurities from the remelted Al. Cu is found almost exclusively in the precipitates at this stage of hot rolling.

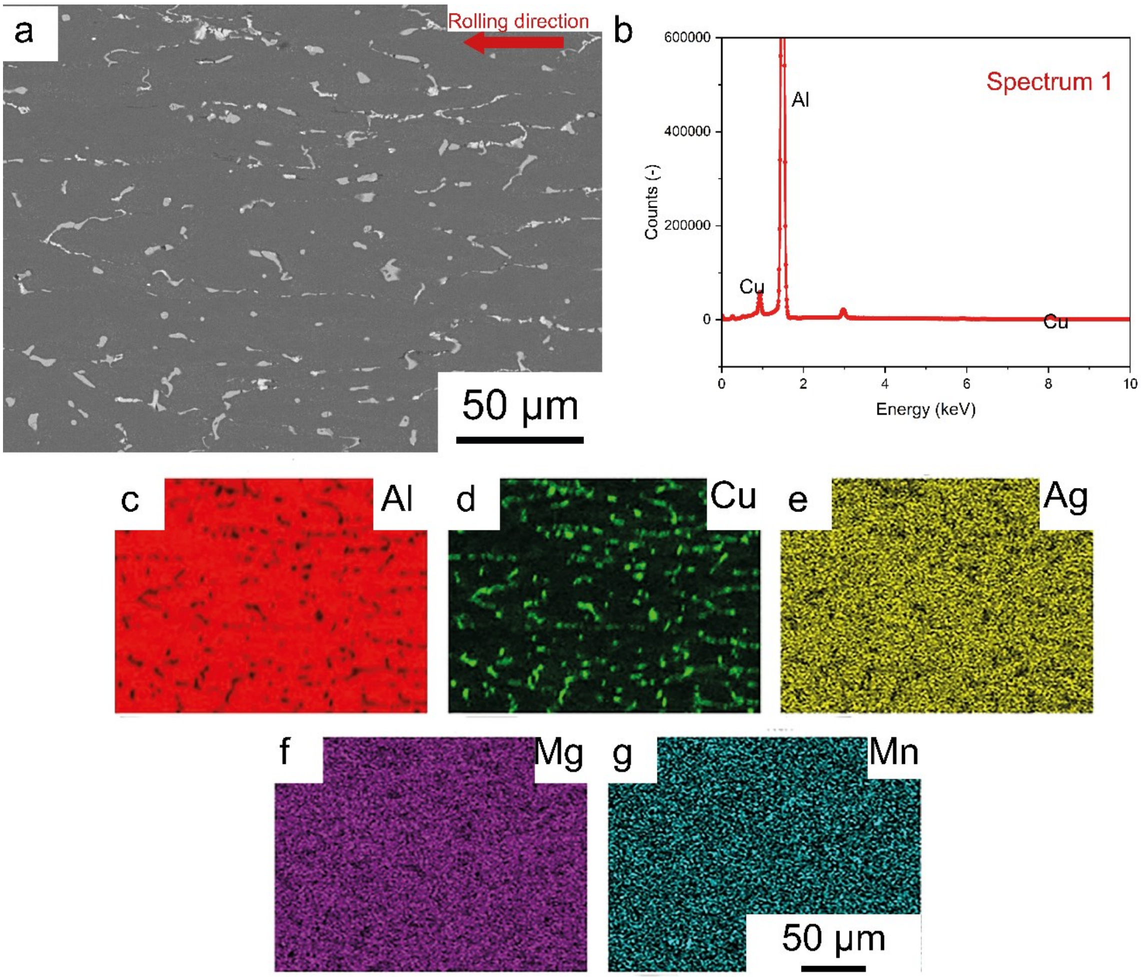

Figure 4-49: (a) SEM image, (b) EDS spectrum taken from the whole region, and (c-g) EDS maps of Al, Cu, Ag, Mg and Mn in the rolled sample with a thickness of 6.74 mm.

Figure 4-50 shows the distributions of the elements visible in the rolled sample with a thickness of 3.14 mm. Compared to the EDS analysis of the first rolling pass, there is hardly any change in the distribution of the elements in the microstructure.

The spectrum for the entire region yields the values of 94.4 % Al, 4.91 % Cu, 0.42 % Mn, 0.15 % Ti, and 0.1 % Fe. This analysis already indicates that it is not always possible to perform an accurate chemical analysis using SEM. Not even if the alloying elements Ag and Mg are specifically investigated.

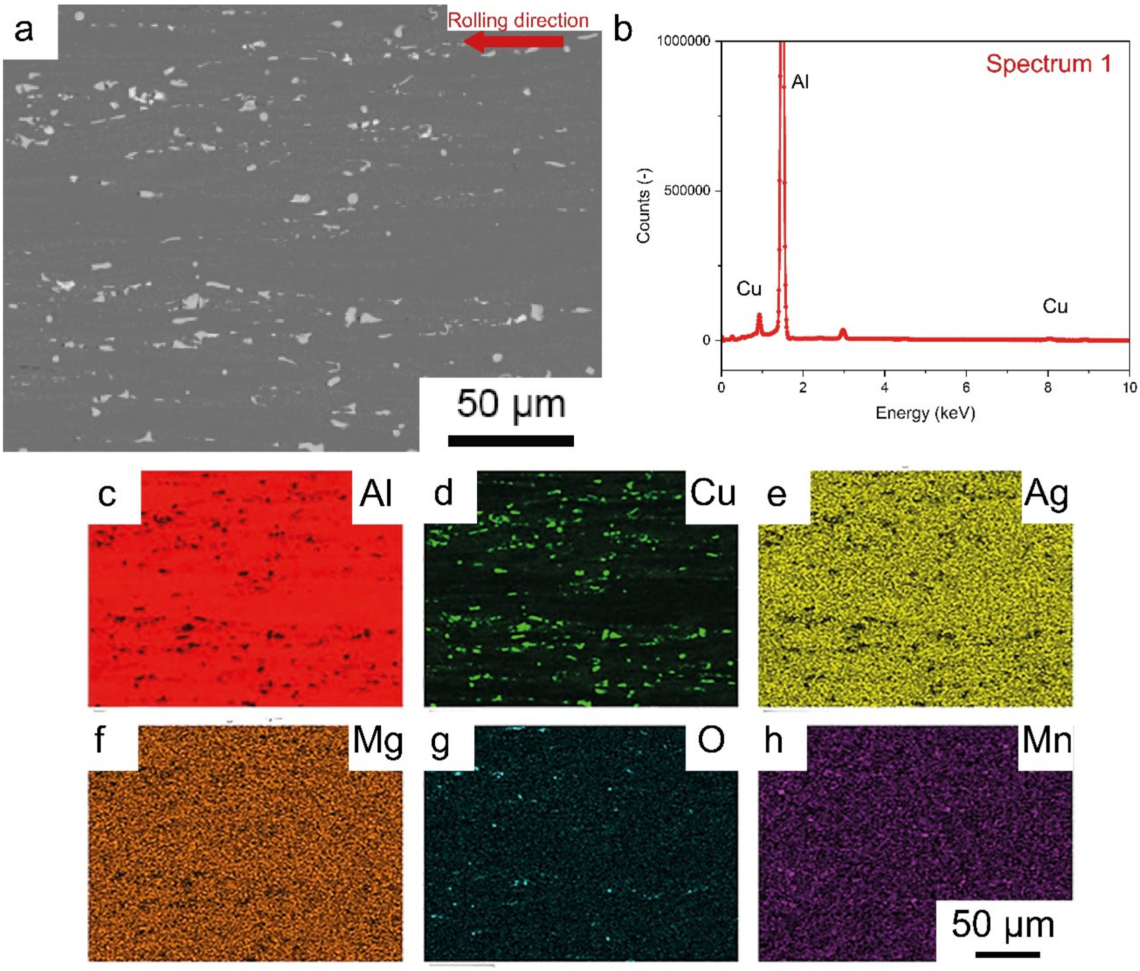

Figure 4-50: (a) SEM image, (b) EDS spectrum taken from the whole region, and (c-h) EDS maps of Al, Cu, Ag, Mg, O and Mn in the rolled sample with a thickness of 3.14 mm.

As the thickness of the sample decreases, the Cu distributes throughout the microstructure, as observed in the EDS analysis in **Figure 4-51**. A progression of the deformation and the increased temperature of 250 °C for a longer period of time causes a dissolution of the Cu-rich precipitates and a more uniform distribution of the atoms. It should be noted that the precipitations are not completely dissolved, but their size is smaller.

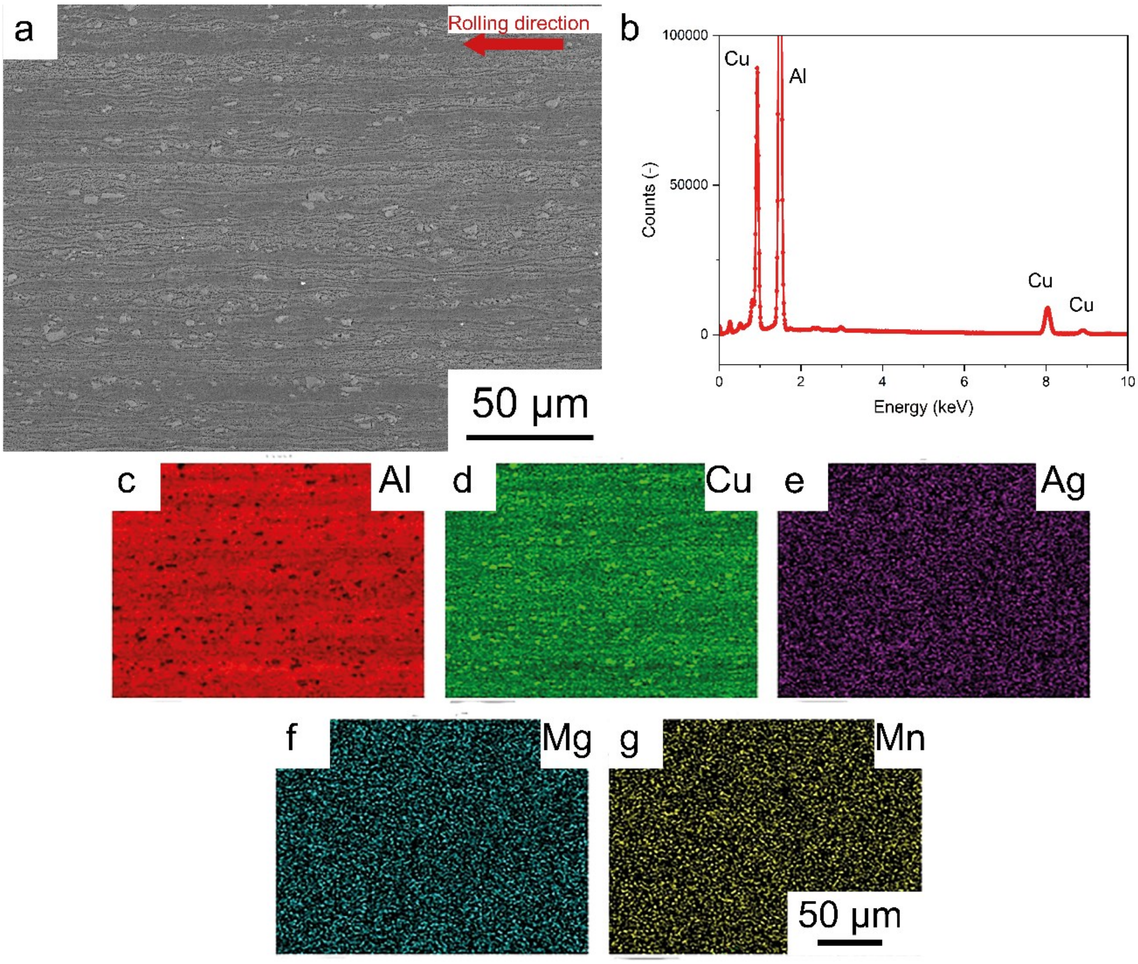

Figure 4-51: (a) SEM image, (b) EDS spectrum taken from the whole region, and (c-g) EDS maps of Al, Cu, Ag, Mg and Mn in the rolled sample with a thickness of 0.3 mm.

4.6.5 Hardness

Figure 4-52 shows the determined hardness of the rolled samples, with all values in the range of about 80 HV. The samples with a thickness of 0.3 mm and 1.2 mm show the highest values. However, the values are significantly lower than those of the samples after casting and T4 solution treatment. This indicates that the recrystallisation during rolling has a negative influence on the hardness.

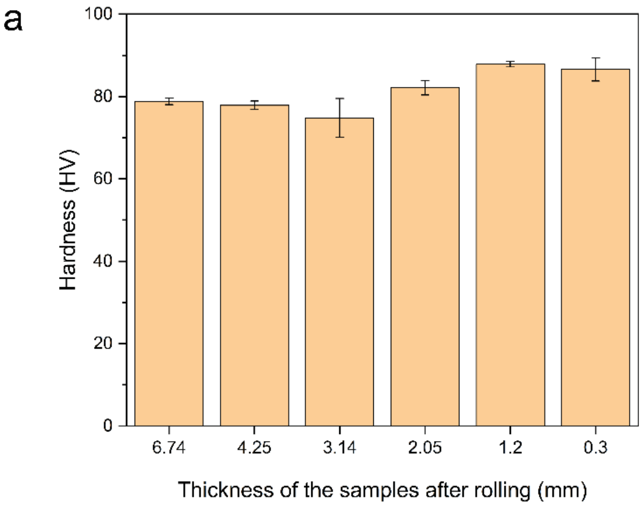

b

Thickness of the sample [mm]	Hardness [HV]
6.74	78.9 ± 0.8
4.25	77.9 ± 1.0
3.14	74.9 ± 4.7
2.05	82.2 ± 1.8
1.2	87.9 ± 0.7
0.3	86.6 ± 2.8

Figure 4-52: Vickers hardness of the samples after rolling.

4.7 Influence of hot rolling and ageing at 170 °C

Ageing these samples at 170 °C for 12 hours causes a growth of the existing phases as well as the formation of new precipitates. This is shown in **Figure 4-53**. Compared to the specimens, which were considered untreated after hot rolling, optically more precipitates are present after ageing.

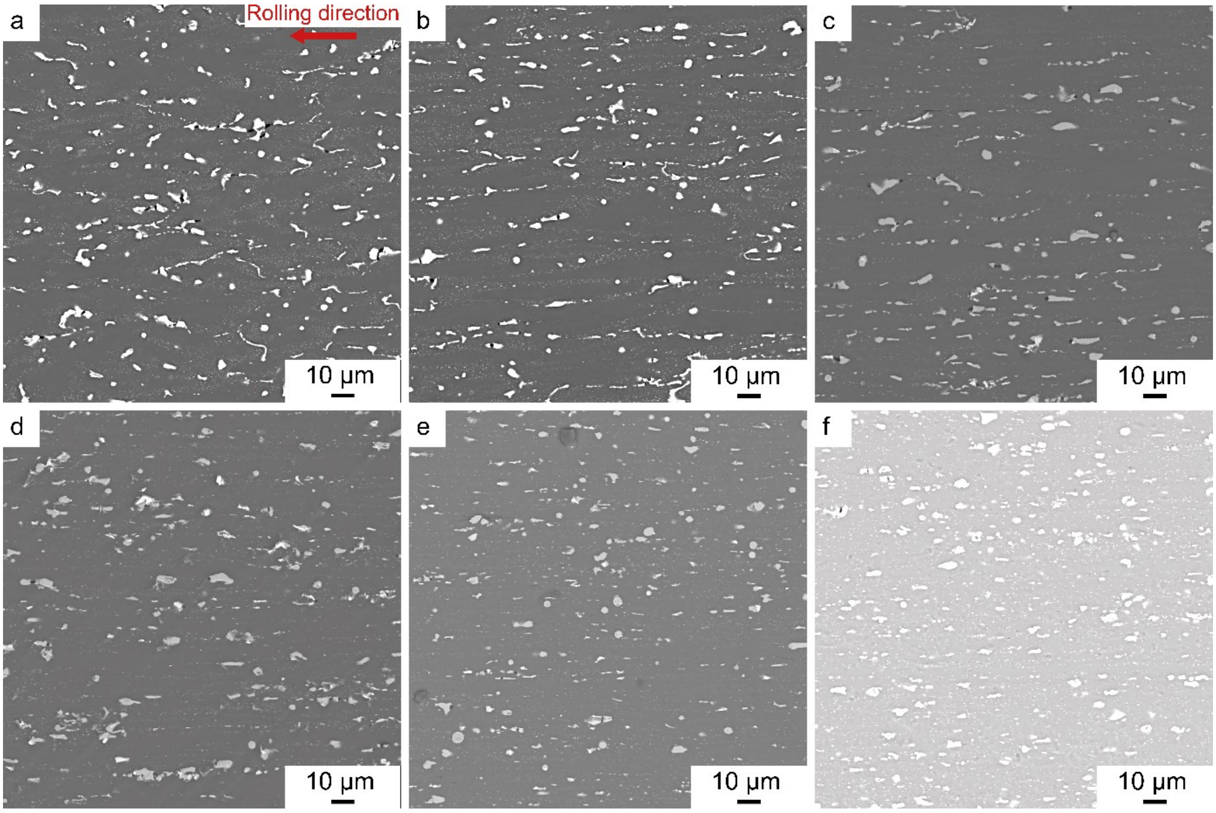

Figure 4-53: SEM image of rolled and aged at 170 °C samples: a) 6.74 mm b) 4.25 mm c) 3.14 mm d) 2.05 mm e) 1.2 mm f) 0.3 mm.

4.7.1 EBSD analysis

When the temperature is exposed to 170 °C for 12 hours, the alignment of neighbouring phases in the same direction occurs, as shown in **Figure 4-54**. In addition, the increase in the rolling pass (a decrease in thickness) causes a reduction in the size of the grains. However, the phases in the rolled alloys are still largely longitudinally stretched.

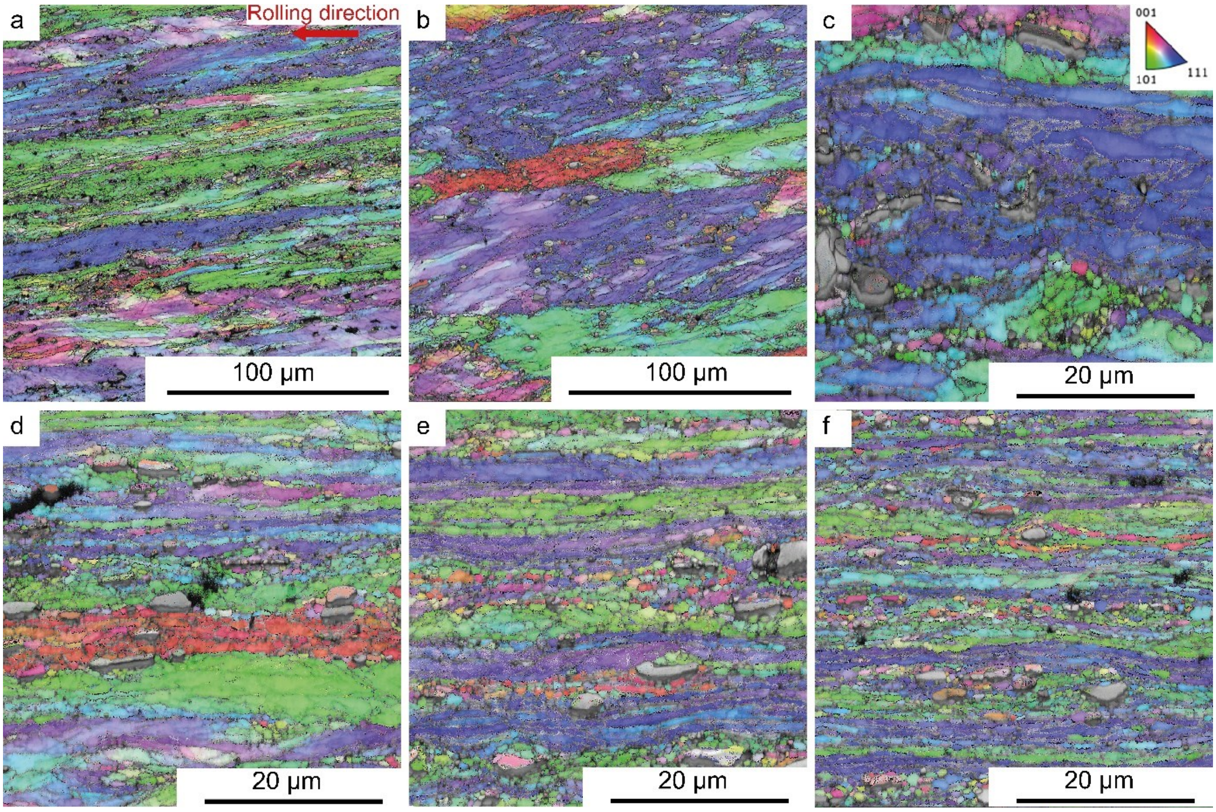

Figure 4-54: IPF image of rolled and aged at 170 °C samples: a) 6.74 mm b) 4.25 mm c) 3.14 mm d) 2.05 mm e) 1.2 mm f) 0.3 mm.

Ageing the rolled sample with a thickness of 6.74 mm at 170 °C for 12 hours results in a reorientation in the <111> direction, as shown in **Figure 4-55**. Also, the orientation of the three thin specimens continues to be in this range after ageing, but there is a slight shift away from this direction. The sample with a thickness of 3.14 mm does not have a preferred crystal orientation even after ageing, and the orientation of the 4.25 mm sample remains nearly the same.

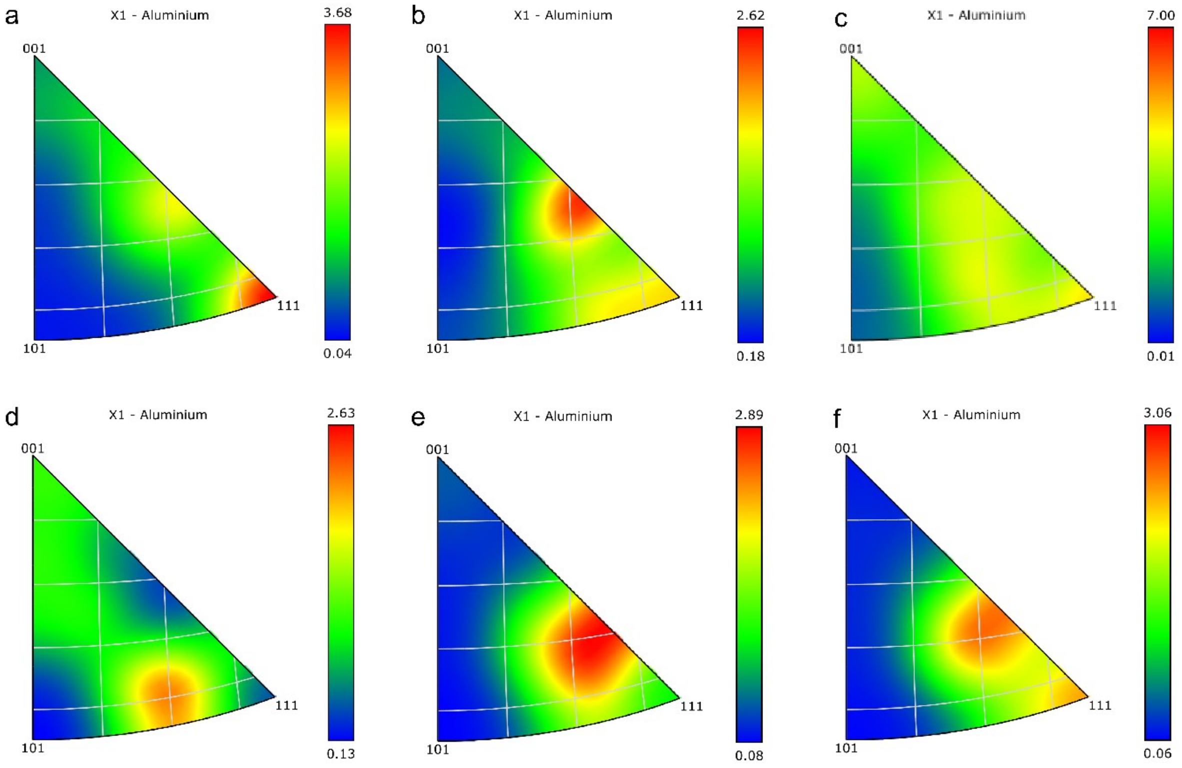

Figure 4-55: Texture analysis (PF) of hot rolled and aged at 170 °C samples: a) 6.74 mm b) 4.25 mm c) 3.14 mm d) 2.05 mm e) 1.2 mm f) 0.3 mm.

4.7.2 Grain size distribution

The evaluation of the grain sizes in **Figure 4-56** shows low values in all samples. The values found also scatter only slightly.

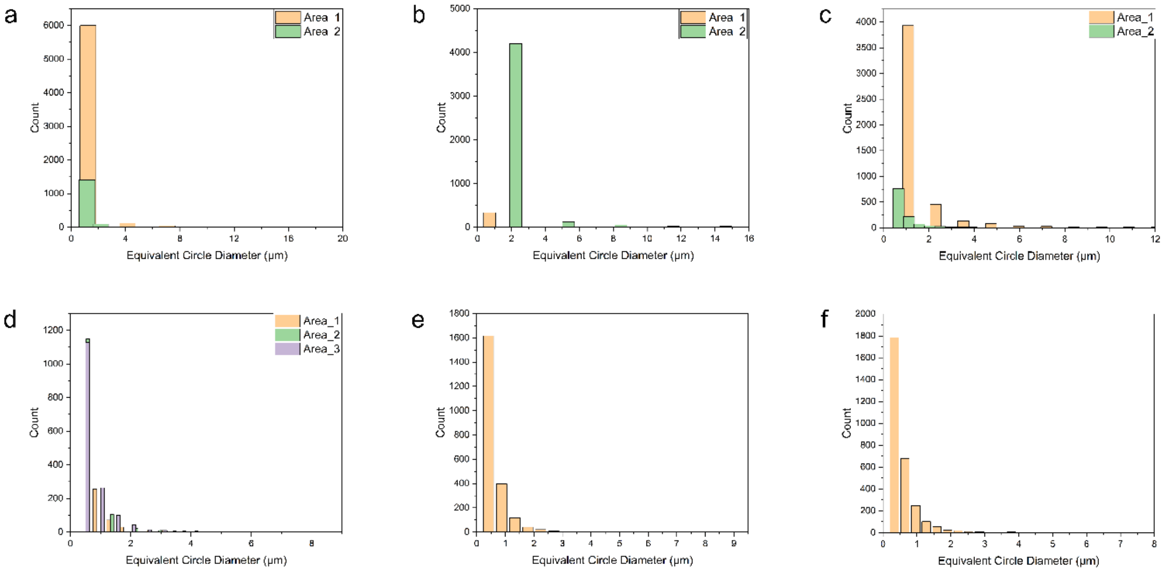

Figure 4-56: Grain size distribution of rolled and aged at 170 °C samples: a) 6.74 mm b) 4.25 mm c) 3.14 mm d) 2.05 mm e) 1.2 mm f) 0.3 mm.

This also becomes clear in the overview of the mean values of the grain sizes determined in **Table 4-3**. The values of the samples with a thickness of 2.05 mm, 1.2 mm and 0.3 mm are very close to each other. The other three samples have a slightly higher mean grain size and standard deviation.

Table 4-3: Average grain size of the Al phase after rolling and ageing at 170 °C for 12 hours.

Sample thickness [mm]	Grain size [µm]
6.74	0.98 ± 2.08
4.25	1.27 ± 2.69
3.14	1.44 ± 1.74
2.05	0.70 ± 1.02
1.2	0.60 ± 0.70
0.3	0.60 ± 0.60

In addition, the size of the Al_2Cu phases was also determined for these samples. The obtained values are listed in **Table 4-4**.

Table 4-4: Average grain size of the Al_2Cu phase after rolling and ageing at 170 °C for 12 hours.

Sample thickness [mm]	Grain size [µm]
6.74	0.60 ± 0.50
4.25	0.70 ± 0.70
3.14	0.80 ± 0.60
2.05	0.30 ± 0.30
1.2	0.40 ± 0.30
0.3	0.40 ± 0.30

4.7.3 Stress distribution

An increase of the temperature to 170 °C for 12 hours already leads to a significant reduction of the stresses in the microstructure. This fact is also shown in **Figure 4-57**. However, these do not disappear completely and areas with even higher values still remain. This means that in the ageing process, the stresses have been relieved by realignment or formation of new grains. It can be seen that even the specimen with a thickness of 4.25 mm and low initial stresses after hot rolling is not completely free of residual stresses. It should be noted, however, that the specimens considered are taken from different areas of the sheet, which means that it is possible that local differences have already occurred as a result of the hot rolling process.

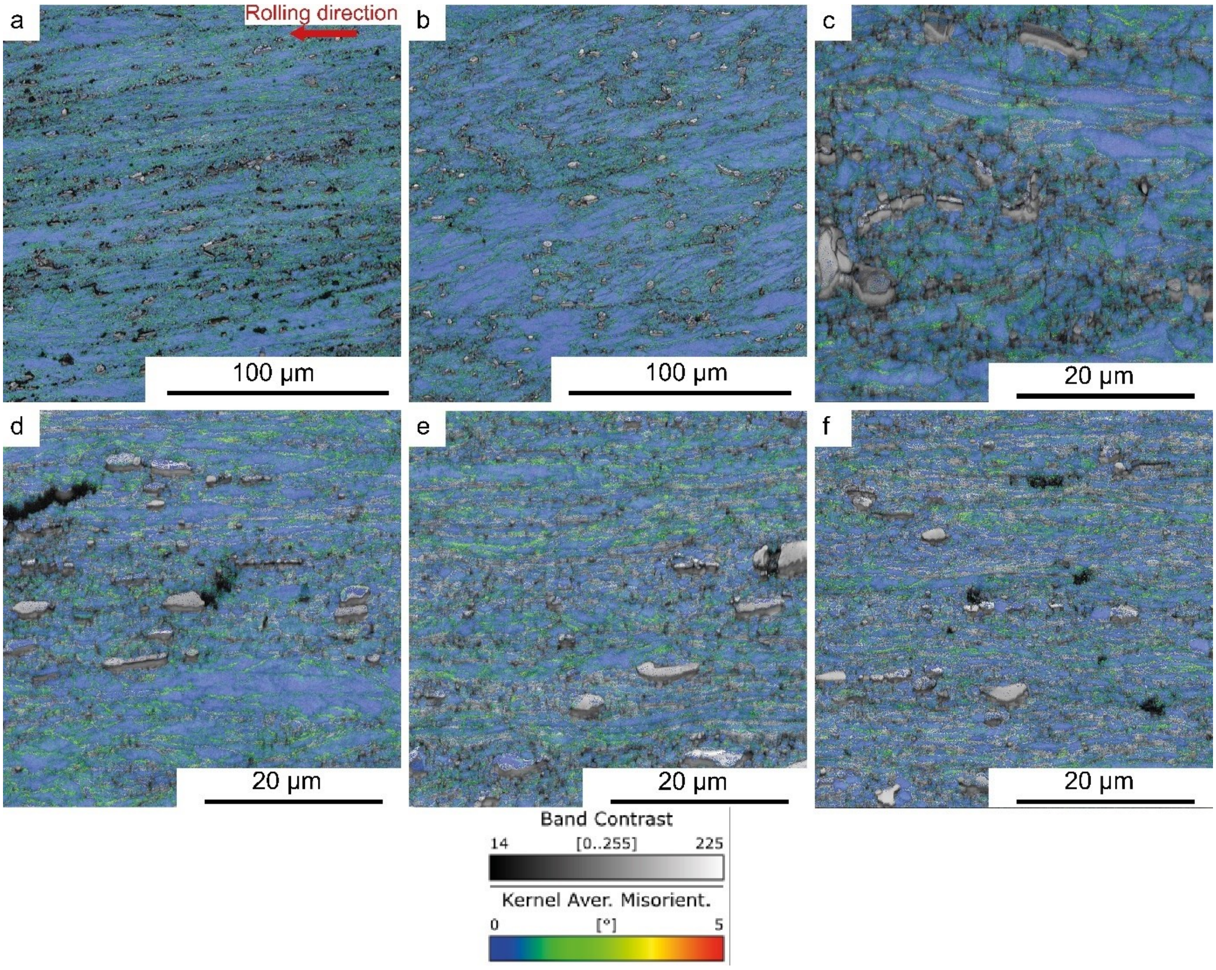

Figure 4-57: KAM of rolled and aged at 170 °C samples: a) 6.74 mm b) 4.25 mm c) 3.14 mm d) 2.05 mm e) 1.2 mm f) 0.3 mm.

4.7.4 SEM EDS analysis

In the following, individual measuring points of the rolled and aged or homogenized sheets are considered. However, the Ω-phase has very small dimensions and often can´t be detected directly in SEM. Nevertheless, this phase also precipitates on Mn-dispersoids, EDS analyses containing Mn could indicate the Ω-phase. [27]

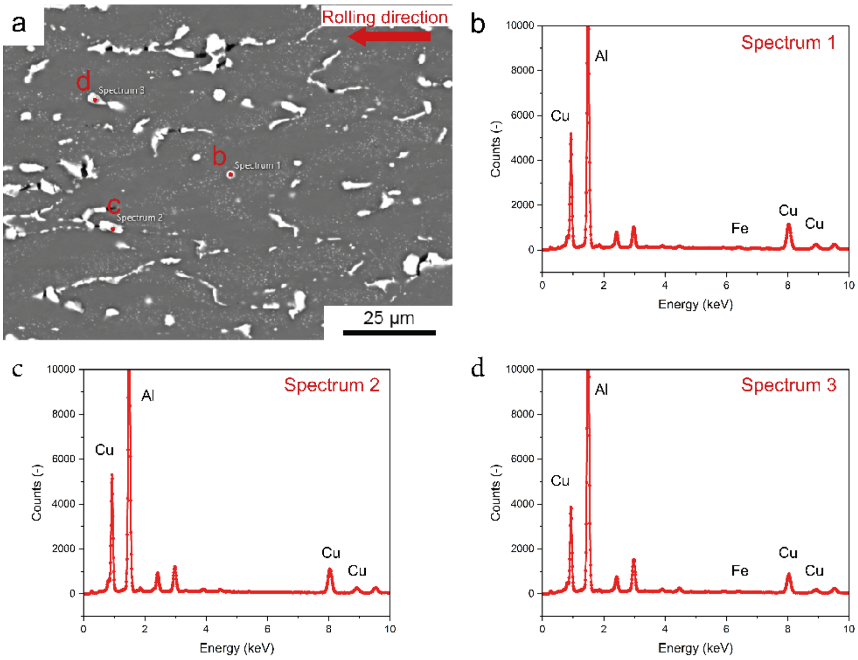

Figure 4-58: (a) SEM image and (b-c) EDS spectra of the rolled sample with a thickness of 6.74 mm after aged at 170 °C for 12 hours taken from specific points as marked in (a).

Table 4-5 clearly shows the results of the above analysis, the elements Ag and Mg could only be partially detected as trace elements. The recorded spectra of the sample with a thickness of 6.74 mm after annealing at 170 °C consist of variable amounts of Al and Cu and occasionally small amounts of Fe and Mn. Converting the mass percentages determined from the acquired spectra into atomic percentages, the composition of the precipitates considered is $Al_4Cu(FeMn)$ phase.

Table 4-5: EDS analysis of the rolled and aged sample with a thickness of 6.74 mm at different points.

Spectrum	Al [at.%]	Cu [at.%]	Fe [at.%]	Mn [at.%]
1	79.33	19.69	0.68	0.29
2	80.98	19.02	0	0
3	84.67	14.35	0.57	0.28

The ageing of the rolled plates should result in a greater amount and growth of the precipitates. The sample with a thickness of 0.3 mm shows a uniform distribution of Cu in the rolled state, after applying a temperature of 170 °C for 12 hours several spectra of the precipitates were recorded. As shown in **Figure 4-59**, these consist mainly of Al and Cu.

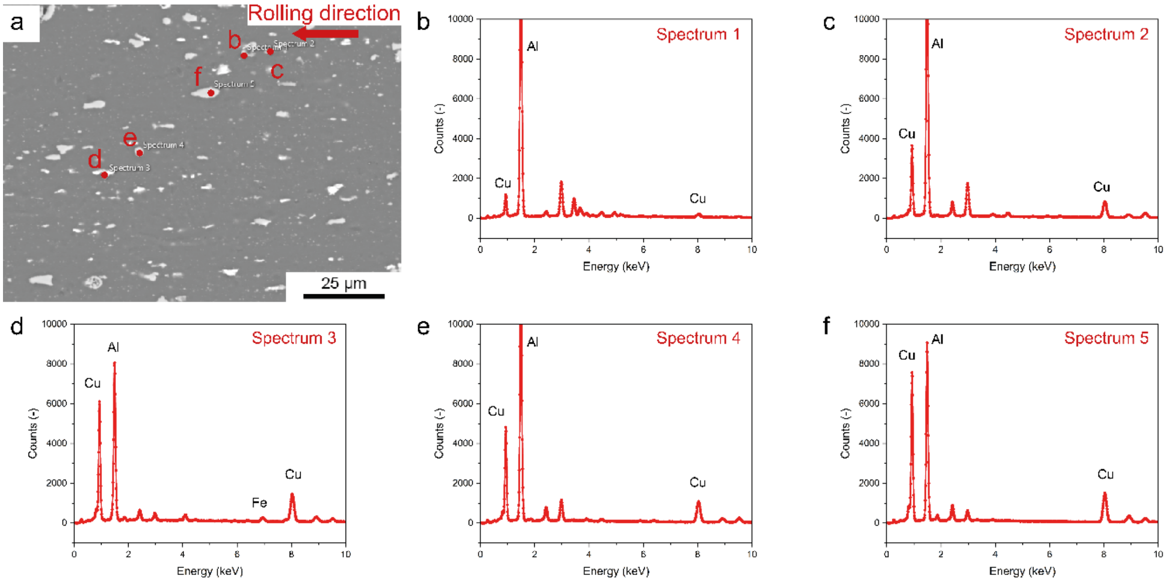

Figure 4-59: (a) SEM image and (b-f) EDS spectra of the rolled sample with a thickness of 0.3 mm after aged at 170 °C for 12 hours taken from specific points as marked in (a).

Table 4-6 lists the determined contents of the sample. Spectrum 3 and spectrum 5 provide a content which approximately corresponds to Al_2Cu in the empirical formula. Spectrum 1 shows a high Al content, which may be caused by the surrounding Al-matrix. Spectrum 1 was recorded at the edge of the precipitate. In addition to Mn, Mg is also found at this location, and the same applies to spectrum 3. However, this was recorded somewhat further in the interior and traces of Fe are also found in this spectrum.

Table 4-6: EDS analysis of the rolled and aged sample with a thickness of 0.3 mm at different points.

Spectrum	Al [at.%]	Cu [at.%]	Fe [at.%]	Mn [at.%]	Mg [at.%]
1	95.36	4.11	0	0.39	0.14
2	85.37	14.63	0	0	0
3	70.73	28.03	0.40	0.43	0.41
4	80.81	18.25	0.56	0.37	0
5	72.31	27.52	0.17	0	0

A detailed examination of a precipitate in the sample with a thickness of 1.2 mm after ageing at 170 °C for 12 hours shows the distribution of elements, as depicted in **Figure 4-60**. It is clear that the precipitate consists mainly of Cu with a slightly smaller area of Fe and Mn. Both Al and Si are found mainly in the matrix. Mg is found to be distributed throughout the sample in small amounts.

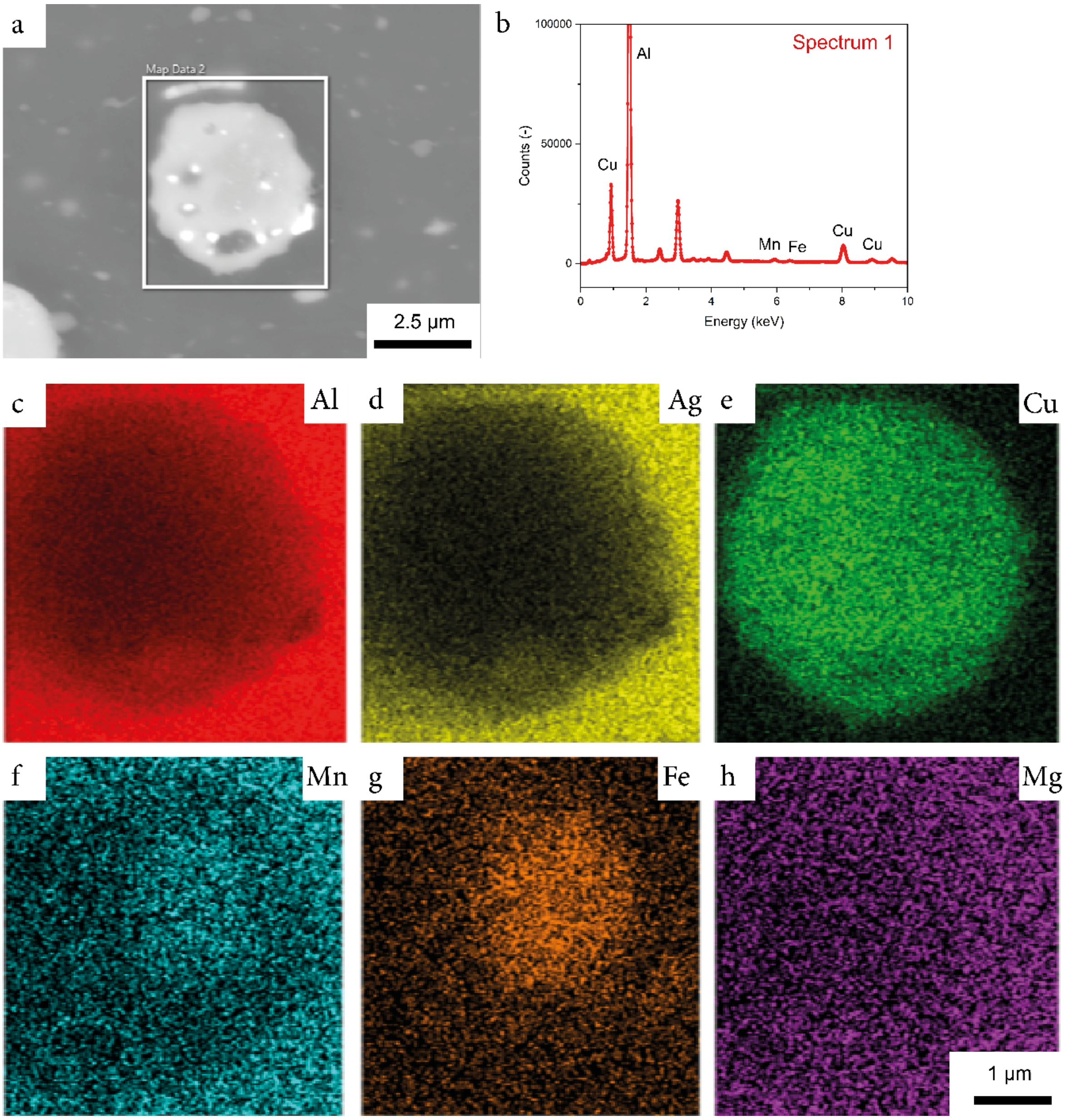

Figure 4-60: (a) SEM image, (b) EDS spectrum taken from the whole region, and (c-g) EDS maps of Al, Ag, Cu, Mn, Fe and Mg in the rolled sample with a thickness of 1.2 mm after aged at 170 °C for 12 hours.

A subsequent analysis of individual points in this precipitation leads to the spectra, as shown in **Figure 4-61**. The brighter areas show a composition consisting mainly of Al and Cu. In the other areas, traces of Fe are found.

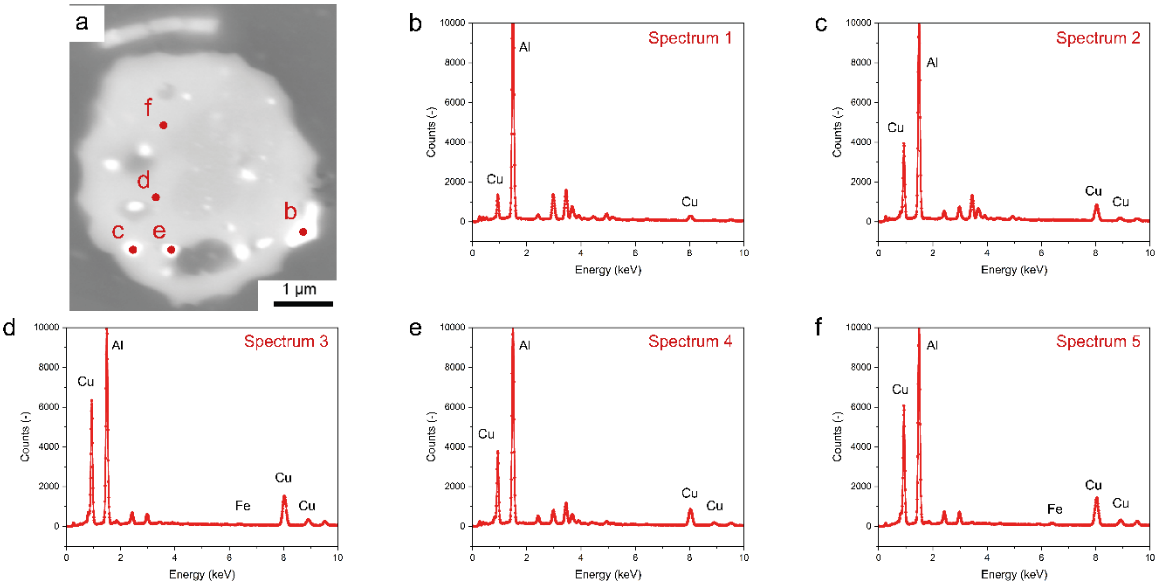

Figure 4-61: (a) SEM image and (b-f) EDS-point analysis in the sample with a thickness of 1.2 mm after aged at 170 °C for 12 hours.

4.7.5 Hardness

The Vickers hardness of the rolled samples after ageing at 170 °C for 12 hours is still in the range of 80 HV, whereby especially the samples with a thickness of 4.25 mm and 1.2 mm yield slightly higher values.

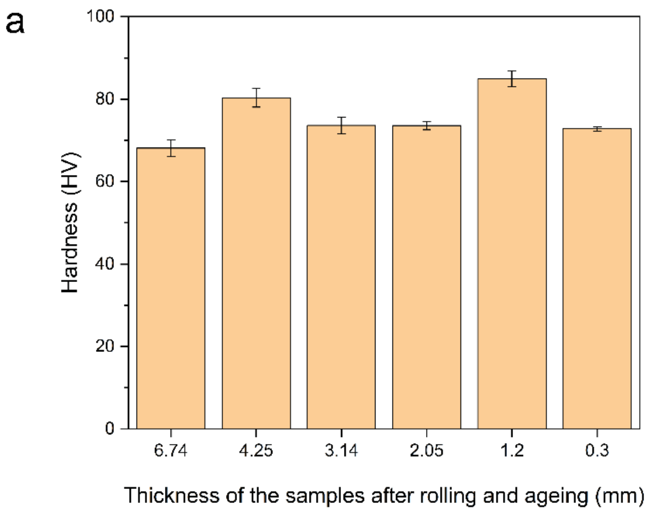

b

Thickness of the sample [mm]	Hardness [HV]
6.74	68.1 ± 2.0
4.25	80.3 ± 2.2
3.14	73.6 ± 2.0
2.05	73.6 ± 1.0
1.2	85.0 ± 1.9
0.3	72.8 ± 0.5

Figure 4-62: Vickers hardness after rolling and ageing at 170 °C.

4.8 Influence of hot rolling and T4

In contrast, T4 solution treatment of the rolled samples leads to a partial dissolution of the precipitates in the microstructure. In addition, the spatial dimensions of the phases decrease. This indicates that the precipitates have not yet completely dissolved after the solution treatment at 540 °C. Whether a further dissolution would have occurred with a longer solution treatment was not investigated in this work. However, as in the untreated samples, the same geometry of the precipitates is shown in **Figure 4-63**, which evolves from lamellar to spherical with decreasing thickness of the rolled plates.

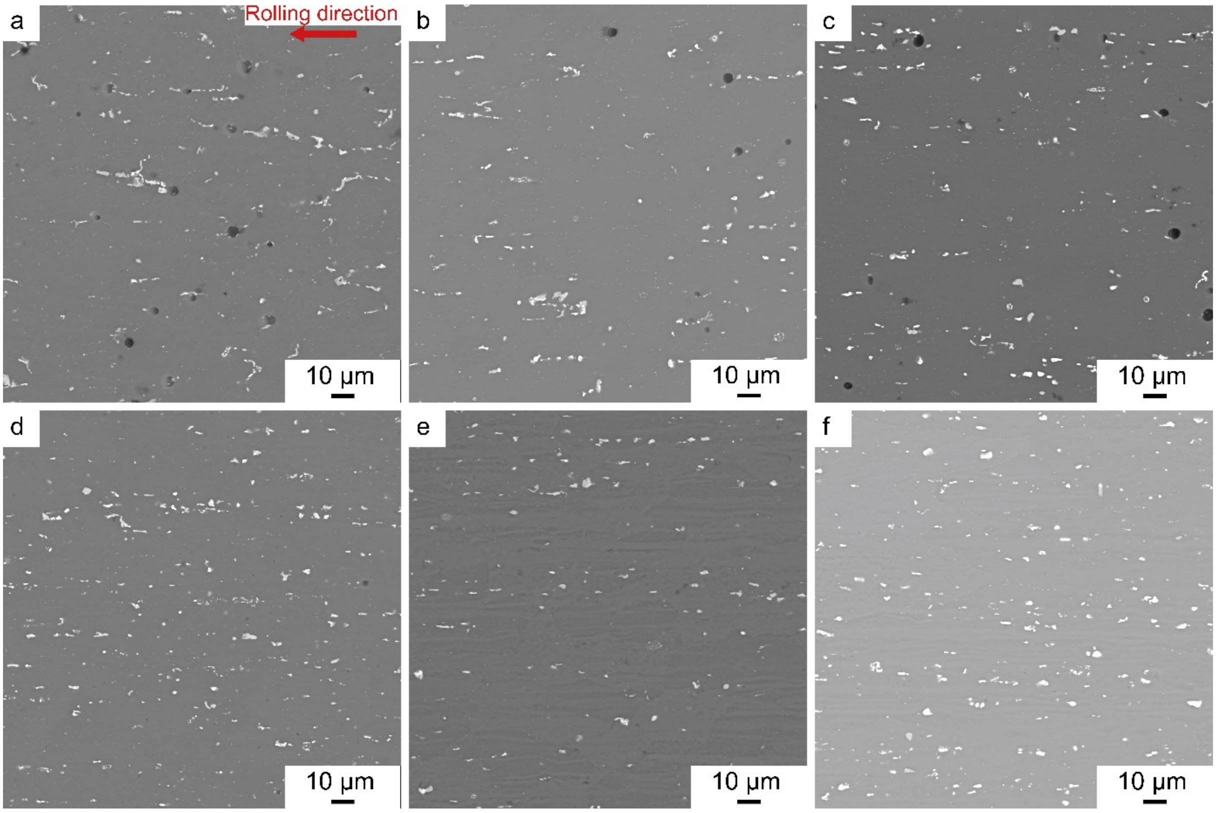

Figure 4-63: SEM images of rolled and T4 treated samples: a) 6.74 mm b) 4.25 mm c) 3.14 mm d) 2.05 mm e) 1.2 mm f) 0.3 mm.

4.8.1 EBSD analysis

In contrast to the ageing after rolling, T4 solution treatment results in the formation of uniformly shaped grains due to recrystallisation. As shown in **Figure 4-64**, only the specimens with a thickness of 0.3 mm, 1.2 mm and 2.05 mm still exhibit an elongated character.

Furthermore, the direction of the formed phases in the thicker samples is now again independent of the rolling direction.

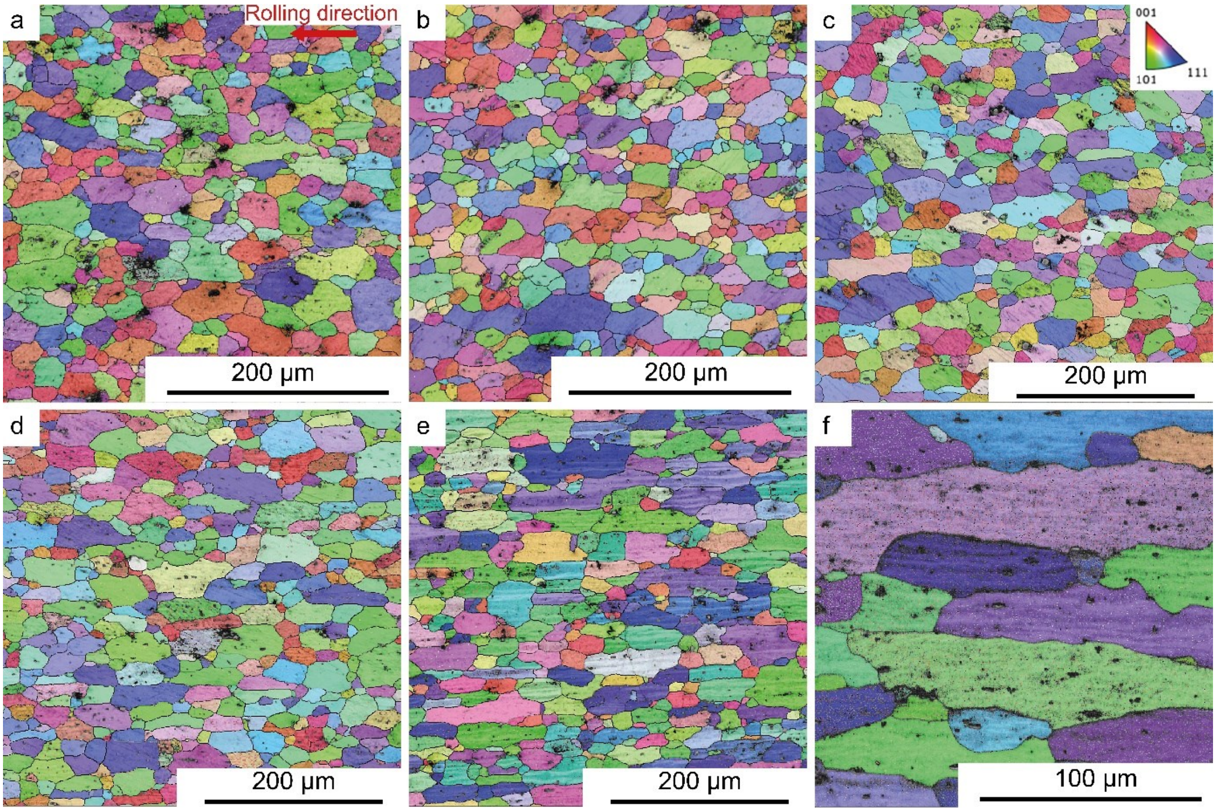

Figure 4-64: IPF images of rolled and T4 treated samples: a) 6.74 mm b) 4.25 mm c) 3.14 mm d) 2.05 mm e) 1.2 mm f) 0.3 mm.

These observations are confirmed when looking at the texture analysis in **Figure 4-65**. The orientation of the phases of the three thin samples is almost entirely in the <101> direction, but even the sample with a thickness of 3.14 mm shows a preferred orientation in this direction. The two thick specimens with a thickness of 4.25 mm and 6.74 mm do not show a preferred direction of the phases.

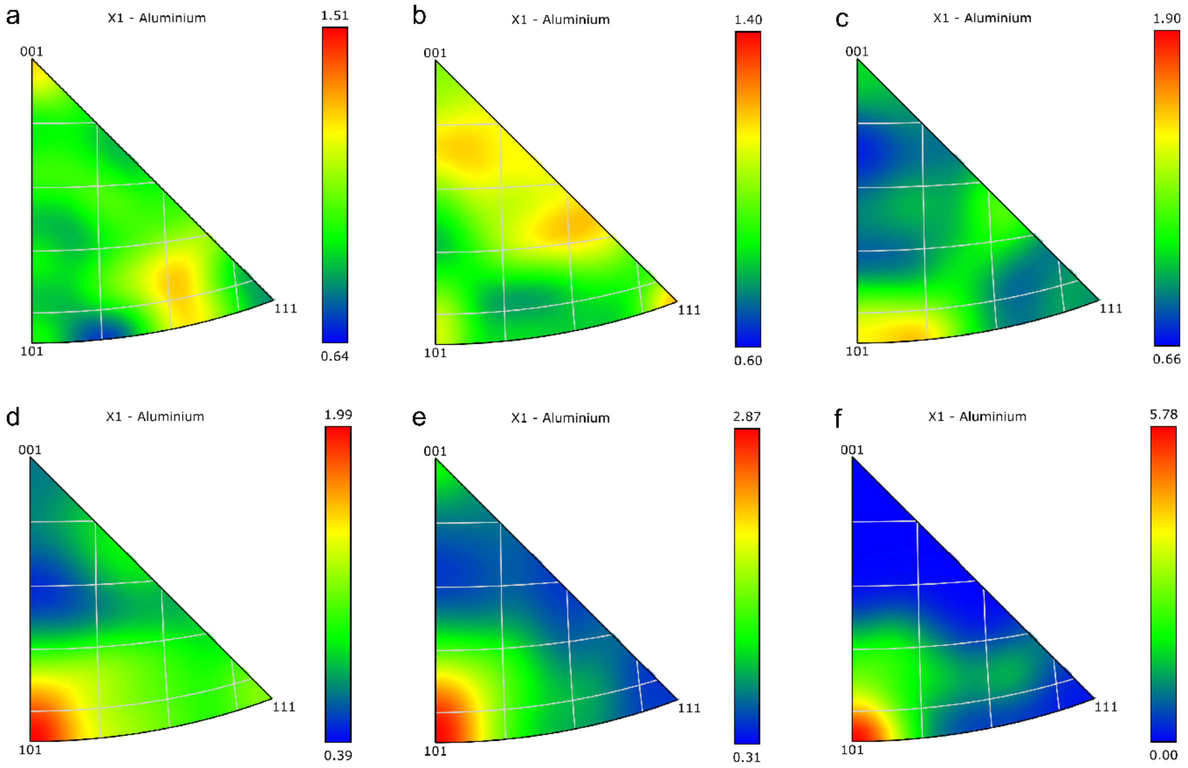

Figure 4-65: Texture analysis (PF) of hot rolled and T4 treated samples: a) 6.74 mm b) 4.25 mm c) 3.14 mm d) 2.05 mm e) 1.2 mm f) 0.3 mm.

4.8.2 Grain size distribution

The grain size distribution of the rolled samples after solution treatment is shown in **Figure** 4-66.

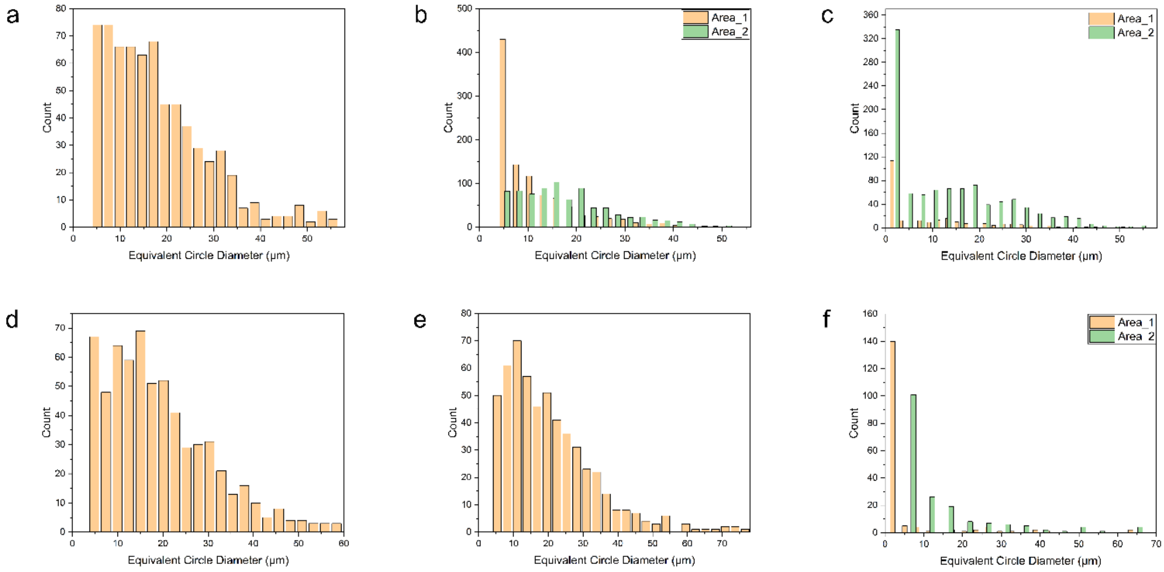

Figure 4-66: Grain size distribution of rolled and T4 treated samples: a) 6.74 mm b) 4.25 mm c) 3.14 mm d) 2.05 mm e) 1.2 mm f) 0.3 mm.

The mean values of the grain sizes determined are presented in **Table 4-7**. The samples show no correlation between the rolling pass and the resulting grain size after a T4 solution treatment.

Table 4-7: Average grain size of the Al phase after rolling and T4 treatment.

Sample thickness [mm]	Grain size [µm]
6.74	18.10 ± 11.00
4.25	13.94 ± 8.92
3.14	12.51 ± 12.06
2.05	19.20 ± 11.60
1.2	20.30 ± 12.90
0.3	12.71 ± 18.65

Compared to the samples after rolling and ageing at 170 °C for 12 h, no Al_2Cu phase was identified in the samples after solution treatment in the SEM.

4.8.3 Stress distribution

Solution treatment of the rolled sheets results in a significant reduction in stresses over the entire microstructure, but phases with high KAM values still remain in all samples, as shown in **Figure 4-66**. It is visible that although there is a reduction in stress in the specimen with a thickness of 0.3 mm, it still persists in the grains.

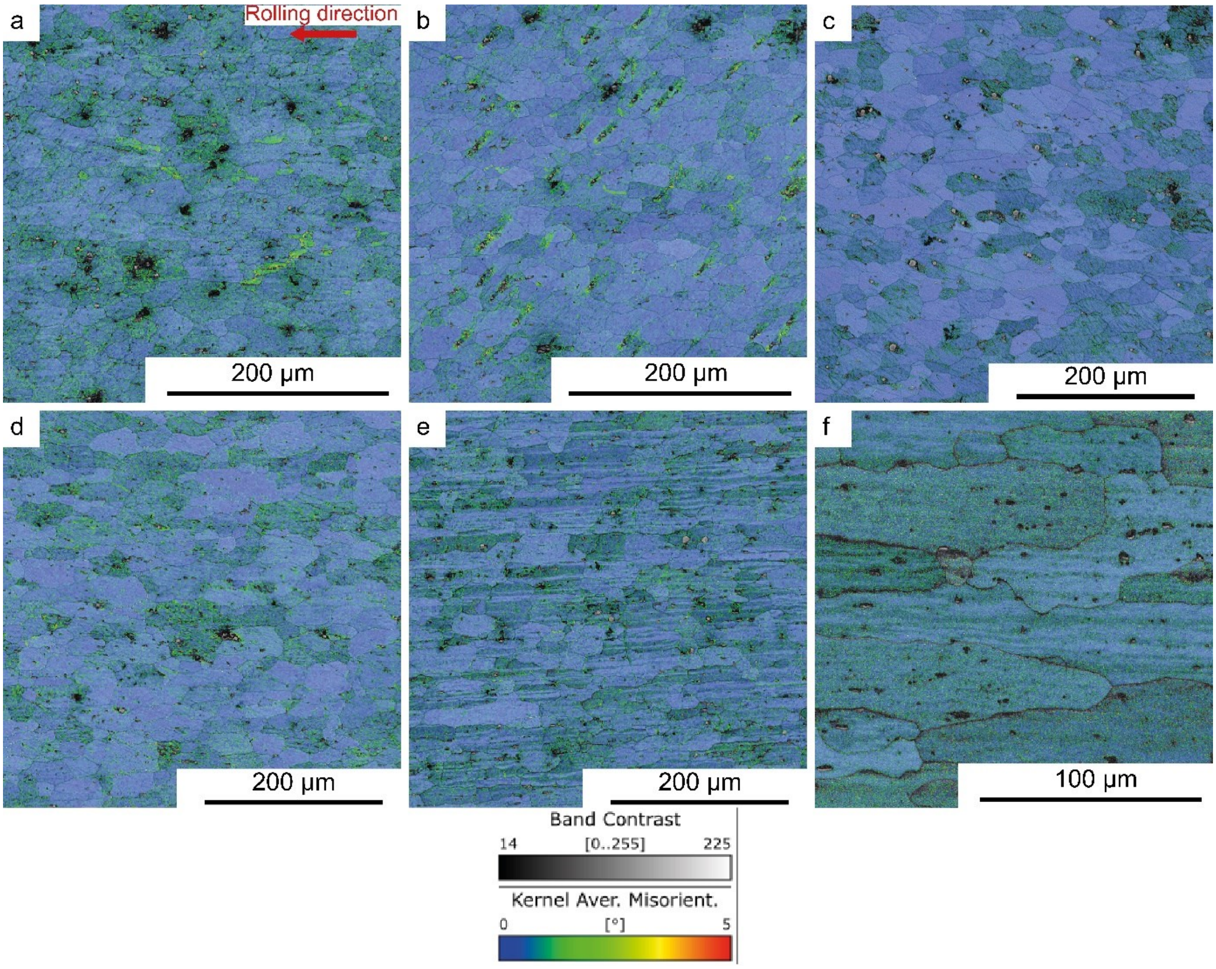

Figure 4-67: KAM of rolled and T4 treated samples: a) 6.74 mm b) 4.25 mm c) 3.14 mm d) 2.05 mm e) 1.2 mm f) 0.3 mm.

4.8.4 EDS analyses

The next step is an observation of the rolled sheets after T4 treatment. For this purpose, various spectra were first recorded on the sample with a thickness of 6.74 mm. **Figure 4-68** shows that almost all spectra after T4 treatment contains Fe and Mn in addition to Al and Cu. This indicates that the complete dissolution of these phases may not have been achieved at a temperature of 540 °C.

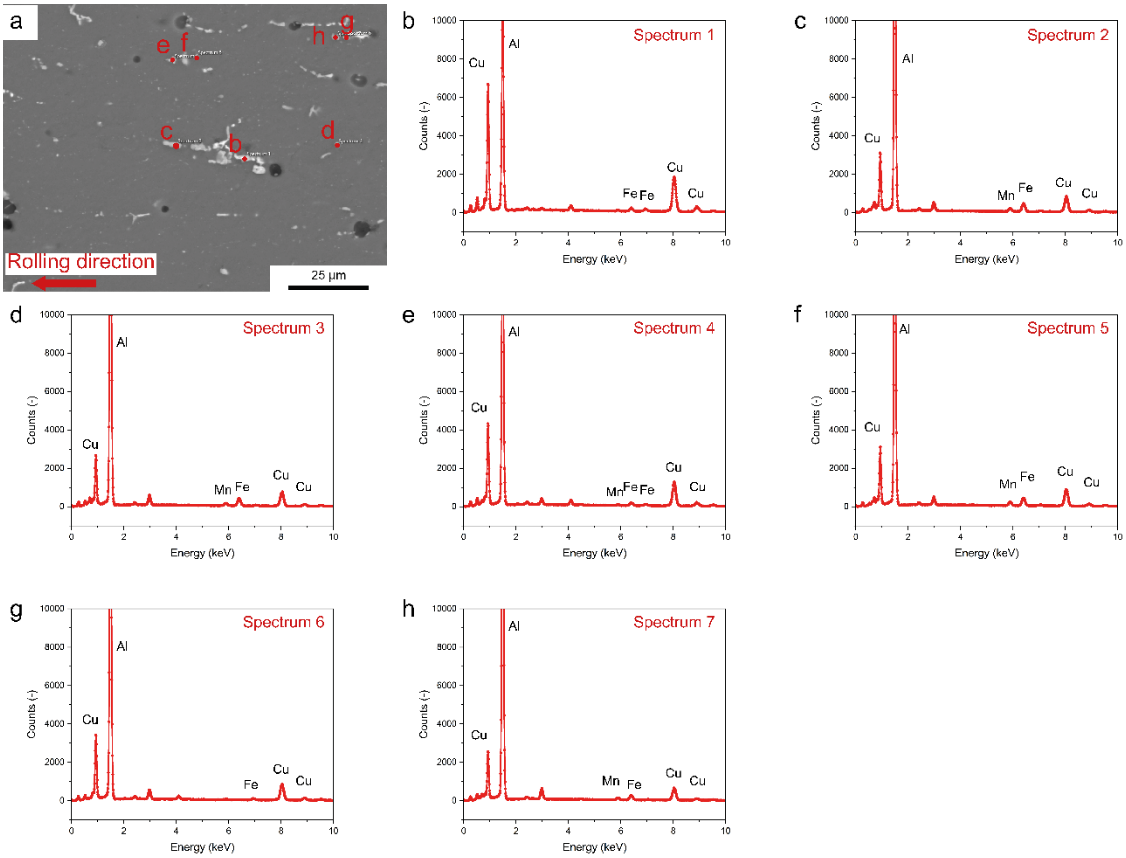

Figure 4-68: (a) SEM image and (b-h) EDS spectra of the sample with a thickness of 6.74 mm after T4 treatment at different points.

In addition to the statements already found, the evaluation of the spectra in **Table 4-8** confirms the assumptions and shows that after T4 treatment of the rolled samples there was even an enrichment of Fe in most precipitates. High values of Fe also usually result in increased contents of Mn. Spectrum 1 corresponds almost to the Al_2Cu phase with traces of Fe, Mn and Mg.

Table 4-8: EDS analysis of the rolled sample with a thickness of 6.74 mm after T4 at different points.

Spectrum	Al [at.%]	Cu [at.%]	Fe [at.%]	Mn [at.%]	Mg [at.%]
1	71.17	27.03	1.32	0.37	0.11
2	84.27	10.94	3.51	1.27	0
3	86.02	9.97	3.07	0.93	0
4	81.86	16.69	1.04	0.37	0
5	83.59	11.76	3.26	1.39	0
6	87.90	11.78	0.15	0.17	0
7	88.29	8.91	2.06	0.74	0

The spectra of the sample with a thickness of 3.14 mm after T4 treatment in **Figure 4-69** also show the same results. In addition to Al and Cu, spectra 1, 2 and 4 show increased amounts of Fe and Mn.

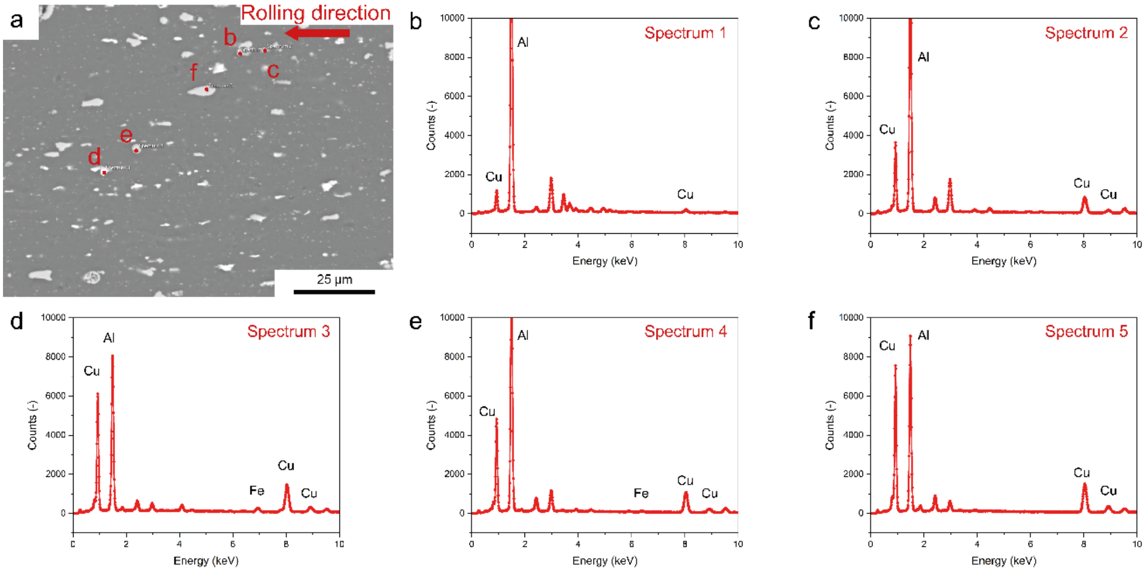

Figure 4-69: (a) SEM image and (b-f) EDS spectra of the rolled sample with a thickness of 3.14 mm after T4 treatment at different points.

The evaluation in the form of **Table 4-9** shows that spectrum 3 also contains low levels of Ag in addition to Mg. It is noticeable that neither Mn nor Fe is found in this phase. The molecular formula of this phase is determined after the conversion of the mass percent to atomic percent to be very close to Al_2Cu. Since the Ω-precipitates have a layer of Mg and Ag between them and the surrounding α-Al, it is possible that this is precisely this phase.

Table 4-9: EDS analysis of the rolled sample with a thickness of 3.14 mm after T4 at different points.

Spectrum	Al [at.%]	Cu [at.%]	Fe [at.%]	Mn [at.%]	Mg [at.%]
1	69.89	24.70	1.89	1.96	0
2	64.60	3.84	0.73	0.39	0.43
3	69.04	30.56	0	0	0.36
4	75.66	2048	0.81	3.05	0

4.8.5 Hardness

In addition, a hardness measurement of the samples after T4 solution treatment was also carried out, the results of these are shown in **Figure 4-70**. The samples with a thickness of 4.25 mm and 0.3 mm still show a hardness of about 80 HV. The samples with a thickness of 6.74 mm and 3.14 mm only achieve a value below 60 HV. This is a significant decrease compared to the values after hot rolling.

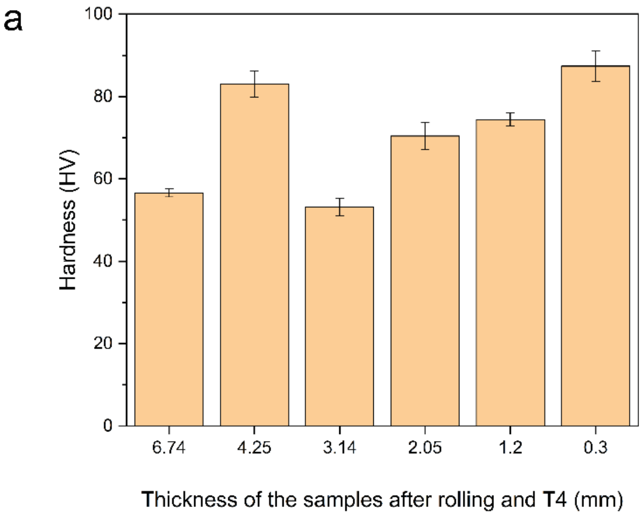

b

Thickness of the sample [mm]	Hardness [HV]
6.74	59.6 ± 1.0
4.25	83.0 ± 3.2
3.14	53.2 ± 2.2
2.05	70.4 ± 3.3
1.2	74.4 ± 1.6
0.3	87.4 ± 3.7

Figure 4-70: Vickers hardness after rolling and T4.

4.8.6 Precipitation behaviour

Investigations were also carried out for the hot rolled sheets after T4 treatment using in-situ SAXS. However, only the first and last rolling step were observed, which means that the specimens with a thickness of 0.3 mm and 6.74 mm were placed in the measuring instrument at 170 °C for 20 hours. Subsequently, the evaluation of the measured intensities is carried out by using the same methodology as in the previous chapter.

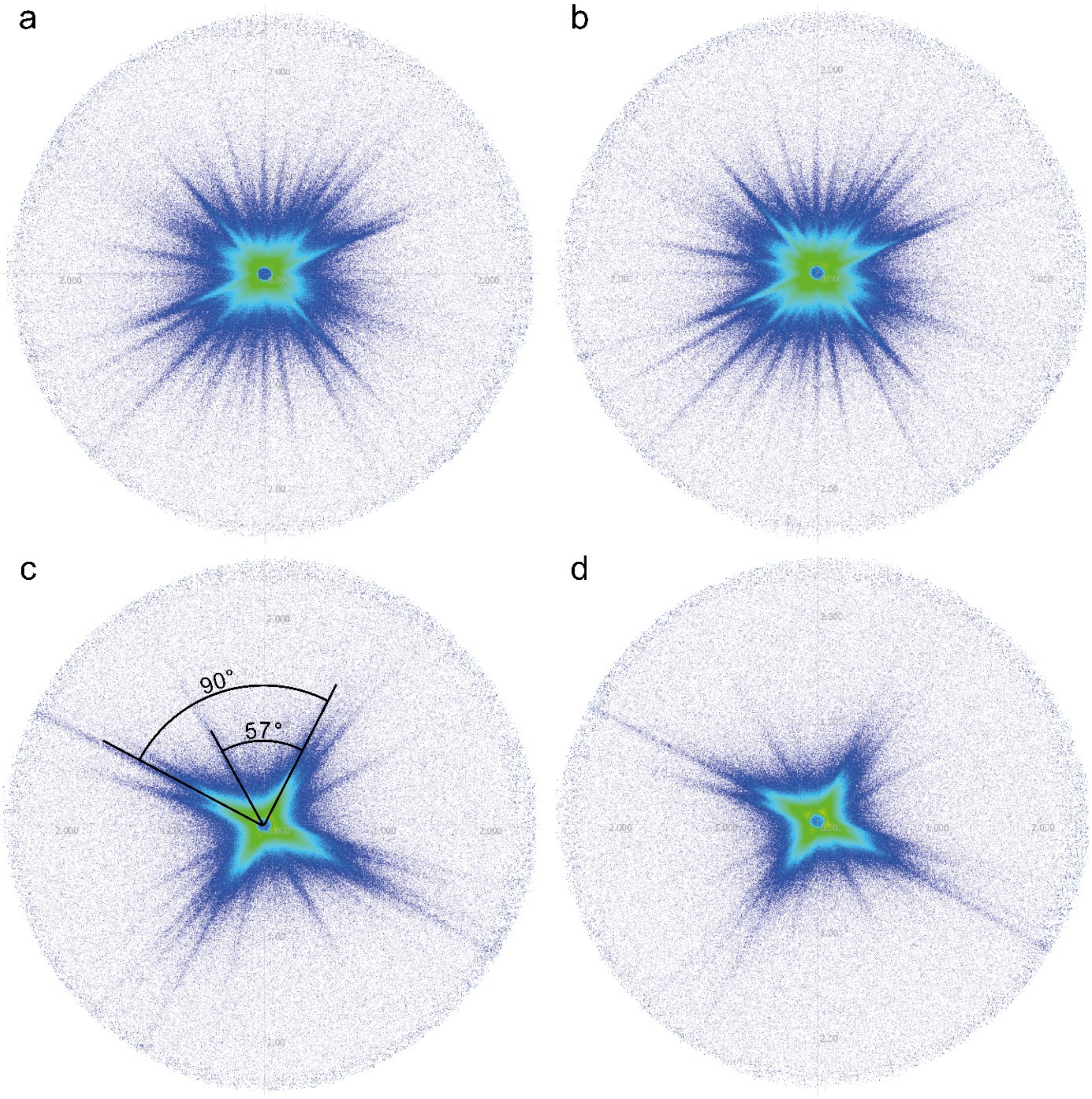

Figure 4-71: 2D scattering images obtained from the in-situ SAXS of the Al-4Cu-0.3Mg-0.7Ag at 170 °C after rolling to different thicknesses and T4 solution treatment: a) 6.74 mm after 1 h b) 6.74 mm after 20 h c) 0.3 mm after 1 h d) 0.3 mm after 20 h.

A small deformation of the plate provides a slight increase in the integrated intensity determined, with the maximum of the 6.74 mm sample being reached after about 2.5 hours. As shown in **Figure 4-72**, a large degree of deformation reduces the volume fraction significantly. Whereby the values decrease steadily from an ageing duration of one hour.

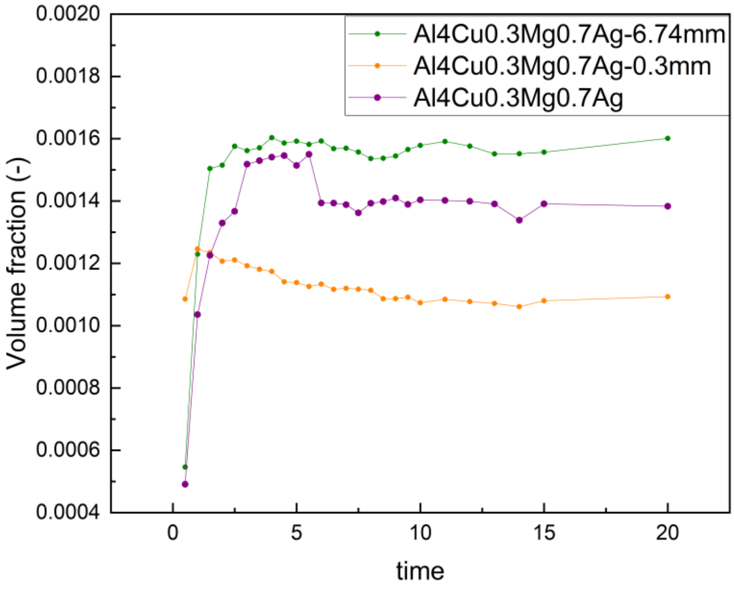

Figure 4-72: Comparison of the values for the integrated intensity in the in-situ SAXS between T4 and rolled plus T4 samples with the composition Al-4Cu-0.3Mg-0.7Ag.

Looking at the number density in **Figure 4-73**, it is noticeable that the values decrease with increasing degree of deformation. The number density of precipitates in an Al-4Cu-0.3Mg-0.7Ag alloy is inversely proportional to the degree of deformation.

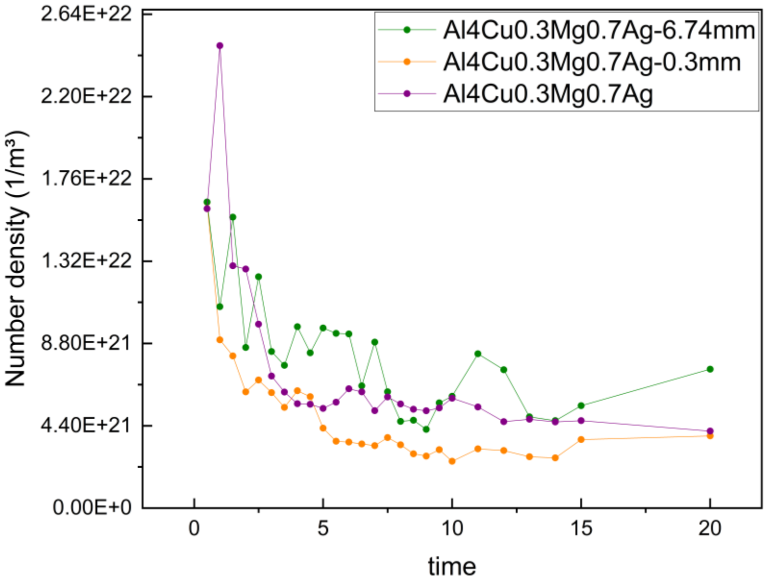

Figure 4-73: Comparison of the values for the number density between T4 and rolled plus T4 samples with the composition Al-4Cu-0.3Mg-0.7Ag.

Finally, the values for the Porod radius are shown in **Figure 4-74**, where it can be regarded that the size of the particles also increases with increasing degree of deformation. This indicates a coarsening behaviour for the hot rolled samples.

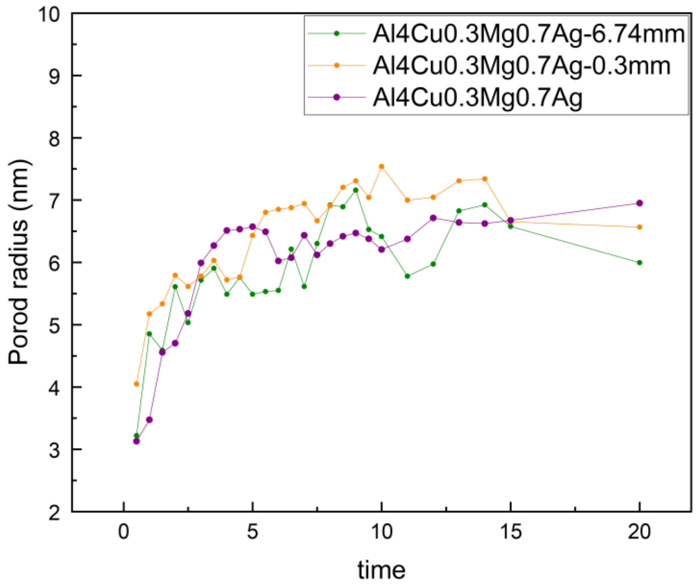

Figure 4-74: Comparison of the values for the Porod radius between T4 and rolled plus T4 samples with the composition Al-4Cu-0.3Mg-0.7Ag.

For the rolled samples, a DSC measurement was also performed after solution treatment at 540 °C for 6 h and subsequent quenching in cold water. The results are shown in **Figure 4-75**. The hot rolled samples no longer show a noticeable peak at around 200 °C. However, the endothermic peak of the rolled sample with a thickness of 6.74 mm is also present at 300 °C, which is similar to that of the sample before hot rolling. The same peak shifts to around 280 °C for the sample with a thickness of 0.3 mm.

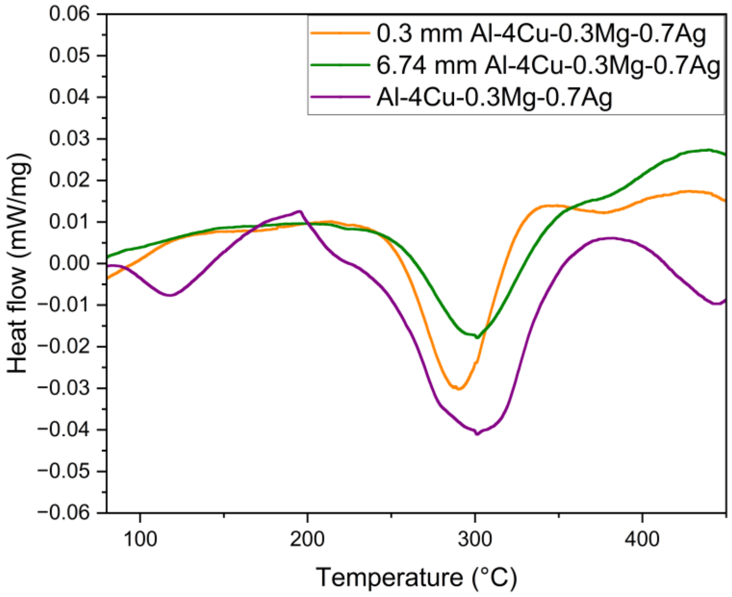

Figure 4-75: DSC curves of the hot rolled samples compared with the sample before rolling with a composition of Al-4Cu-0.3Mg-0.7Ag after solution treatment.

.

5 Discussion

At the beginning, the evaluation of the grain sizes using the line intercept method showed that the trace elements such as Fe and Mn in the Al lead to lower average grain sizes being determined compared to the high purity Al. The Cu content influences the determined grain sizes of the Al-Cu alloys up to a content of 2 %, from this point the values remains nearly unchanged. A T4 heat treatment also showed hardly any influence on the determined grain sizes of the Al-Cu alloys. The hardness of the alloys after a T4 solution heat treatment and natural ageing increases with increasing Cu content. The results of the SAXS measurements clearly show that precipitates are only formed in larger quantities from a Cu content of 4 %. The subsequent investigation of the precipitate formation by using DSC also confirms this. Only from a content of 4 wt.% can the formation of phases be clearly observed. An addition of only 1 % Cu did not lead to any significant precipitation, from a content of 2 % Cu the first clusters and precipitates formed. The precipitates in the Al-4Cu alloy coarsen considerably in the first 5 hours until their growth slows down, but never stops completely. An increase in the Cu content also has an influence on the position of the peaks of the GP zones in **Figure 4-9**. Higher Cu contents lead to a shift of the peaks to lower values for the time. One reason for this could be the increased diffusion rate due to the increased Cu concentration.

In this work, the addition of 0.7 wt.% Ag resulted in the grain size of the alloy remaining almost constant after solution treatment. In the previous report, Peng et al. [28] show a correlation between the addition of a small amount of Ag and the precipitation density and size of the precipitates at low Cu contents. This is consistent with the correlations found in this work, even with larger amounts of Cu and Ag. The addition of 0.7 wt.% Ag to an Al-4Cu alloy only shows a clear influence on the volume fraction, but hardly any difference can be seen in the other two parameters. The Ag causes a slight increase in the precipitation density and the coarsening of the particles in the alloy. The reason for this is the increase in the nucleation of the θ-phase due to Ag. After 5 hours, the coarsening of the precipitates decreases for both the Al-4Cu and the Ag-containing alloy.

The addition of Mg to an Al-4Cu alloy causes a slight increase in the number of precipitated particles, but the size decreases significantly. Due to the additional Mg present in the alloy, the S-phase is formed next to the θ-phase, which can be assumed by the observation of the DSC. Furthermore, the addition of Mg causes a temporal shift in the formation of the GP zones at later stages.

Compared with the other three alloys, an Al-4Cu-0.3Mg-0.7Ag has the highest number density and at the same time the lowest values for the Porod radius. The presence of Ag next to Mg in the alloy again shifts the formation of the GP zones to an earlier stage. However, the formation of the clusters takes place somewhat later compared to the Al-4Cu alloy. It appears that both Mg and Ag have an influence on the rate of the formation of the GP zones, with Mg retarding the formation and Ag showing opposite influences. After about 3 hours, both the number density values and the radius of the precipitates remain constant. All alloys considered so far, except the Al-1Cu and Al-4Cu-0.3Mg-0.7Ag showed an increase in Porod radius during ageing. It indicates that the θ-phase continues to coarsen at elevated temperatures, whereas the Ω-phase shows an increase in size up to a certain value, then remains approximately constant at least for the duration of the experiment. This behaviour is also consistent with the well-known information about the thermally stable Ω-phase. The observation under SEM shows that the alloy has lower values for the dislocation in the microstructure compared to the alloy without Ag, with an almost identical grain size distribution. In addition, the microstructure also shows a preferential texture in the <111> direction. This leads to the conclusion that the addition of 0.7 % Ag on the one hand has no influence on the size of the grains, but strongly influences the texture and above all the formation of precipitates. Therefore, higher values for the hardness after T4 and natural ageing compared to the other samples can be observed. This shows that even at room temperature a higher amount of strengthening phases is formed.

Overall, the hot rolling of an Al-4Cu-0.3Mg-0.7Ag alloy results in a coarsening of the precipitates with increasing deformation. At the same time, the number density decreases. The mean grain size before in-situ SAXS measurement of the T4 sample without rolling is 18 µm, also the rolled sample with a thickness of 6.74 mm is about 18 µm and that of the 0.3 mm sample is 12 µm. This means that although the mean size of grains in the 0.3 mm sample is the smallest, larger precipitates occur. The observation of the DSC curves also shows a similarity between the sample before hot rolling and the rolled sample with a thickness of 6.74 mm. The deviation of the sample with a thickness of 0.3 mm indicates that the dissolution of the phases takes place earlier in this sample due to the greater degree of deformation. This can be attributed to the shorter diffusion paths due to the smaller grain size and more vacancy. Hot rolling at 250 °C leads to a coarsening of the precipitates in a single rolling pass and an associated shorter duration at 250 °C compared to the original alloy. Heating the sample to this temperature for several rolling passes and thus maintaining the temperature for a longer period of time leads to a dissolution of the precipitates on one hand and a growth of the precipitates on the other hand. Also, an increase in lattice defects and vacancies is associated with a greater deformation. The observation of the internal stresses in the material using SEM (EBSD) also showed that high values for these could still be observed after T4 treatment. It can be concluded that there is probably still a larger number of defects in the material, which in turn affects the diffusion rate.

6 Summary and future outlook

This work deals on the one hand with the influence of the elements Cu, Mg, Ag, the cooling condition and on the other hand of the degree of deformation of an Al-4Cu-0.3Mg-0.7Ag alloy on the solidification and precipitation microstructure as well as hardness. Special attention is paid to the precipitates, since in the alloy system without Mg and Ag mainly α-Al and θ-phase are found. In contrast, the two alloying elements lead to the additional formation of the thermally more stable Ω-phase. The investigations include the observation of the morphology with the help of the optical microscope and SEM. With these, in addition to the determination of the grain sizes, the observation of the internal stresses and a chemical analysis with the help of EDS are carried out. The samples used in this work are in the as-cast condition, after hot rolling, aged at 170 °C for 12 hours, as well as after T4 treatment. Some samples are further investigated after T4 treatment using in-situ SAXS, where conclusions about precipitation at 170 °C can be drawn. The addition of Mg and Ag increases the precipitate density and decreases the size of the precipitates. In addition, the number of precipitates decreases with a simultaneous coarsening of the precipitates due to greater degrees of deformation of this alloy after hot rolling.

Influence of alloying elements

For the evaluation of the influence of the alloying elements, the line intercept method for grain size determination is used at the beginning after a Barker etching of the pure Al samples and Al-xCu alloys in the as-cast condition and after T4 heat treatment. It is shown that from a content of 2 wt.% Cu onwards the average grain size hardly changes, even solution treatment has only a slight influence on the size. In the following, the influence of Ag and the cooling rate on the solidification microstructure is examined with the use of SEM. Rapid cooling produces a finer grain in both alloys, but there is no significant difference in the sizes found. In contrast to the microstructure of the Al-4Cu-0.3Mg alloy, the addition of Ag leads to an orientation of the grains in the <111> direction. In the subsequent in-situ SAXS measurement at 170 °C for 20 hours, it is shown that the addition of 1 % Cu does not lead to any precipitation. Increasing the Cu content leads to a growth and coarsening of the precipitates, due to the increased diffusion rate with increasing Cu contents. The separate addition of Ag and Mg leads to only a slight change in the precipitate density. In contrast to the addition of Ag, where no significant change in the size of the precipitates can be observed compared to the Al-4Cu alloy, the addition of Mg alone results in a comparatively smaller size of the precipitates. The Al-4Cu-0.3Mg-0.7Ag alloy shows the highest precipitate density and smallest grain size in in-situ SAXS compared to the other samples considered. The Ω-phase coarsens in the first 5 hours at 170 °C, after which the values for the precipitate density and the Porod radius level off.

Influence of hot rolling

The influence of the hot rolling on the solidification microstructure is considered mainly by SEM, subsequently the samples with the lowest and the highest thickness are examined in in-situ SAXS with respect to the precipitates. The hot rolled specimens are considered in detail in the rolled condition, aged at 170 °C for 12 hours and T4 treated. It is found that with increasing degree of deformation, solution treatment at 540 °C for 6 hours results in a microstructure with a texture in the <101> direction. Whereas the samples from the rolled sheets with a thickness of 4.25 mm and 6.74 mm show no preferred texture of the grains. The T4 treatment as well as the ageing at 170 °C cause a reduction of the internal stresses, but also here the samples from the thinner plates still show increased values after the temperature exposure. When considering the EDS element maps, the distribution of the Cu outside the precipitates at higher deformation degrees is particularly noteworthy. The observation of the grain sizes in the different treatment states does not reveal any influence of the degree of deformation. Ageing at 170 °C after hot rolling reduces the grain sizes, while a T4 treatment provides a significant grain coarsening. The final examination of the precipitates with the aid of in-situ SAXS makes it clear that an increasing degree of deformation leads to a reduction in number density and coarsening of the precipitates.

Future outlook

The formation of the thermally more stable Ω-phase by adding Mg and Ag extends the application range of the alloy system. However, Ag is also an expensive element, which one would like to add only in the smallest necessary quantities from an economic point of view. Thus, a database with different compositions of the alloy system is desirable. Further investigations are also necessary with regard to the alloy used in the area of mechanical properties and the resistance of the precipitates at higher temperatures and extended holding times at these temperatures. Finally, following this work, the precipitates formed after the in-situ SAXS measurements will be further investigated using a transmission electron microscope and / or atom probe tomography in order to identify them more closely.

7 Literaturverzeichnis

[1] CHEN, T. et al. (2015) *Microstructure and crystal growth direction of Al–Cu alloy* in: Transactions of Nonferrous Metals Society of China 25, H. 5, S. 1399–1409. https://doi.org/10.1016/S1003-6326(15)63739-6

[2] Mokhtari, O. et al. (2014) *Investigation of Formation and Growth Behavior of Cu/Al Intermetallic Compounds during Isothermal Aging* in: Transactions of The Japan Institute of Electronics Packaging 7, S. 1–7. https://doi.org/10.5104/jiepeng.7.1

[3] Fuss, V. (1934) *Metallographie des Aluminiums und seiner Legierungen*. Berlin, Heidelberg: Springer Berlin Heidelberg.

[4] Köster, W.; Altenpohl, D. (1965) *Aluminium und Aluminiumlegierungen*. Berlin, Heidelberg: Springer Berlin Heidelberg.

[5] Eschbach, L. (1997) *Entwicklung von sprühkompaktierten AlCuMgAg-Legierungen mit hoher Warmfestigkeit und Zähigkeit*. ETH Zurich.

[6] Huang, B.-P.; Zheng, Z.-Q. (1998) *Independent and combined roles of trace Mg an Ag additions in properties precipitation process and precipitation kinetics of Al-Cu-Li-(Mg)-(Ag)-Zr-Ti alloys* in: Acta Mater 46, H. 12, S. 4381–4393.

[7] Bai, S. et al. (2019) *On the role of the solute partitioning and chemistry in initial precipitation of Ω plates* in: Materials Science and Engineering: A 766, S. 138339. https://doi.org/10.1016/j.msea.2019.138339

[8] Umantsev, A. (2011) *On the Origin of Biological Functions* in: Journal of Modern Physics 02, H. 06, S. 602–614. https://doi.org/10.4236/jmp.2011.226070

[9] Schulze, G. (2010) *Die Metallurgie des Schweißens – Eisenwerkstoffe - nichteisenmetallische Werkstoffe*. 4. Aufl. Berlin, Heidelberg: Springer.

[10] Bargel et al. (2008) *Werkstoffkunde*. 10. Aufl. Berlin: Springer.

[11] Schawe, J. E. K. (2015) *The Gibbs free energy difference between a supercooled melt and the crystalline phase of polymers* in: Journal of Thermal Analysis and Calorimetry 120, H. 2, S. 1417–1425. https://doi.org/10.1007/s10973-015-4453-z

[12] (17.03.2023) *Homogeneous Nucleation* [online]. https://polymerdatabase.com/polymer%20physics/Spherulites.html [Zugriff am: 31. Jul. 2023].

[13] Ashby, M. F. (2017) *Materials selection in mechanical design*. Amsterdam, Boston, Heidelberg …: Butterworth-Heinemann.

[14] Kamano, Y. et al. (2014) *Quantitative evaluation on the heterogeneous nucleation of amino acid by a thermodynamic analysis* in: Journal of Molecular Liquids 200, S. 474–479. https://doi.org/10.1016/j.molliq.2014.11.021

[15] Daeho Industries Ltd. (2015) *Aluminum Mast Alloys & Grain Refiner* [online]. http://www.daeholtd.co.kr/?page_id=1834&lang=en&ckattempt=1 [Zugriff am: 19. Aug. 2023].

[16] Hasse, S. (op. 2007) *Giesserei Lexikon*. 19. Aufl. Berlin: Schiele & Schön.

[17] Fan, Z. et al. (2015) *Grain refining mechanism in the Al/Al–Ti–B system* in: Acta Materialia 84, S. 292–304. https://doi.org/10.1016/j.actamat.2014.10.055

[18] (19.08.2023) *Boron Grain Refinement: Part One :: Total Materia Article* [online]. https://www.totalmateria.com/page.aspx?ID=CheckArticle&site=ktn&NM=405 [Zugriff am: 19. Aug. 2023].

[19] Panchal, H. et al. (2020) *Effect of Titanium and Boron on grain refining mechanism of aluminum: A Review* 5, S. 624–628.

[20] (19.08.2023) *Boron Grain Refinement: Part Two :: Total Materia Article* [online]. https://www.totalmateria.com/page.aspx?ID=CheckArticle&site=ktn&NM=407 [Zugriff am: 19. Aug. 2023].

[21] (17/07/2023) *Precipitation Hardening of Aluminum Alloys : Total Materia Article* [online]. https://www.totalmateria.com/page.aspx?ID=CheckArticle&site=ktn&LN=DE&NM=235 [Zugriff am: 17. Jul. 2023].

[22] *Wärmebehandlung von Aluminiumlegierungen* [online]. https://docplayer.org/47446107-Merkblatt-aluminium-zentrale-w-7-waermebehandlung-von-aluminiumlegierungen.html [Zugriff am: 21. Jul. 2023].

[23] Frederic De Geuser, Francoise Blez and Alexis Deschamps (2010) *Earlz Stages of Sigma Phase Precipitation in Al-Cu-Mg-Ag Observed in Situ with and without Applied Stress by Small Angle X-ray Scattering* [online]. The Japan Institute of Light Metals.

[24] Chen, M.-C. et al. (2023) *Quantitative evaluation of the effect of Ag-addition on the concurrently-existing precipitation kinetics in the aged Al-Cu-Mg(-Ag) alloys* in: Materials & Design 227, S. 111766. https://doi.org/10.1016/j.matdes.2023.111766

[25] Swapp S. (26/05/2017) *Scanning Electron Microscopy (SEM)* [online]. University of Wyoming. https://serc.carleton.edu/research_education/geochemsheets/techniques/SEM.html [Zugriff am: 17. Jul. 2023].

[26] Schnablegger H.; Singh Y. *The SAXS Guide – Getting acquainted with the principles*. 4. Aufl.

[27] Mukhopadhyay, A. K. (2002) *Coprecipitation of Ω and σ phases in Al-Cu-Mg-Mn alloys containing Ag and Si* in: Metallurgical and Materials Transactions A 33, H. 12, S. 3635–3648. https://doi.org/10.1007/s11661-002-0238-7

[28] Peng, Z. et al. (2022) *Tensile Property and Corrosion Performance of Ag Microalloying of Al-Cu Alloys for Positive Electrode Current Collectors of Li-Ion Batteries* in: Materials (Basel, Switzerland) 15, Nr. 15. https://doi.org/10.3390/ma15155126

8 List of figures

9 List of tables